Bachelor's thesis

NTNU
Norwegian University of Science and Technology
Faculty of Engineering
Department of Energy and Process Engineering

Eirik Odinsen
Benjamin Trondsen
Sivert André Woll

Digital twin for next generation PEM electrolyzer

Development of a dynamic digital twin of the Balance of Plant using Modelica

Bachelor's thesis in Engineering Renewable Energy
Supervisor: Alejandro Oyarce Barnett, NTNU
Co-supervisor: Eddy Van Oort, Hystar
May 2022

NTNU
Norwegian University of
Science and Technology

Eirik Odinsen
Benjamin Trondsen
Sivert André Woll

Digital twin for next generation PEM electrolyzer

Development of a dynamic digital twin of the Balance of Plant using Modelica

Bachelor's thesis in Engineering Renewable Energy
Supervisor: Alejandro Oyarce Barnett, NTNU
Co-supervisor: Eddy Van Oort, Hystar
May 2022

Norwegian University of Science and Technology
Faculty of Engineering
Department of Energy and Process Engineering

NTNU
Kunnskap for en bedre verden

NTNU

Institutt for energi- og prosessteknikk

Bachelor thesis

Project title: Digital twin for next generation PEM electrolyzer **Project title (NOR):** Digital tvilling for neste generasjons PEM-elektrolysør	**Project assigned:** 13.01.2022 **Submission deadline:** 20.05.2022 **Number of pages/ appendices:** 69/0
Project participants: Eirik Odinsen Benjamin Trondsen Sivert André Woll	**Supervisors:** Alejandro Oyarce Barnett Eddy Van Oort **Project number:** 22BIFOREN-014
Client: Hystar	**Contact person at client:** Eddy Van Oort

Freely available: ☒

☐

Preface

This BSc is the final part of the three-year study program Bachelor in Engineering, Renewable Energy, Department of Energy and Process Engineering at the Norwegian University of Science and Technology. The thesis is written in the course FENT2900 - Bachelor Thesis Renewable Energy and is valued at 20 credits.

The project description was given by Hystar with the objective of developing a digital twin for a PEM electrolyzer, with focus on development of the surrounding auxiliary equipment called the Balance of Plant. While both challenging and frustrating at times, creating the digital twin has been an inspiring and interesting experience.

We would like to express our utmost gratitude towards our internal supervisor from NTNU, Alejandro Oyarce Barnett, and our external supervisor from Hystar, Eddy Van Oort. Without their weekly guidance and support concerning the development of the digital model and writing of the thesis, our finalized results would not have been possible.

Trondheim, 20. May 2022

Eirik Odinsen Benjamin Trondsen Sivert André Woll

Abstract

A digital twin is a virtual representation that serves as the real-time digital counterpart of a physical object or process.

This thesis presents the development of a digital twin for a next generation PEM electrolyzer. The main task is centered around the development of the auxiliary equipment which is required in the electrolysis process, called the Balance of Plant. The thesis is supported by Hystar, a company that specializes in PEM electrolyzers with high-end technology for green hydrogen production. The digital twin is created with the open-source modeling program Modelica, a program that excels at component-oriented modeling of complex systems.

The Balance of Plant is made up of several components which maintain the process at its desired operational performance point and ensure that this is upheld through monitoring and controlling. The Balance of Plant includes centrifugal pumps, regulative valves, ion exchangers, liquid-gas separators, heat exchangers, coolers, sensors, controllers, and a power supply unit. Each digital component developed is thoroughly described with included parameters, variables, and equations.

Simulations from Modelica were presented, initially from individual models before a more complex, combined system was created and connected to an electrolyzer stack provided by Hystar. From the simulations done in Modelica, it was found that the digital twin achieved its intended behaviour, as well as delivering realistic results if provided with accurate input parameters. Controlling the system towards desired operating conditions was also achieved. The models in general proved simple to utilise and alter in order to fit specific needs.

Simulations of all the models as well as subsystems proved the digital twin worked as intended. The simulations and following discussion highlighted several aspects suitable for further improvement. Improvements like an increase to the digital twin's complexity and implementation of certain subsystems could be done in order to address the limitations and shortcomings in this thesis.

.

Sammendrag

En digital tvilling er en virtuell representasjon som fungerer som den digitale motparten til en fysisk gjenstand eller en prosess.

I denne oppgaven presenteres utviklingen av en digital tvilling for en neste generasjons PEM-elektrolysør. Hovedaspektet er sentrert rundt utvikling av tilleggsutstyret som kreves i elektrolyseprosessen, kalt balanse av anlegget. Oppgaven er støttet av Hystar, et selskap som spesialiserer seg på PEM-elektrolysører med avansert teknologi for grønn hydrogenproduksjon. Den digitale tvillingen er utviklet med modelleringsprogrammet Modelica, et program som er egnet til komponentorientert modellering av komplekse systemer.

Balansen av anlegget består av flere komponenter for å opprettholde prosessen ved ønsket ytelse. Dette inkluderer sentrifugalpumper, reguleringsventiler, ionevekslere, væske-gass-separatorer, varmevekslere, kjølere, sensorer, kontrollere og en strømforsyningsenhet. Hver digitale komponent som utvikles er grundig beskrevet med inkluderte parametere, variabler og ligninger.

Simuleringer fra Modelica ble presentert, først fra individuelle modeller før en mer kompleks kombinasjon av systemet ble utviklet med elektrolyse stacken levert av Hystar tilkoblet. Fra simuleringene som ble utført i Modelica ble det bevist at den digitale tvillingen fungerte som forventet, samt leverte realistiske resultater om den ble gitt riktige parameter verdier. Kontroll av systemet mot ønskede driftsforhold ble oppnådd. Modellene viste seg å være fleksible og anvendbare til sine formål.

Simuleringer av alle komponentene samt undersystemene viste at den digitale tvillingen fungerte som antatt. Simuleringene fremhevet også flere aspekter ved den digitale tvillingen som egnet seg for ytterligere forbedring. Forbedringer som en økning av den digitale tvillingens kompleksitet og implementering av neglisjerte delsystemer kan blir gjort for å adressere begrensningene og manglene som eksisterer i oppgaven.

Contents

List of Symbols

Symbol	Unit	Description
A	m^2	Area
C_{max}	W/K	Maximum heat capacity rate
C_{min}	W/K	Minimum heat capacity rate
Cp	$J/(kg \cdot K)$	Specific heat capacity
C_r	-	Heat capacity ratio
D	m	Diameter
e^-	-	Chemical symbol of electron
f	Hz	Frequency
g	m/s^2	Standard gravity
h	J/kg	Specific enthalpy
H	m	Total head
H^+	-	Chemical symbol of positively charged hydrogen
H_2	-	Chemical symbol of hydrogen gas
H_2O	-	Chemical symbol of water
I	A	Current
k	W/K	Convective heat transfer
k_v	-	k factor
Kp	-	Proportional gain
Ki	-	Integral gain
L	m	Length
m	kg	Mass
$\dot{m}$	kg/s	Mass flow rate
N	-	Number of windings
O_2	-	Chemical symbol of oxygen gas
P	Pa, bar	Pressure
$P_{AC/DC}$	W	Electric power
P_c	W	Full load copper/ohmic losses
P_i	W	Iron losses
q	W	Heat transfer rate
q_{max}	W	Theoretical maximum heat transfer rate
Q	m^3/h	Volume flow rate
R	Ω	Resistance
T	K, °C	Temperature
U	$W/(m^2 \cdot K)$	Overall heat transfer coefficient
U	J	Internal energy
V	V	Voltage
W	W	Power input
X	-	Medium composition
ϵ	-	Efficiency of heat exchanger
η_{pump}	-	Efficiency of centrifugal pump
η_{rect}	-	Efficiency/conversion ratio of rectifier
η_{trans}	-	Efficiency of transformer

List of Abbreviations

Abbreviation	Description
AC	Alternating current
BoP	Balance of Plant
DC	Direct current
HEX	Heat exchanger
IEA	International energy agency
NTU	Number of transfer units
OMEdit	Open Modelica Connection Editor
PEM	Proton exchange membrane
PEMEL	Proton exchange membrane electrolyzer
PF	Power factor
PI	Proportional Integral
RMS	Root mean square
RPM	Revolutions per minute
SG	Specific gravity

List of Figures

List of Tables

1 Introduction

This thesis aims to develop a dynamic digital model of a next generation polymer electrolyte membrane electrolyzer. The digital model will contain descriptions of the most important electrolyzer system auxiliary components to investigate the electrolysis system's dynamic behavior. The thesis is written with the purpose of giving the reader insight of the digital model created, and describe the thought process behind choices made.

1.1 Background

Today, modern society faces arguably its greatest challenge yet, the ongoing climate crisis. Sustainable energy systems are required, as the energy sector is the source of around three-quarters of the global greenhouse gas emissions [1]. Fortunately, a transition is already happening from fossil-fueled energy production to renewable energy. However, with this change energy is produced more intermittently, with increased implementation of sources such as wind energy and solar energy. This changes the intermediate steps in the energy supply chain, and energy carriers need to be implemented. To contribute to this transition, hydrogen as an energy carrier can prove to play a crucial role in the said transmission of energy. The use of hydrogen as an energy carrier has the potential to reduce greenhouse gas emissions across many applications.

About 3% of the global energy consumption is used to produce hydrogen today [2]. According to Hydrogen Council, the long-term potential of hydrogen is substantial. By 2050, hydrogen could cover 18% of the final, global, energy demand [3]. Today the dominant source of hydrogen production is grey hydrogen, which is hydrogen generated from natural gas or methane. This process is called steam reforming and generates carbon dioxide emissions. Green hydrogen on the other hand is hydrogen produced by the electrolysis process powered by renewable energy [4].

With increased desire and demand for green hydrogen, the PEM water electrolysis technology has seen increased interest. Due to numerous operational advantages, the electrolyzer produces hydrogen with high purity at high energy efficiency, in the range of 80-90% [5]. Advantages include a higher rate of hydrogen production and a more compact design, compared to the two other main hydrogen production methods such alkaline water electrolysis and anion exchange membrane water electrolysis [5]. Figure 1 illustrates the working principle of a PEM electrolyzer.

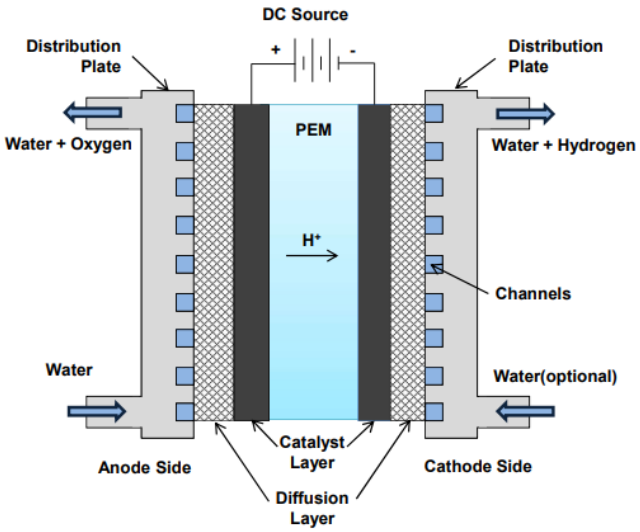

Figure 1: Schematic of a PEM electrolyzer stack [6]

PEM is an abbreviation for proton exchange membrane, originating from the use of protons as the ionic agent. The PEM electrolyzer stack consists of two half cells separated by a thin polymer electrolyte membrane. The half-cell reaction of the electrodes and the overall reaction is presented in equation 1 [5].

$$\begin{aligned} Anode: & H_2O \rightarrow 2H^+ + \frac{1}{2}O_2 + 2e^- \\ Cathode: & 2H^+ + 2e^- \rightarrow H_2 \\ Overall: & H_2O(l) \rightarrow H_2(g) + \frac{1}{2}O_2 \end{aligned} \tag{1}$$

The water is fed in on the anode side, where the water is reduced to oxygen, O_2, positively charged hydrogen protons, H^+, and electrons, e^-. The oxygen produced in this half-cell reaction is extracted from the anode fluid cycle in the gas-liquid separation unit. The hydrogen protons move through the membrane and to the cathode side, where it reacts with electrons from the direct current power source and form the hydrogen gas. Water can optionally be fed in on the cathode side to facilitate the effective removal of the hydrogen gas. This is not necessary in all cases as proton drag carries substantial amounts of water through the membrane [7]. The digital model created is categorized as an anode feed system.

The electrochemical reactions occur at the catalyst layer. The catalyst layer is coated on the electrodes and is crucial to ensure desired reactions. The stack's performance is significantly influenced by the construction and structure of the layers. A diffusion layer on each electrode is beneficial for efficient current distribution. The distribution plates, also called bipolar plates, serve the purpose of evenly distributing water in the electrolyzer stack to cool the device and evacuate gases produced by the electrochemical reactions. A PEM electrolyzer is a complex system involving non-linear relations to describe the dynamics as the system combines various physical phenomena such as electro-chemical, thermo-electric, and thermo-fluidic [7].

1.2 Motivation

When constructing a polymer electrolyte membrane electrolysis system, costs are involved in both the electrolysis stack itself and all the equipment surrounding the stack. The different equipment around the electrolysis stack is referred to as the Balance of Plant, or BoP in short, and includes the necessary auxiliary components for the system to operate normally. Typical BoP equipment can be described as controlled valves, heat exchangers, pumps, a power supply unit, a water conditioning system, liquid-gas separators, sensors, and safety equipment. According to an IEA report prepared for the G20 meeting in 2019, the electrolyzer stack is responsible for around 50% of the total system cost [8]. This implies that the Balance of Plant costs makes up the remaining 50%. The BoP equipment also has a large impact on the performance and efficiency of the electrolysis system, which further reinforces its significance.

Considering how important and expensive all the BoP equipment is, a digital twin of the electrolysis system would be a preferable way to cut potential costs and optimize the system sufficiently before physical production starts. The digital twin would also be a tool that could contribute to the continuous development of electrolyzers, as technology rapidly undergoes changes and improvements. Such changes could quickly be applied to the digital twin, allowing for transparent and updated testing conditions at all times.

The techno-economical aspect related to the BoP equipment within the electrolysis system requires the project to develop parametric models of BoP equipment which then can be combined into a single model, representative of the digital twin of the electrolysis system. These models need to be tested and validated against real-world data and realistic component behavior. Optimization and documentation are required so that the models are easy to use, implement and understand for the client of this bachelor thesis, Hystar.

1.3 Limitations and Prerequisites

This bachelor thesis is supported by the high-tech company Hystar, a company that specializes in PEM electrolyzers with new high-end technology, and the production of green hydrogen from water electrolysis. The project consists of digital modeling and validation of the BoP equipment for the electrolysis system. A model of the electrolysis stack itself will be provided by Hystar. The physical limitations of the project encompass that most of the BoP equipment surrounding the electrolyzer stack will be modeled in this project. Certain assumptions and simplifications are required to keep the project within its limited scope, which is 20 credits.

The end product of the project is a result of close collaboration with Hystar to ensure that the product satisfies the desired properties and purpose. Assumptions and simplifications done have been determined in agreement with Hystar.

1.4 Structure

The thesis aims to describe the digital twin that is developed in detail. The methodology applied to establish the basis of the project is described. Further, each component in the Balance of Plant is presented and thoroughly described. The individual components are then connected into their respective subsystems. Finally, the subsystems are connected into a combined system where further improvements are made until desired behavior with the electrolyzer stack provided by Hystar is achieved.

Simulations of important and wanted parameters are presented in the results section. In the discussion section, these results are then explained more thoroughly. The design choices, assumptions and sources of error are also discussed. The models are then compared to real world data and real component behavior in a subsection about the models' validity as a part of the discussion. Further work and suggested improvements to the digital model are presented before the work done is concluded.

2 Methodology

Today, society stand on the brink of a technological revolution that will fundamentally alter the world. The fourth industrial revolution is a digital transformation that conceptualizes rapid change to technology, processes, and industries due to increasing interconnectivity and smart automation. The development of digital twins is a product of this change. A digital twin is a digital representation of a physical object, process or service. It is in its most simplistic form a computer program that applies real world data to create simulations that can predict how a process or product will perform [9].

The application of digital twins are drastically increasing, as additional industries and corporations find the importance and benefits which digital models provide. One benefit can be economic efficiency. The ability to adapt and change parameters and system dynamics of the digital model without having to produce costly prototypes are important. Digital twins facilitate more efficient research and design of products, with belonging performance outcomes. This information provides crucial insight into potential product refinements required before production starts.

The methodology of creating a digital model differs from the more traditional academic research approach. Acquisition of theory is greatly replaced with the learning of modeling language and research of system behavior. A substantial theory section is replaced with the theory and method behind each component in the digital model. Initially, the scope of the project was defined, and relevant academic papers were retrieved and reviewed. To better illustrate the models created, multiple schematics and illustrations are presented in chapter 3. All schematics are, unless stated otherwise, created by the authors using the online diagram software *Draw.io* [10].

2.1 Modelica

To develop the digital model of the electrolysis system the open-source modeling program Modelica was applied. The program is well suited for object-oriented programming and supports the acausal connection of components governed by mathematical equations. Modelica is often applied to engineering systems and is suited to describe the behavior of typical engineering components. The Modelica language is developed by the Modelica Association, a nonprofit organization with seat in Linkoping, Sweden [11]. The program is distributed as an open language and is available online for free [12].

The Modelica language excels at component-oriented modeling of complex systems. The user is therefore not required to re-arrange model equations to suit the system boundary conditions or the desired application of the system. This enhances efficiency and ease of use by encapsulating mathematical behavior into reusable component models. Modelica allows for an efficient organizational structure, combining components into subsystems, systems, or architectures. The compilers allow users to focus on the mathematical descriptions of component behavior and get high-performance simulation capability in return. All this is possible without needing to be well versed in complex topics such as differential-algebraic equations, symbolic manipulation, numeric solvers, code generation and post-processing [13].

The Modelica language offers several compilers, and the one chosen for this project is OpenModelica Connection Editor, OMEdit. OMEdit has an advanced and user-friendly graphical interface and easy-to-use model creation. Including connection editing, plotting of results, and simulations of models. Models can be both textual and graphical, which offers valuable user flexibility when developing models. It gives the ability to check and instantiate models, which again makes troubleshooting and debugging easier. The implementation of OMEdit is based on the programming language C++ and the Qt software [14].

In order to have a determined system in Modelica, the system is required to have the same number of variables and equations. If this relation is unequal, the result is an under- or overdetermined system. In the case of this occurring, the system may find infinitely many solutions or no solutions at all.

Open Modelica was decided as the modeling program to be used, chosen over other programs such as Python and Matlab' Simulink. This decision was made mainly because of the Modelica models' simple understanding as it keeps the models' physical structure. The models are also extremely versatile and allow extensive model reuse for several applications. It was also desired by Hystar that Modelica should be used for the project, due to the necessary compatibility between the created digital twin and their own electrolyzer stack model developed in Modelica.

2.1.1 Library

In computer science, a library is a collection of resources used by computer programs for software development. Modelica offers a collection of free and commercially available libraries. In total there are around 30 libraries submitted by the Modelica Association, and the license allows both copying and modifying of them. In addition to these models, a vast selection of libraries provided by users is available online. The largest library, The Modelica Standard Library, contains fundamental components for modeling mechanical, electrical, magnetic, thermal, fluid, control systems, and hierarchical state machines [13]. Numerical functions and functions for strings, files, and streams are also included. In the process of developing the digital twin of the electrolyzer inputs or parts of components from external libraries are utilized, and sufficient inheritance and documentation are attached.

2.2 Literature

To accumulate the knowledge required to develop the digital model, learning the Modelica programming language is essential. In order to learn the Modelica language, literature consisting of academic articles, which were either found online or provided by Hystar, were used. Articles that involved development of models with similar behavior to the planned BoP equipment models were especially sought after. However, the articles found indicated that there was not much work done on the modeling of PEM electrolyzers and electrolysis systems, as opposed to PEM fuel cells [15]. Despite this, there are several structural and process similarities which can be adapted between the models for the PEM electrolyzers and the already exsiting models of the PEM fuel cells. A digital model of a PEM fuel cell was developed by SINTEF in 2020, where parts of this model, including the structural approach, have been used as inspiration for the digital twin of this thesis [16].

Modelica by Example is an electronic book which was used extensively to learn the describing behavior of the program initially [13]. It is built up with examples with gradually increasing complexity, analogous to the project progress. Peter Fritzon, a founder of Modelica has also created a tutorial course called "Introduction to Object-Oriented Modeling and Simulation with Modelica Using OpenModelica" [11]. This course was used in the initial phases of the project work in order to grasp the basics of the Modelica language and its interfaces.

2.3 Assumptions

For a project of this scope, some assumptions have been made in order to keep the thesis well within its credit score of 20 points. As previously mentioned when discussing the limitations of the project, the assumptions were discussed and agreed upon with Hystar.

In PEM electrolysis, an important parameter is the water purity. Pure water is required with a specific desired conductivity, normally acquired in a water purification unit. This unit is neglected due to its complexity, and pure water is assumed fed into the system.

In the process of separating gas and liquids, there will in most cases be a small substance of liquid extracted with the gaseous fluid. As for the digital models case this is assumed to be false, and pure oxygen and hydrogen is extracted for the system with no liquid trace substance. Following this, a hydrogen purification unit is a normal auxiliary component included to purify the hydrogen produced, but is excluded for limitation purposes of the thesis.

Another simplification done is that the medium flow out of the electrolysis stack is transported separated in its constituent phases, meaning that the gas and liquid flows in separate inlets and outlets. The reasoning behind this is that the modeling of multi-phase mediums increased the complexity of the digital twin to be outside the scope of the thesis.

The electrical balance was deemed to be generally false where electrical pin connectors were not used in the electrical models of the digital twin. This assumption was made due to the complex nature of power electronics and how they interact with each other. In order to simplify, custom connectors were used instead to allow better customization options of which variables that could be transferred between models. How this decision impacted the simulations and design of the models is discussed later in chapter 5.3.

3 The Balance of Plant

The Balance of Plant is a term commonly used in the power industry and other technical facilities. It can be described as all infrastructural components surrounding the main product, which in the case of this thesis is the electrolyzer stack. This chapter will describe the applied port connectors in Modelica, the medium used in the system, the different BoP components present in the digital twin and the applied sensors. The different subsystems of the digital twin, as well as the combined system as a whole, will also be described.

3.1 Ports

When connecting multiple components in Modelica, such as the auxiliary equipment that makes up the BoP, ports have to be implemented. Ports can be described as connectors and can be of various types such as fluid ports, signal ports, heat ports, and power ports. Fluid ports are the most common type of ports in the digital twin, as fluids are transported through the anode and cathode flow circuit, the stack itself, and the cooling circuits. The properties and values of the fluid are described using the Modelica standard library fluid port, located in *Modelica.Fluid.Interfaces.FluidPort*. This port is an interface for quasi-one-dimensional fluid flow in a piping network, with one or more phases and substances.

To describe the behavior of the fluid port four variables are included. The mass flow rate is defined as a flow, *m_flow*. This represents the flow rate from the connection point into the component. The specific enthalpy, *h_outflow*, is defined as a stream with medium-specific attributes at the connection point, or close to the connection point if m_flow < 0. The mass fraction, *Xi_outflow*, is defined as a stream at the connection point, or close to the connection point if m_flow < 0. An extra property, *C_outflow*, is included as a type for unspecified, mass-specific property transported by flow. Heat ports are used as a thermal port for one dimensional heat transfer. The connector includes the port temperature, T, and the heat flow rate, Q_{flow}.

In order to connect electrical components, connector pins from *Modelica.Electrical.Analog.Interfaces.Pin* are applied. This type of connector contains two variables, the potential at the pin, v, and the current flowing into the pin, i. To distinguish between the positive and negative pin of an electric component, the connectors are often named *PositivePin* and *NegativePin*. Both are identical except for differences in their icons.

To transfer signals, primarily used for regulation and controlling of systems, signal ports are utilized. It is implemented from the Modelica standard library, under *Blocks.Interfaces.RealInput* for input signals, and *RealOutput* for output signals. Both function as connectors with one signal of type Real, a type that represents real valued variables.

3.2 Mediums

When modeling with fluid ports a medium has to be defined in the system. Modelica library mediums are used to define the wanted and realistic medium compositions in the system. The medium is defined as a replaceable package in the model and can be redeclared within wanted parts.

As the electrolysis reaction occurs, ions are transferred through the membrane and the fluidic composition in the circuit changes. However, due to the complexity of multi-phase compounds in Modelica, the mediums are for simplicity sake kept in separate streams as previously mentioned.

The water fed into the system on the anode side is defined as the Modelica medium *Media.Water.StandardWater*. The gas extracted from the anode side separator is the Modelica medium *Media.IdealGases.SingleGases.O2*. The gas extracted from the cathode side separator is the Modelica medium *Media.IdealGases.SingleGases.H2*. Modelica retrieves the ideal gas data from NASA Glenn coefficients, a computer program developed by NASA for calculating thermodynamic properties. For the cooling circuit the Modelica medium *Media.Water.StandardWater* is used.

To describe the streams of the mediums in connectors the Modelica operators *inStream* and *actualStream* are used. InStream is used if the medium flows from the connection point to the component. For bi-directional flows the operator actualStream is used, allowing flow in both directions.

To describe the thermodynamic state of the medium the function *setState_phX* is applied. This returns the thermodynamic state as a function of pressure, enthalpy, and composition X, and is useful to retrieve unknown temperatures at known pressure and enthalpy states. If multiple thermodynamic states are of interest, the Modelica record ThermodynamicState can be applied. This returns a selection of variables that uniquely defines the thermodynamic state.

The Modelica model *BaseProperties* is used to return the base properties of a declared medium. Included properties are medium density, specific enthalpy, specific internal energy, molar mass, gas constant, absolute pressure, and temperature.

3.3 The BoP components

The Balance of Plant components included in the digital twin are presented individually with graphical illustrations where it is deemed of use. Governing equations, relevant parameters, and variables specific to each model are presented. In addition to this, the components' behavior, role, and usefulness to the electrolysis system of the digital twin are also described. Other assumptions or simplifications made for the models are explained in detail. Discussions around the design choices and assumptions are further elaborated on later in chapter 5.

3.3.1 Centrifugal pump

For the system to work under optimal conditions, the PEMEL stack needs to operate at a given pressure and a desired flow rate. A centrifugal pump is a simple component that creates flow, where due to increasing resistance in the flow the pressure also increases. Centrifugal pumps are often powered by an electric motor [17].

For a pump under stationary conditions, Bernoulli's equation could be used to calculate the pressure increase[18]. However, for a pump operating under varying conditions, pump curves are of interest. These curves describe the correlations between displaced volume, Q, total head, H, and the pumps operating rpm. The pump curves can be represented by an equation correlating H and Q to simplify things [19]. In this model, a simple replica of a typical pump curve is used. This can easily be changed later as it is only necessary to fit an equation for the pump curve.

For this pump, the outlet and the inlet pipes are of the same size. To further simplify things the difference in height of the suction and discard of the pumps are assumed to be zero, meaning that the only attributes relevant to the pump is its potential to create flow under varying pressure by the power added. An illustration of the centrifugal pump is shown in figure 2.

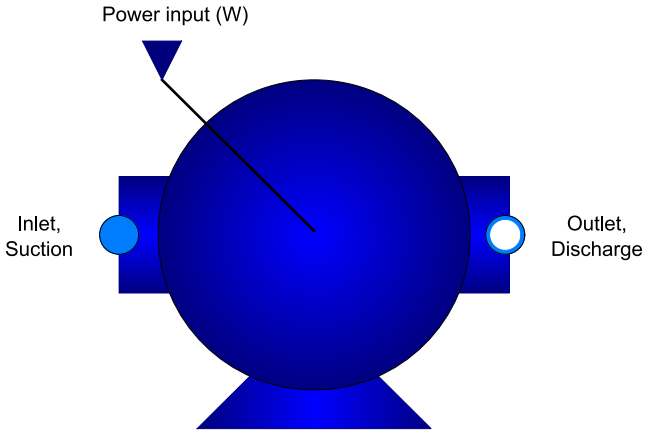

Figure 2: Illustration of a centrifugal pump

All parameters and variables concerning the development of the centrifugal pump are presented in table 1 and table 2 respectively.

Table 1: Parameters of the centrifugal pump

Parameter	**Unit**	**Comment**
ρ	kg/m^3	Mass density
W	W	Power input
P_1	Pa	Pressure at inlet
g	m/s^2	Standard gravity
h_1	J/kg	Specific enthalpy at inlet

Table 2: Variables of the centrifugal pump

Variable	**Unit**	**Comment**
H	m	Total head
η	-	Efficiency of pump
$\dot{m}$	kg/s	Mass flow rate
Q	m^3/h	Volumetric flow rate
P_2	Pa	Pressure at outlet
h_2	J/kg	Specific enthalpy at outlet

$$Q = \frac{\dot{m} \cdot 3600}{\rho} \tag{2}$$

Calculating the volumetric flow rate, as done in equation 2, is of great interest as most manufacturers state their pump curves as a function of head and volumetric flow rates [18].

$$H = \frac{P_2 - P_1}{\rho \cdot g} \tag{3}$$

To find the value of the total head, equation 3 is used. Both the kinetic term and the elevation term is ignored as it is assumed that the inlet velocity and outlet velocity, as well as the inlet height and outlet height as mentioned previously, are the same [18].

$$H = W \cdot 10^{-1} - \frac{1}{100} \cdot Q^2 \tag{4}$$

Equation 4 is a gross simplification of the pump curve as this in reality should take into account both rpm, efficiency at different operating conditions and the power, head, and volumetric flow rate [19]. This does however make the model mimic characteristic pump behavior and is in this thesis used to describe a certain behavior between the head and volumetric flow rate at differing power inputs. For later use, a more fitting pump curve can, and should, be added in order to acquire desired pump curves and behavior.

$$h_1 + \frac{W}{\dot{m}} = h_2 \tag{5}$$

The outflow enthalpy from the pump is also of interest since it is a variable within the stream. The equation 5 relates the inflowing and outflowing enthalpy. For the digital twin created in Modelica there is also included an additional pump designed for a predescribed mass flow rate. For this pump the pump curve calculated in equation 4 is neglected, and power is a variable needed to deliver said mass flow rate at given difference in pressure.

3.3.2 Valve

Valves are components often designed to limit flow and can thus also be applied to hydraulic systems to ensure a certain pressure [20]. In the digital twin, valves are instrumental for keeping the desired operating conditions. In this system, the applied valves are pressure-regulated. These valves regulate their openings from fully open to fully closed to control the inlet pressure. This is illustrated in figure 3. In addition to regulating the pressure, the operation of the valve is increasing the pressure drop of a stream and is therefore also affecting the mass flow rate of the system. There are several types of valves such as quick opening and equal percentage, the one applied in this model is a valve of type linear [21].

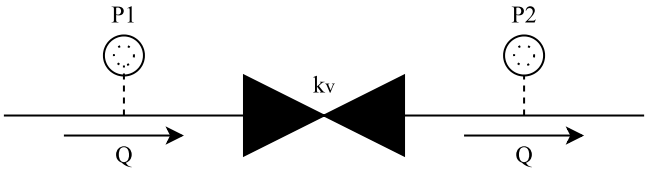

Figure 3: Schematic representation of a simple valve

Table 3: Parameters of the valve

Parameter	**Unit**	**Comment**
P_2	Pa	Pressure at outlet port
k_v	-	k factor
SG	-	Specific gravity of working fluid
Nominal pressure drop	Pa	Pressure drop at full opening
u	-	Input signal varying from 1 to 0
ρ	kg/m^3	Density of fluid at inlet
P_{ref}	Pa	Desired pressure set point for a regulated valve

Table 4: Variables of the valve

Variable	**Unit**	**Comment**
$\dot{m}$	kg/s	Mass flow rate through component
Q	m^3/h	Volumetric flow rate
P_1	Pa	Inlet pressure
opening	-	Opening varying from (almost) closed to open

In tables 3 and 4, the parameters and variables used in the valve model are given.

$$Q = \frac{\dot{m} \cdot 3600}{\rho} \tag{6}$$

As most producers of valves give the k_v factor according to the volume flow rate in m^3/h, equation 6 finds the given volume flow rate from the mass flow rate [22].

$$SG = \frac{\rho_{Xi}}{\rho_{water}} \tag{7}$$

Since the valve should be applicable for a variety of mediums, the term specific gravity, SG, is introduced in equation 7 [23]. The reference medium is water.

Since a fully closed valve is expected to have a small amount of leakage and a fully open valve is expected to have a minor pressure drop, a way to implement this expected behavior into the valve model has to be done [20].

This is necessary since allowing there to either be no pressure drop or no mass flow in the model creates singularities. A variable, *opening*, as seen in table 4, solves this problem by following an u value from 0.01 to 0.99.

For a valve, an increasing k factor allows more flow through the valve which decrease the pressure drop. The flow is also dependent on the opening of the valve [20].

$$k_v \cdot opening = Q \cdot \sqrt{\frac{SG}{\Delta P}} \tag{8}$$

The valve curve is defined by equation 8, which is the governing equation for the valve behavior. The relations in this equation can be altered in order to acquire the desired behavior of the pump.

$$\Delta P = P_1 - P_2 \tag{9}$$

ΔP is the change in inlet and outlet pressure, as seen in equation 9. In addition to the regular valve, a simple regulated valve is included in the model. The regulated valve regulates the opening after the actual inlet pressure and the pressure set point. For an actual system this should be determined by a regulator. However, algorithm 1 and equation 10 can still manage to recreate this, although in a much simpler fashion.

$$der(u) = P_1 - P_{ref} \tag{10}$$

Algorithm 1 Calculate the opening of the valve

```
if der(u) < 0 then
    opening = 0.001
else
    opening = der(u)
end if
```

Since this is just a simplification made, adding a constant to the derivative of u to either increase or decrease gain can be done as part of the further development of the digital twin.

3.3.3 Ion exchanger

Ion exchange resins are normally placed in both the anode and cathode water circulation loops of electrolysis systems. The purpose of the exchanger is to maintain conductivity within desired specifications [24]. This component will only affect the pressure in the water circuit.

$$P_{1IonEx} = 1.05 \cdot P_{2IonEx} \tag{11}$$

The ion exchanger is modeled as a minor pressure drop in the digital twin, presented in equation 11. If further development of the digital twin with the inclusion of a water purification unit is desired, more complex relations in the ion exchanger could be implemented.

3.3.4 Liquid-gas separator

A liquid-gas separator is used in applications to separate a vapor-liquid mixture into its constituent phases [24]. This component is modeled as a vessel mimicking separation by gravitational force, though the actual separation in this model is assumed to be instantaneous.

A separator is required on both the anode and cathode sides of the electrolysis fluid circuit. On the anode side, purified H_2O with desired conductivity is fed into the separator vessel. As the electrolysis process occurs the O_2 produced has to be removed from the system. This process is controlled by a regulated valve. The liquid-gas separators function as buffer storage vessels for the fluids to assure sufficient flow levels at all operational times. In the electrochemical reactions occurring in the stack, hydrogen ions combine with electrons from the external circuit to form hydrogen gas, H_2. This gas is extracted from the system in the liquid-gas separator unit on the cathode side, again controlled by a regulated valve

Liquid level monitoring is required in the separators. The separators can fail if the inlet supply of liquid is too great, or if the outlet drain is unable to handle the liquid collected. To control this a set maximum and minimum volume level of the liquid-gas separator, V_{max} and V_{min}, is defined. These values are monitored by a sensor, where the output signal regulates the inlet flow of liquid feedwater in the anode side, and the fluid discharged on the cathode side. It is important to include a fluid discharge at the cathode as this prevents the volume of the vessel from containing too much liquid. As proton drag transports water to the cathode side, excess water is released out of the system when the liquid reaches a certain volume in the vessel.

A simplification made to the vessel is that the enthalpy outflow from any port is equal to the given media's specific enthalpy inside the vessel at any moment.

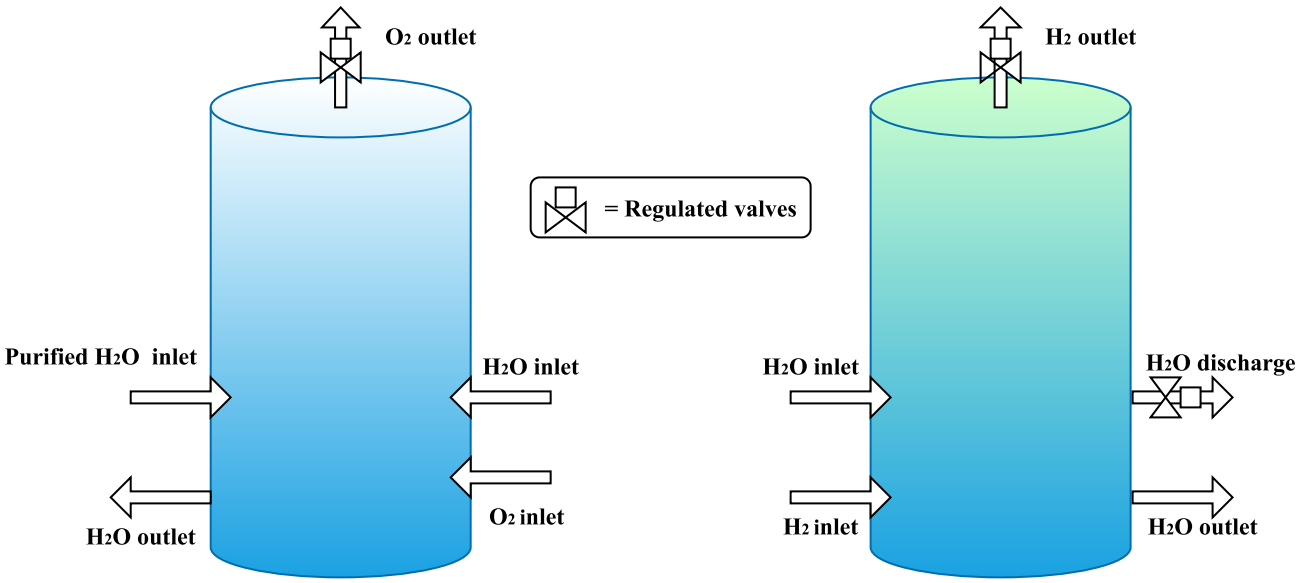

Figure 4: Schematic representation of the anode and cathode side liquid-gas separator vessels respectively

Figure 4 illustrates a simple schematic of the liquid-gas separators in the system. The outlet streams are assumed to be pure H_2O. The pressure of the vessels is regulated by the valves on the gas outlets.

Table 5: Parameters for the liquid-gas separator vessel

Parameter	**Unit**	**Comment**
V	m^3	Volume of vessel
V_{max}	m^3	Maximum liquid volume
V_{min}	m^3	Minimum liquid volume
k	W/K	Constant for convective heat transfer

Table 6: Variables for the liquid-gas separator vessel

Variable	**Unit**	**Comment**
P	Pa	Pressure inside the vessel and at all ports
m	kg	Total mass
m_{gas}, m_{liquid}	kg	Mass of gas and liquid inside the vessel
V_{gas},V_{liquid}	m^3	Volume of gas and liquid inside the vessel
h_{gas}, h_{liquid}	J/kg	Specific enthalpy of the gas and liquid inside the vessel
U_{gas}, U_{liquid}	J	Internal energy of the gas and liquid inside the vessel
ρ_{gas}, ρ_{liquid}	kg/m^3	Density of liquid and gas inside the vessel
q	W	Heat transfer rate

Tables 5 and 6 presents the different parameters and variables used in the calculations for modeling the behavior of the liquid-gas separator in Modelica. As the liquid-gas separator contains two working mediums, each with the same set of equations, certain equations of the liquid-gas separator vessel are noted with Xi.

$$\rho_{Xi} = \frac{m_{Xi}}{V_{Xi}} \tag{12}$$

For both the liquid and the gas in the vessel, equation 12 correlates the respective mass, volume and density for both fractions [23].

$$V = V_{liquid} + V_{gas} \tag{13}$$

Equation 13 dictates that the volume of the gas and the liquid is the same as the total volume of the vessel.

$$m = m_{gas} + m_{liquid} \tag{14}$$

The total mass of the vessel is given by equation 14. This equation states the total amount of mass inside the vessel.

$$\frac{dm_{Xi}}{dt} = \dot{m}_{Xi,in} - \dot{m}_{Xi,out} \tag{15}$$

The mass balance in the vessel is given by equation 15. This dictates the total mass of each faction within the vessel, and also the change of each faction [25]. For this to to work during simulations an initial value of both the mass of gas and mass of liquid must be given.

$$\frac{dU_{Xi}}{dt} = \dot{m}_{Xi,in} \cdot h_{Xi,in} - \dot{m}_{Xi,out} \cdot h_{Xi,out} \pm q \tag{16}$$

For the energy balance within the vessel, the internal energy is used. One could use enthalpy, but the correlations between volume and pressure are already given. The change in internal energy is given by equation 16 [26]. This equation gives the change in internal energy for both liquid and gas. Since the compression of the gas increases the gas' temperature, heat transfer between the different mediums inside the vessel will occur [23].

$$q = k \cdot (T_{gas} - T_{liquid}) \tag{17}$$

The value of the heat transfer rate is given by equation 17. This states that there will be a heat flux from the hotter medium to the colder. The value k is an approximated value, which can later be substituted by a more precise variable such as the convection heat transfer coefficient. The value k is used for now in order to keep things simple.

3.3.5 Heat exchanger

In the electrolysis system, the electrolyzer stack generates heat during the separation of water [24]. Due to this, the need for components that can exchange the heat generated by the stack and transport it outside of the system arises. This feat is possible by using heat exchangers.

A heat exchanger works by exchanging heat between two flowing mediums. Different types of heat exchangers could for example be liquid/gas, gas/gas, or liquid/liquid heat exchangers . Additionally, the heat exchangers can also work with the flows of the gasses or liquids moving either as a counter-current or co-current flow [27]. It is important to decide early on whether the heat exchanger model will work as a co-current or counter-current flow, as this will directly affect which equations are used and in turn the code, the placement of ports, and more in Modelica. In this thesis, it was assumed that the heat exchangers work by the *counter-current flow* principle. One of the main advantages of having a counter-current flow heat exchanger is that the heat exchanger can extract a higher proportion of heat from the hot fluid than compared to a generic co-current flow heat exchanger [27]. Since this decision has been made, some calculations can be done to model and eventually simulate the heat exchanger in Modelica.

Determining which flow that requires to be cooled and which flow should transport the excess heat in the heat exchanger model is vital. For the electrolysis system in this thesis, the fluid that circulates within the electrolyzer stack needs to be cooled. Therefore, the heat should be moving from within the electrolysis system and out of it. To do this, the heat exchanger needs a total of at least *four* ports. Two ports, namely port a and b will act as the inlet and outlet of the hot fluid flow within the electrolysis system. The two remaining ports, ports c and d, will correspond to the inlet and outlet of the cold fluid flow. Since the flows are counter-current within the heat exchanger, ports a and d are placed on one side and ports b and c are placed on the other side. The exact placement of the ports can be viewed in figure 5.

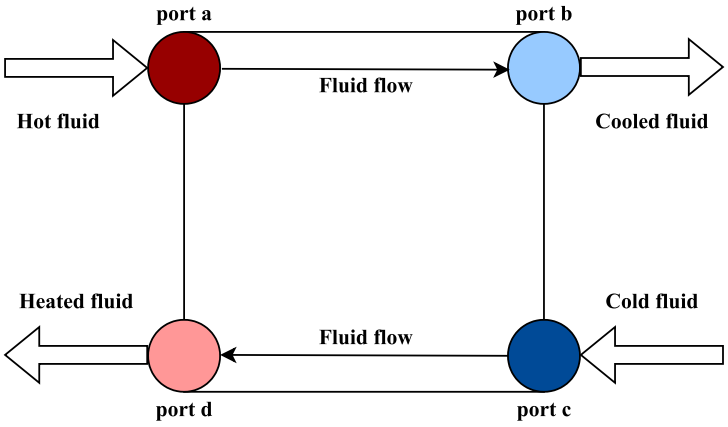

Figure 5: Schematic illustrating the fluid flows and ports of the heat exchanger

In order to accurately model the heat exchanger, there are some parameters, variables and equations that need to be implemented. The heat exchanger will from now on be referred to as the HEX.

Table 7: Parameters of the HEX

Parameter	**Unit**	**Comment**
h_a,h_c	J/kg	Specific enthalpy at inlet ports
U	W/(m^2· K)	Overall heat transfer coefficient
$\Delta\ T_{max}$	K	Temperature difference between port a and c
P_a,P_c	Pa	Pressure at port a and c
L,D	m	Length and diameter of HEX pipe
Cp_{min},Cp_{max}	$J/(kg \cdot K)$	The specific heat capacity of the cold and hot fluid

Table 8: Variables of the HEX

Variable	**Unit**	**Comment**
q, q_{max}	W	Heat transfer, Theoretical maximum heat transfer
ϵ	-	Efficiency
NTU	-	Number of Transfer Units
C_{max},C_{min}	W/K	Max and min heat capacity rates
C_r	-	Heat capacity ratio
h_b,h_d	J/kg	Specific enthalpy at outlet ports
$\dot{m}_a$,$\dot{m}_c$	kg/s	Mass flow rate of hot and cold inlet fluid

With the parameters and variables of the HEX model defined in both table 7 and table 8, it is necessary to also define the equations. The equations used in the HEX model take the known parameters and variables into consideration and finds the value of the unknown variables. The main goal for all these equations is to accurately calculate the heat transfer between the fluids, as well as the temperatures at the outlets so that the HEX model can obtain information externally, process it, and deliver the processed information to other models of the subsystem. Since the outlet temperatures are unknown variables but the inlet temperatures are known, the NTU method is used. The NTU method is often used when there is insufficient information about the HEX like there is in this specific HEX model [27]. In cases where all temperatures are known the method of Log Mean Temperature Difference could be used to determine the driving force for heat transfer [28].

First, the heat capacity rates for both the cold and hot fluid needs to be calculated. This is calculated from the in-flowing state at the port. For simplicity's sake, the specific heat rates are constants in the fluid, even though this in reality changes as the fluid is either cooled or heated. The specific heat capacity in the cold fluid is lower than the hot fluid, therefore the cold fluid is related to the C_{min} and Cp_{min} variables as stated in table 8. The same relation is true for the hot fluid being related to the C_{max} and Cp_{max} variables.

$$C_{min} = Cp_{min} \cdot \dot{m}_c \tag{18}$$

$$C_{max} = Cp_{max} \cdot \dot{m}_a \tag{19}$$

Equation 18 and equation 19 both calculate the heat capacity rates of the fluids based on their respective specific heat capacities and mass flow rates at the inlets of the HEX model. These variables can then be used to calculate the ratio between the heat capacity rates in the HEX model [27].

$$C_r = \frac{C_{min}}{C_{max}} \tag{20}$$

The ratio found in equation 20 is important for calculating the effectiveness of the HEX model later on, which is a vital part of the NTU method to determine the unknown temperatures at the outlets [27].

The overall heat transfer coefficient, U, is assumed to be constant, although this is not the case in reality. It is dependent on the heat transfer coefficients of the mediums, which again is derived from the nusselts number. Calculating this proved to be difficult without certain simplifications such as a uniform heat flux, therefore it was assumed to be a parameter.

$$NTU = \frac{U \cdot A}{C_{min}} \tag{21}$$

With the overall heat transfer coefficient determined, as well as C_{min} and the area of heat transfer, the number of transfer units can be found in equation 21.

$$\epsilon = \frac{(1 - e^{-NTU \cdot (1 - C_r)})}{(1 - C_r \cdot e^{-NTU \cdot (1 - C_r)})} \tag{22}$$

Equation 22 shows how the effectiveness is calculated in a counter-current flow HEX, based on the heat capacity rate and number of transfer units which were previously calculated in equations 20 and 21 respectively [27].

With the effectiveness for the HEX model found, the heat flux can be calculated in order to subsequently find the temperatures at the outlets.

$$q = \epsilon \cdot C_{min} \cdot \Delta T_{max} \tag{23}$$

The actual heat flux is determined in equation 23 by using the effectiveness of the HEX model which was found in equation 22. The mass flow rates are then modeled by considering the conservation of mass, so the mass flow rate at port a is the same as the mass flow rate at port b. This is also the case for the cold fluid between ports c and d [27].

$$h_a - \frac{q}{\dot{m}_a} = h_b \tag{24}$$

$$h_c + \frac{q}{\dot{m}_c} = h_d \tag{25}$$

With the assumption of no pressure drop in the HEX, the energy balance can be used for both the cooling and heating side to compute the outflowing enthalpies. This is calculated by using equations 24 and 25.

3.3.6 Cooler

Cooling is required to extract surplus heat generated in the electrolysis process. Water is used as a coolant source and is attached to the cold side of the heat exchanger model. A centrifugal pump is required in the circuit to ensure a sufficient mass flow rate of the medium. The power output of the pump is controlled by a regulated signal measuring the desired temperature in the stack, and a mass flow rate is calculated to maintain said temperature. The desired temperature for the stack's operation is 60 °C, or 333 K. The cooling system extends the heat exchanger and is connected to its cold side. A simple schematic of the system is presented in figure 6.

The temperature setpoint is a Modelica connector called *RealInput*, defining the desired temperature of 333 K. A regulator is then used to control the temperature by varying the mass flow rate of cold coolant through the pump

and into the heat exchanger. The cooling side is directly contiguous with the HEX model, and variables from that model combined with new parameters are used to determine the behavior of the cooling side, shown in table 9 and table 10.

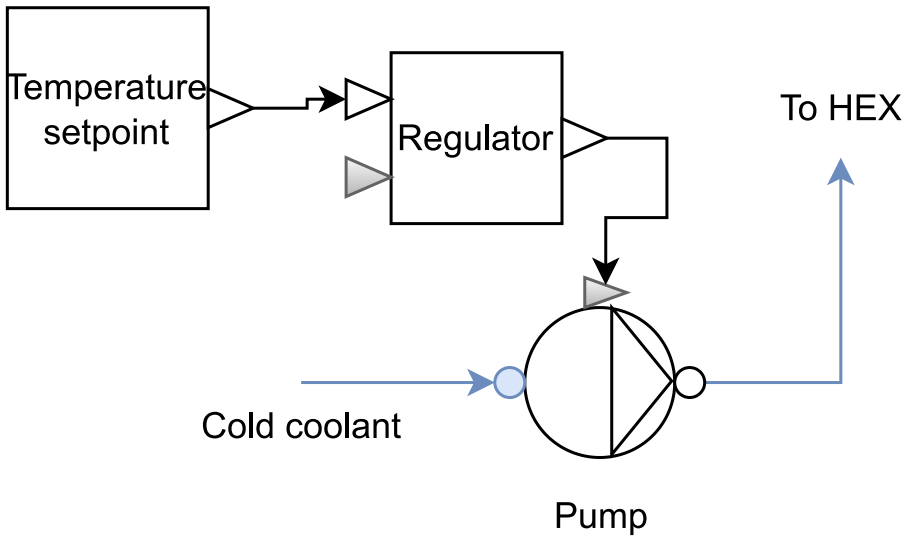

Figure 6: Illustration showing the cooling component

Table 9: Parameters of the cooler

Parameters	**Unit**	**Comment**
$T_{ambient}$	K	Ambient temperature
ref	-	Reference temperature
K_p	-	Proportional gain

Table 10: Variables of the cooler

Variables	**Unit**	**Comment**
u	-	Input signal
y	-	Output signal
$\dot{m}_c$	kg/s	Mass flow rate of coolant medium

Equation 26 is used to calculate the output signal from the regulator to the pump. With u being the monitored sensor temperature from the HEX, and Ref being the temperature setpoint. The required coolant mass flow to maintain the desired temperature of the fluid is then determined in the pump by the output signal y.

$$\frac{dy}{dt} = Kp \cdot (u - ref) \tag{26}$$

3.3.7 Power supply

The model for the power supply in the digital twin acts as the source for the voltage and current supplied to the electrolyzer stack. The power supply model is the first model in a series of electrical models, where the information generated by the power supply model will be transferred to the other models. Therefore, accuracy, as well as flexibility in how the model for the power supply can be customized, are important design considerations.

Table 11: Parameters of the power supply

Parameter	**Unit**	**Comment**
V_p	V	Rms voltage in the power supply
Phase	rad	Phase shift of the voltage
f	Hz	Frequency of the three-phase voltage
point	-	Determines where on the y-axis the sine waves are mirrored
startTime	s	Offset of the time variable that is used when simulating in Modelica

Table 12: Variables of the power supply

Variable	**Unit**	**Comment**
Va	V	Amplitude of the three-phase AC voltage
$Phase_2$	rad	Phase shift of second AC voltage
$Phase_3$	rad	Phase shift of third AC voltage
u_{t1}	V	Value of the first AC voltage wave at a specific time
u_{t2}	V	Value of the second AC voltage wave at a specific time
u_{t3}	V	Value of the third AC voltage wave at a specific time

Table 11 and table 12 shows all the different values that are either input or calculated in the power supply model. It is important to note that the parameter Vp is assumed to be a line-to-neutral voltage, as this will impact the choice and use of relevant equations in the rest of the electrical models. These parameters and variables were deemed necessary to implement in the model in order to create three symmetric sine waves, imitating the three-phase sinusoidal nature of AC voltage and current [29]. This measure is important to implement when modeling an alternating power source since the sinusoidal AC voltage will have a direct impact on how for example the rectified DC voltage will behave. The modeling of three-phase AC voltage was achieved by using several simple equations as well as algorithms.

$$Va = Vp \cdot \sqrt{2} \tag{27}$$

Equation 27 is used to calculate the amplitude of the AC voltage waves in the power supply model based on the input parameter Vp. This step is necessary in order to model the alternating voltage waves correctly, where the amplitude is assumed to be the same in all three sine waves. The peak AC voltage also provides useful information directly, as it shows the maximum possible voltage value each sine wave can possibly have [29].

$$Phase_2 = Phase + \frac{2 \cdot \pi}{3} \tag{28}$$

$$Phase_3 = Phase - \frac{2 \cdot \pi}{3} \tag{29}$$

The phase shifts have to be determined in order to properly model and simulate a three-phase AC voltage from the power supply. The equations for the phase shifts, with respect to the phase of the first voltage wave, are given in equation 28 for the second wave and 29 for the third wave. Their specific values were given in order to create symmetric waves for the three-phase voltage with equal distance between each wave. The values used in equations 28 and 29 are given in radians, and can be directly translated into 60°.

Algorithm 2 Creation of the three-phase AC voltage $u_{t1/2/3}$ as sine waves

if $time < startTime$ **then**
  0
else
  $point + Va \cdot cos(2 \cdot \pi \cdot f \cdot (time - startTime) + Phase/2/3)$
end if

Algorithm 2 creates the sine waves used to imitate the three-phase AC voltage, based on the parameters and variables from tables 11 and 12. It is important to note that in algorithm 2, the variable *time* is not defined as a variable in table 12. This is because time in this regard is a pre-existing variable within Modelica that is taken into consideration every time a simulation is run. Algorithm 2 was heavily inspired by the pre-existing model for a sine voltage located in the Modelica standard library, as well as literature describing the sinusoidal nature of AC voltage [29]. Algorithm 2 is used to calculate all three sine waves.

3.3.8 AC/AC transformer

In order to supply the electrolyzer stack with electricity that is within an acceptable voltage range, a transformer is necessary in order to lower the AC voltage from the power supply [30]. In order to lower the AC voltage, some calculations can be done including the number of windings in the inductors on both the primary and secondary side of the transformer. A simple illustration of a transformer can be seen in figure 7.

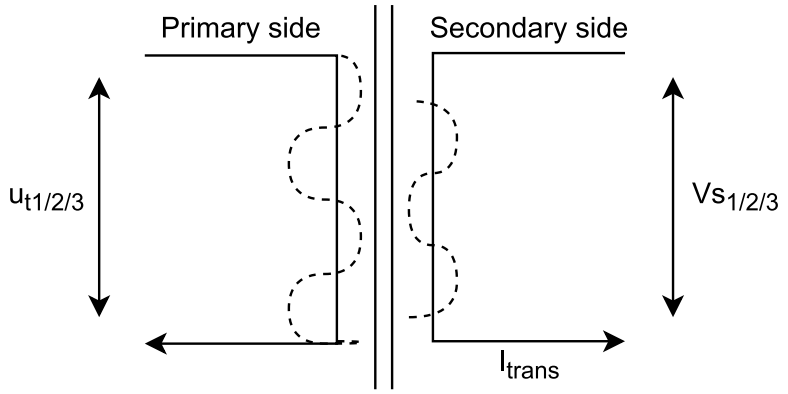

Figure 7: Illustration showing the primary and secondary side of a transformer

As seen in figure 7, the number of windings on the primary side are greater than on the secondary side. This is done intentionally in order to lower the AC voltage on the secondary side. This phenomena is based on Faraday's law of induction [31]. The three-phase AC voltage from the power supply, as well as the lowered three-phase AC voltage and rms current on the secondary side of the transformer are also visible in figure 7.

Table 13: Parameters of the transformer

Parameter	**Unit**	**Comment**
Np	-	Number of windings on the primary side of the transformer
Ns	-	Number of windings on the secondary side of the transformer
Pi	W	Iron losses (eddy current losses + hysteresis losses)
Pc	W	Full load copper/ohmic losses
PF	-	Power factor of the transformer

The parameters and variables presented in tables 13 and 14, are the values which are applied and taken into consideration in the transformer model. The parameter PF, or power factor, is a parameter used in the model to implement the percentage of actual power output of the transformer compared to the apparent power output.

Table 14: Variables of the transformer

Variable	**Unit**	**Comment**
$u_{t1/t2/t3}$	V	Three-phase AC voltage on the primary side
$Vs_{1/2/3}$	V	Lowered three-phase AC voltage on the secondary side
Vs	V	Rms AC voltage on the secondary side of the transformer
I_{rect}	A	DC current from the rectifier based on the load resistance
I_{trans}	A	Rms AC current on the secondary side of the transformer
P_{AC}	W	Power output of the transformer
η_{trans}	-	Efficiency of the transformer

The power factor is included since some of the apparent power becomes reactive power and can therefore not be utilised as actual power [32]. An interesting variable to look further into is I_{rect}, which is the DC current from the rectifier. This current is calculated by taking into consideration the current from the rectifier which is based on the connected load resistance. This will be discussed further in section 3.3.11.

$$I_{trans} = \frac{\frac{P_{AC}}{3}}{Vs} \tag{30}$$

In equation 30 the current on the secondary side of the transformer, as well as the AC power output, is calculated. This is done by dividing the power output by a value of three, due to the AC power being three-phase line-to-neutral [33]. This expression is then further divided on the Vs variable to find the current on the secondary side of the transformer. How the rectifier current I_{rect} is found will be explained later in section 3.3.11. The variable P_{AC} was found by using equation 33 in section 3.3.9.

$$Vs_{1/2/3} = \frac{Ns}{Np} \cdot u_{t1/t2/t3} \tag{31}$$

In equation 31, the lowered AC voltage on the secondary side is calculated using the AC voltage from the power supply and the number of windings on both the secondary and the primary side of the transformer. Note that in equation 31 and table 14 the variables for the three-phase AC voltage are three different variables that together simulate the three-phase AC voltage in Modelica.

Within a transformer, some losses are bound to occur which will affect its efficiency. Among these losses are the copper/ohmic losses, which occur mostly due to the resistance in the transformer windings, and the iron losses. The iron losses in the transformer can further be divided into both hysteresis losses and eddy current losses. The hysteresis losses occur when the alternating current from the grid side is applied to the transformer core which in turn will cause the magnetic field to be reversed. The eddy current losses can briefly be explained as energy being expended for no useful purpose in the transformer since some of the current flowing through a core path with a specific resistance will convert some of its energy into heat [34][35].

In the created model for the transformer in Modelica, these losses are only taken into consideration after they have been found. This means that the losses themselves are input as parameters into the model with a specific value of power as seen in table 13, presented as Pi and Pc. These values are then used to calculate the efficiency of the transformer.

$$\eta_{trans} = \frac{3 \cdot Vs \cdot I_{trans} \cdot PF}{(3 \cdot Vs \cdot I_{trans} \cdot PF) + Pi + Pc} = \frac{P_{AC}}{P_{AC} + Pi + Pc} \tag{32}$$

In equation 32 the efficiency of the transformer is calculated by looking at the power output divided by the power output plus losses. The factor of three is included in this equation as well since the source for the power is three-phase, and the voltage used in equation 32 is derived from the line-to-neutral voltage Vp of the power supply [33]. The transformer efficiency is calculated based on the assumption that it is operating at full load, meaning that the transformer efficiency is expected to be relatively high regardless of the losses [32].

3.3.9 AC/DC rectifier

The main task of the rectifier is to turn the AC voltage into DC voltage [36]. A model for this is necessary due to the fact that the electrolyzer stack uses DC voltage. To do this, a simple model was created which is based on calculating the DC components of the individual AC voltage waves, in order to find the rectified voltage which should be supplied to the electrolyzer stack after it has been controlled. A three-phase six diode bridge full wave rectifier was chosen as the template for designing this rectifier in Modelica. This type of rectifier allows both the positive and negative sine waves of the three-phase AC voltage to be rectified, which in turn allows for high rectifier efficiencies [37].

Table 15: Parameters of the rectifier

Parameter	**Unit**	**Comment**
η_{rect}	-	Efficiency of the rectifier

Table 16: Variables of the rectifier

Variable	**Unit**	**Comment**
V_s	V	Lowered rms voltage from transformer
V_{avg}	V	DC voltage of the rms AC voltage Vs
$Vs_{1/2/3}$	V	Lowered three-phase AC voltage from the transformer
$V_{DC1/DC2/DC3}$	V	DC voltages of $Vs_{1/2/3}$
V_{rect}	V	Rectified voltage from the three-phase AC voltage
R_{load}	Ω	Load resistance from the electrolyzer stack
I_{rect}	A	Current in the rectifier based on the rectified voltage and load resistance

There is only one parameter in the rectifier model, presented in table 15. The different variables used in the rectifier model are presented in table 16. The rectifier efficiency was implemented in the rectifier model to simply be input as a parameter. This allowed the AC power input into the rectifier, as well as the transformer current to be calculated as seen in equations 33 and 30 respectively.

$$P_{AC} = \frac{V_{avg} \cdot I_{rect}}{\eta_{rect}} = \frac{P_{DC}}{\eta_{rect}} \tag{33}$$

Since the rectifier efficiency was implemented as a parameter, the AC power input of the rectifier from the transformer could be calculated in equation 33. Although this decision undoubtedly removes some depth from the rectifier model, it was necessary due to the already simple nature of the electrical models. Still, discussion around plausible rectifier efficiencies will be done later on in section 5.5.8.

$$V_{avg} = V_{DC} = \frac{3 \cdot \sqrt{6} \cdot Vs}{\pi} \approx 2.34 \cdot Vs \tag{34}$$

In equation 34 the average voltage is calculated. The average voltage from the lowered rms value of the AC voltage can be described as the DC component of the AC voltage [38]. Important to note is that this variable is not a valid representation of the actual DC voltage.

The actual DC voltage from the rectifier will still have some fluctuations in the form of ripple that occur due to the sinusoidal form of the three-phase AC voltage. Therefore, the ripple in the DC voltage wave will occur because it has been derived from an AC power supply [39]. Ripple is an unwanted characteristic of the rectified voltage wave, since it is responsible for power losses [40].

$$V_{DC/Top} = \sqrt{3} \cdot Vs \tag{35}$$

$$V_{DC/Bottom} = \sqrt{3} \cdot Vs \cdot sin(60°) \tag{36}$$

Equations 35 and 36 signify the maximum and minimum value of the rectified voltage from the three-phase AC voltage [41]. These equations will be important in the following algorithms 3 and 4 as they determine the boundaries for the rectified voltage wave.

Algorithm 3 Calculate the first of three parts of the rectified voltage

if $(|Vs_2| + |Vs_3|) > V_{DC/Bottom}$ **then**
  $(|Vs_2| + |Vs_3|)$
else
  0
end if

Algorithm 3 is used in order to calculate the DC voltage of the first AC voltage wave coming from the transformer. This is done simply by taking the absolute value and sum of the two other AC voltage waves. If this calculated value is *above* the value calculated in equation 36, $V_{DC/Bottom}$, then it is taken into consideration and used. However, if the calculated value in algorithm 3 is below $V_{DC/Bottom}$, then it is not taken into consideration at all. Algorithm 3 is also applied when calculating the other DC voltage waves, V_{DC2} and V_{DC3}, by using the other AC voltage waves in a similar fashion. The absolute value taken from the AC waves in algorithm 3 can be done since the rectifier is based on a full wave rectifier, where the negative values of the sine waves are also taken into consideration as previously explained.

Algorithm 4 Calculate the actual rectified voltage V_{rect}

if $(V_{DC1} + V_{DC2} + V_{DC3}) < V_{DC/Top}$ **then**
  $(V_{DC1} + V_{DC2} + V_{DC3})$
else
  $V_{DC/Bottom}$
end if

As explained previously in algorithm 3, the separate parts of the rectified voltage were calculated for each of the three different AC voltage waves. In order to merge these waves together into a single, rectified voltage wave, algorithm 4 was applied. Algorithm 4 sums all the DC voltages from algorithm 3 together while still making sure that the merged wave for the rectified voltage does not move out of its boundaries. As previously mentioned, the value for V_{rect} will unlike V_{avg}, which is derived from equation 34, include some ripple from the AC voltage waves. The effect of this can be viewed in figure 31 and figure 32 in section 4.3.3.

3.3.10 Electrical control

In order to determine and control the voltage and current which flows from the rectifier and into the electrolyzer stack, an intermediate model, called electrical control, is beneficial. A model for the electrical control allows for calculations in order to achieve a desired current, based on inputs into the model.

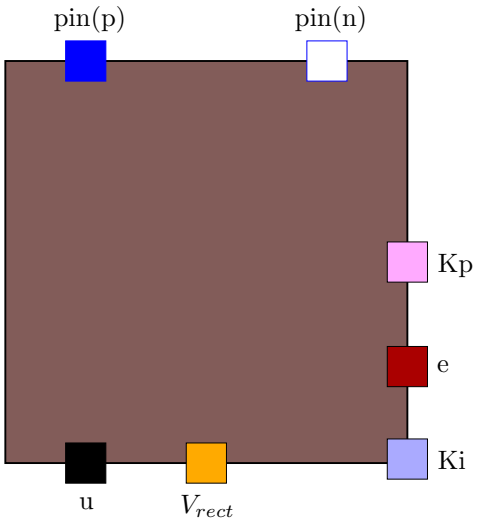

Figure 8: Schematic illustrating the electrical control model and its ports

Table 17: Parameters of the electrical control

Parameter	**Unit**	**Comment**
I_1	A	The "first" desired current of the stack
I_2	A	The "second" desired current of the stack
$setTime$	s	The time at which the desired current changes
R_{ref}	Ω	Reference resistance used to determine feed forward
K_p	-	The proportional gain component used in the PI-controller model
K_i	-	The integral gain component used in the PI-controller model

Table 18: Variables of the electrical control

Variable	**Unit**	**Comment**
$I_{desired}$	A	The desired current of the stack
V_{output}	V	DC voltage based on the u signal
I_{rect}	A	The DC current in the rectifier based on the load resistance and voltage
$Error\ signal$	A	The error signal between the desired and actual current
$feed\ forward$	V	The error signal between the desired and actual current

Tables 17 and 18 shows the different parameters and variables used in the electrical control model. Most of the parameters and variables are presented in figure 8 as well. The I_{rect} variable is directly calculated when the output voltage is applied to the load resistance based on ohm's law, and requires therefore no explanatory equation [42].

In algorithm 5, the parameters I_1, I_2 and $setTime$ are used in order to determine the variable $I_{desired}$. This algorithm is mainly implemented in order to allow for more flexibility when testing the model in Modelica. If a constant current is desired, where there is no sudden current change, the I_1 and I_2 parameters can receive the same input value and no sudden change in the current will occur. The parameter $setTime$ could also be set as zero, meaning that the only parameter for the desired current that is taken into consideration is I_2.

Algorithm 5 Implementation of time dependent ramp change of the desired current

if $time < setTime$ **then**
  $I_{desired} = I_1$
else
  $I_{desired} = I_2$
end if

$$feed\ forward = I_{desired} \cdot R_{ref} \tag{37}$$

The $feed forward$ variable, which is calculated in equation 37, is implemented in order to manipulate and minimize the deviations of the set point variable [43]. The calculated feed forward value is then directly used in equation 41 within the PI-controller model to determine the u signal.

$$Error\ signal = I_{desired} - I_{actual} = I_{desired} - I_{rect} \tag{38}$$

Equation 38 shows how the error signal is calculated based on the difference between the desired current and the actual current. The actual current is the same as the rectifier current. The error signal will then be used in a feedback loop which gradually corrects the measured error in order to reach the desired current. There are additional equations used in the electrical control model, but these equations will be explained in the section for the PI-controller model as these equations uses the calculated u signal.

3.3.11 PI-controller

In order to limit the voltage and current that is supplied to the electrolyzer stack, a controller is necessary. The model for the PI-controller works as an add-on to the electrical control model, where it determines the u signal based on the error signal received from the electrical control as well as the Ki and Kp values.

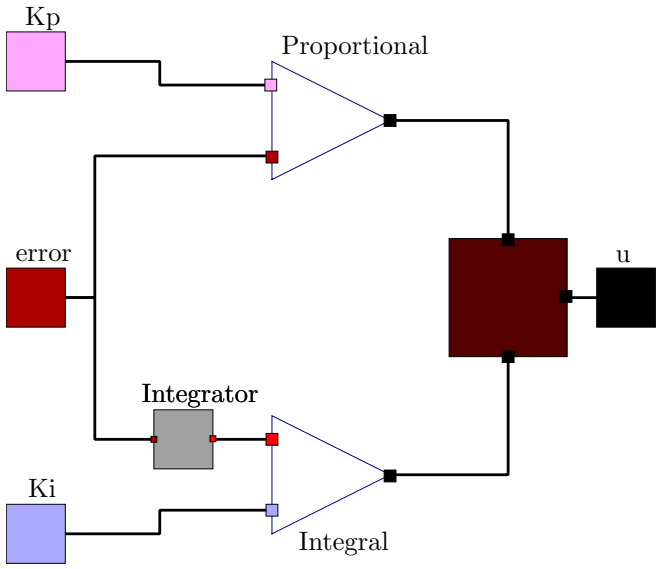

Figure 9: Schematic illustrating the blocks within the PI-controller model

The PI-controller model was created by dividing the different operations inside the controller into smaller parts or blocks as seen in figure 9. This was done to keep the model relatively simple while still providing transparency to the user.

Table 19: Variables of the PI-controller

Variable	**Unit**	**Comment**
Error signal	A	The error signal from the current difference in the load
K_p	-	The proportional gain component
K_i	-	The integral gain component
u signal	A	The feedback loop signal used as the output current of the load

In figure 9, the error signal as well as the values for Kp and Ki are transferred from the electrical control model and into the PI-controller model. These values are then transferred to either the proportional gain block or the integral gain block, with an integrator block in front of the integral gain block. The error signal is sent to both blocks. The PI-controller has no parameters and is therefore solely used to process information to and from the electrical control model with variables presented in table 19.

$$Proportional\ gain = Kp \cdot error\ signal \tag{39}$$

Inside the PI-controller model, equation 39 is used to calculate the proportional gain of the error signal where the Kp value is multiplied with the error signal inside the proportional gain block.

$$Integral\ gain = Ki \cdot \int (error\ signal) \tag{40}$$

The integral gain part of the PI-controller model has an integrator in front of it which integrates the error signal as a function of time. The integrated error signal is then multiplied with the integral gain value Ki as seen in equation 40 in the integral gain block.

$$u\ signal = Proportional\ gain + Integral\ gain \tag{41}$$

The gains from the proportional integral blocks within the PI-controller are then added together in another block in order to calculate the u signal as seen in equation 41. The u signal is then sent back to the electrical control and is in this case directly used as the regulated voltage output of the electrical control model.

$$V_{output} = pin\_p.v = u\ signal + feed\ forward \tag{42}$$

Equation 42 shows how the voltage output is simplified to be based on the u signal from the PI-controller model and sent back into the electrical control model. The use of the u signal in such a way is inaccurate. However, since the other electrical models are quite simplified in relation to their real-world counterparts, it proved difficult to implement the u signal in any other meaningful way. Normally the u signal would be implemented to determine for example the duty cycle in relation to a switching frequency in a more complicated rectifier model [44]. This depth was not added to the electrical models, hence why the u signal was used in such a simplified manner.

From the electrical control model the V_{output} variable is connected to a signal voltage model retrieved from the Modelica standard library. By doing this, the voltage can then be transferred to a resistor model through the connections of electrical pins. A current is drawn from the resistor based on the output voltage. This current is then used as the current in the rectifier I_{rect}, which can calculate the DC power output as seen in equation 33.

3.3.12 Sensors

An important component in a PEM electrolyzer system is the sensors, as the sensor can read the value of a parameter and transform it into a signal which can be used. The signal in this model is transferred to the Real Output block in the standard Modelica library under *Modelica.Blocks.Interfaces.RealOutput*. The medium of any sensor must be defined, as it is unable to determine values without fluid flow. Three types of sensors are developed for the digital model.

Table 20: Monitoring method for temperature sensor

Measurement	Calculation	Unit	Output
Temperature	T of phX	K	Real output = T

The first sensor is the absolute temperature sensor. This sensor detects the temperature at any fluid port and based on the pressure, enthalpy, and mass fractions return the absolute temperature. Absolute in this sense means a thermometric scale where a reading of zero coincides with the theoretical absolute zero of temperature, achieved by using the standard measure of temperature in Kelvin, K. Table 20 summarizes the monitoring method.

Table 21: Monitoring method for the mass flow sensor

Measurement	Calculation	Unit	Output
Mass flow rate	m_flow at port	kg/s	Real output = m_flow

The second sensor is the absolute mass flow sensor. The mass flow rate is fetched from the mass flow value at the connected port. Table 21 showcases the monitoring method for the sensor.

Table 22: Monitoring method for absolute pressure sensor

Measurement	Calculation	Unit	Output
Pressure	P at port	Pa	Real output = P

Lastly, the absolute pressure sensor is described. The absolute pressure is fetched from the pressure value at the connected port. Absolute meaning the pressure relative to the zero pressure in the ideal or absolute vacuum. Table 22 summarizes the monitoring method.

3.4 Subsystems of the electrolysis system

In the previous section, the relevant BoP components were introduced and explained in detail. By having defined the different Balance of Plant components, it is advantageous to divide these components into different subsystems. Doing so allows for a more broad understanding of how the different BoP components interact with each other within the digital twin.

3.4.1 The liquid-gas separator unit

When the electrolyzer stack is operating, oxygen and hydrogen gases will be generated and flow along with the liquid, which in this system is assumed to be pure water. These gases need to be separated from the liquid and sorted accordingly. The oxygen gas is a by-product of the production of hydrogen and can either be released out of the system or captured and used for other purposes. The hydrogen gas is desired and will therefore be separated from the liquid in the liquid-gas separator component and then directed to the gas treatment unit.

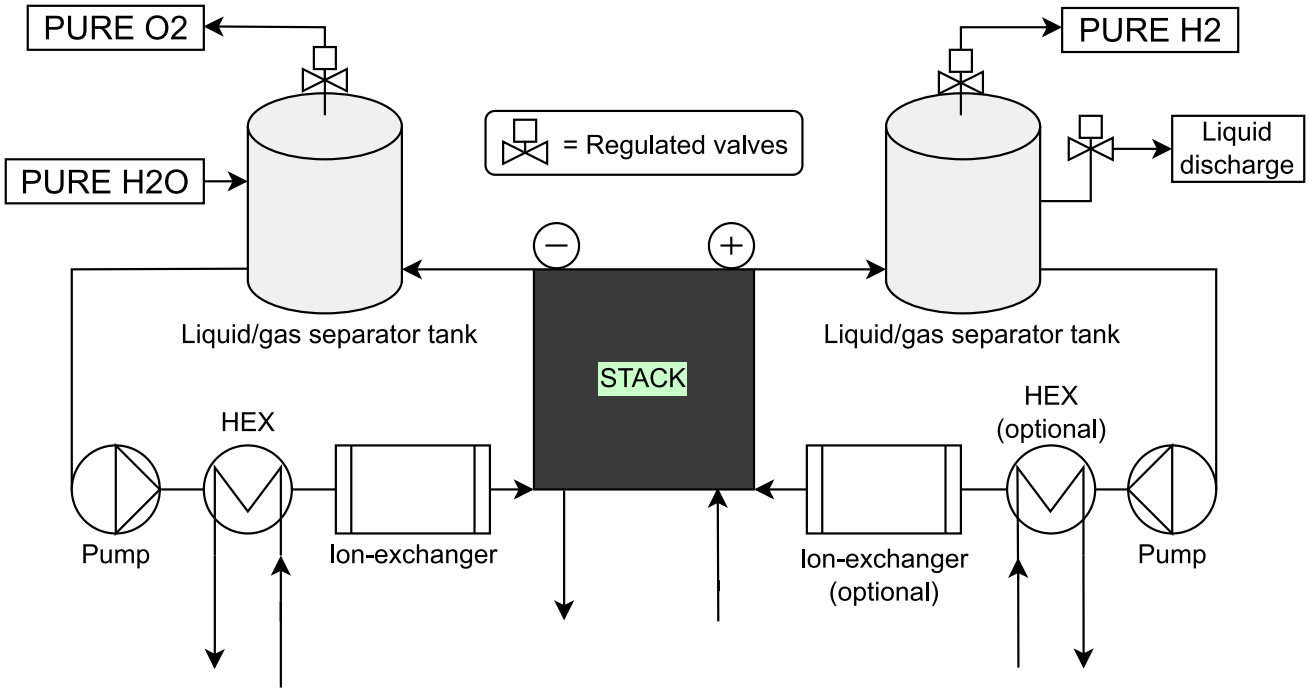

Figure 10: Schematic illustrating the different BoP models involved in the liquid-gas separator unit

In figure 10, some of the different components introduced previously in section 3 make up the subsystem. The cathode and anode side are almost identical, which helps make the subsystem more simple to both model and simulate. Water is only fed in on the anode side, as there is sufficient proton drag that carries substantial amounts of water through the membrane and to the cathode side. The main objective of this multi component unit is to keep the fluid flowing at the desired pressure, mass flow, and temperature. This is achieved by the all components in the anode and cathode flow, together with sensors and appropriate regulator settings.

3.4.2 The cooling system unit

The source of cooling in the cooling system unit used to cool the hot side is simple water. As the heat exchange system is coupled to the coolant water, it is forced through the cooling side of the heat exchanger. Thereafter the heated water is transported to an ambient sink modeled in Modelica. The centrifugal pump in the system is coupled to a sensor that relays the measured output temperature of the heat exchangers hot side, which is then compared to the desired outlet temperature, in this case the reference temperature set point. The difference between the temperature and the desired temperature affects the rate of change in the output of the pump, thus affecting the output temperature to reach a desired set point. For the sake of simplicity and ease of use, the signal directly controls the mass flow rate of the pump, with the power output being a variable. This variable is thus a calculation of power needed for desired cooling.

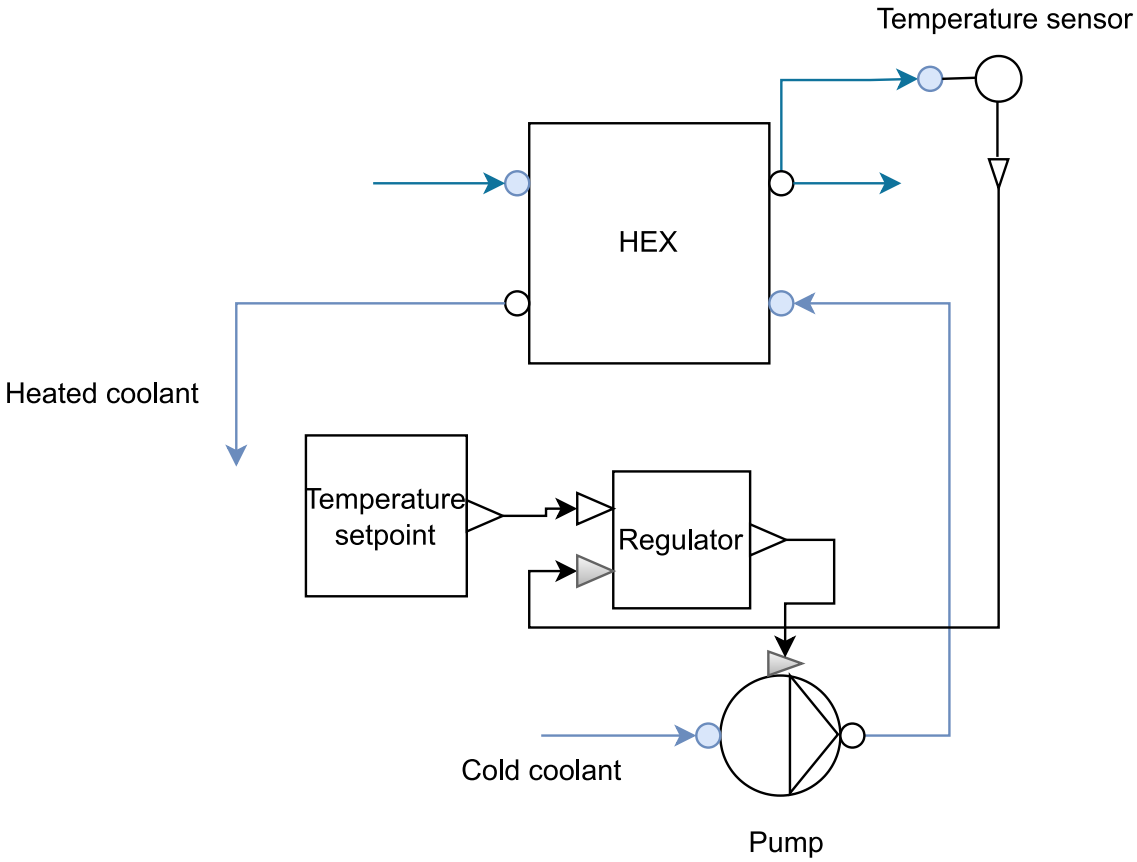

Figure 11: Schematic illustrating the cooling system unit

The cooling system unit is illustrated in figure 11, and it works by having a pump which circulates the fluid of a specific HEX in the electrolysis system. The fluid is pumped into the HEX with its main task being to cool the fluid down to a desired operational temperature of the electrolysis stack. The cooling system unit will be implemented in each of the heat exchangers on the anode and cathode side of the BoP.

3.4.3 The power supply unit

The electrolyzer stack is unable to operate unless it is supplied with electricity from the power supply unit. The electricity supplies the electrolyzer stack with electrons through its current, as seen previously in equation 1, chapter 1. This action allows the electrochemical reactions within the stack to occur, which emphasises why a stable, continuous supply of electricity is necessary in order to operate the electrolyzer stack efficiently.

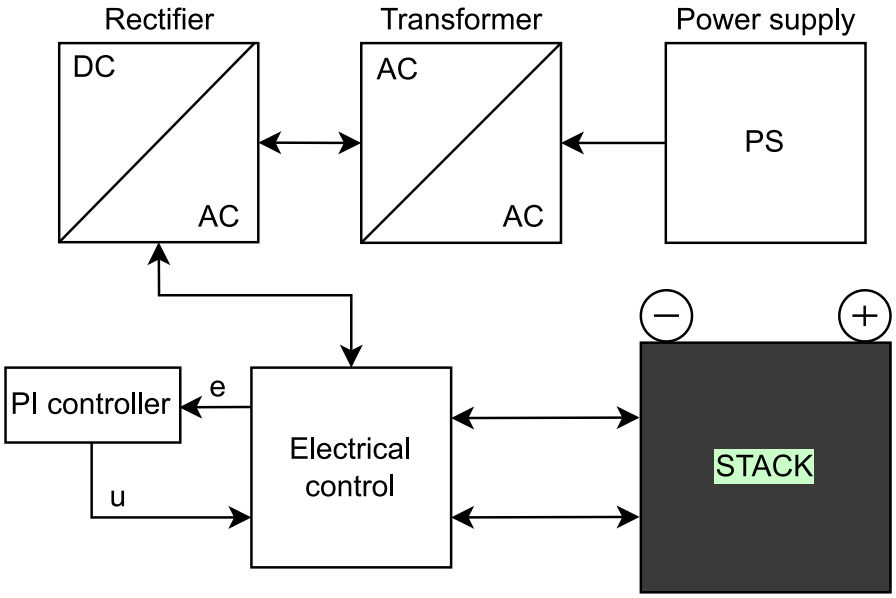

Figure 12: Schematic illustrating the different BoP models involved in the power supply unit

The models within the power supply unit, which are visible in figure 12, have all been explained on an individual level and in great detail previously in this chapter. However, a quick summary of how the models are designed to interact with each other is useful in order to understand the different design choices that has been made.

As established previously, the main task of the power supply unit is to supply the electrolyzer stack with electricity. To simulate this action in Modelica, the power supply model generates three sine waves that imitate the three-phase AC voltage. This information is then sent into the transformer model which in turn lowers these waves based on previous equations like equation 31. When the waves have been lowered, they are transported to the rectifier model where they are combined into a single wave with smaller fluctuations. This wave is meant to imitate the rectified voltage. The output voltage is based on the u signal derived from the electrical control and PI-controller. When the output voltage has been supplied, a current is drawn based on the output voltage and load resistance. This current is then supplied back into the rectifier and transformer models in order to determine their power outputs and so on. Further discussion around the advantages and disadvantages of these design choices are presented in section 5.3.2.

The different intermediate models within the power supply unit, between the power supply and the electrical control, are referred to in general as power electronics. Power electronics, like the transformer and rectifier, are equipment that is connected to the field of electrical engineering. This type of equipment is meant to be able to deal with processing high voltages and currents in order to deliver power that can be used in different appliances. Types of appliances that are supplied might be everything from household electronics to special equipment used in different industries like for example hydrogen production through electrolysis [45].

3.5 The combined system

The complete combined BoP system connected to the electrolyzer stack is illustrated in figure 13. This illustration shows all the different subsystems connected into a single system or model, which acts as the created digital twin. The assumptions previously made of pure water fed into the system, as well as pure oxygen and hydrogen exported from the system, are also visible in the illustration. The anode and cathode side are referred to as anode flow unit and cathode flow unit respectively.

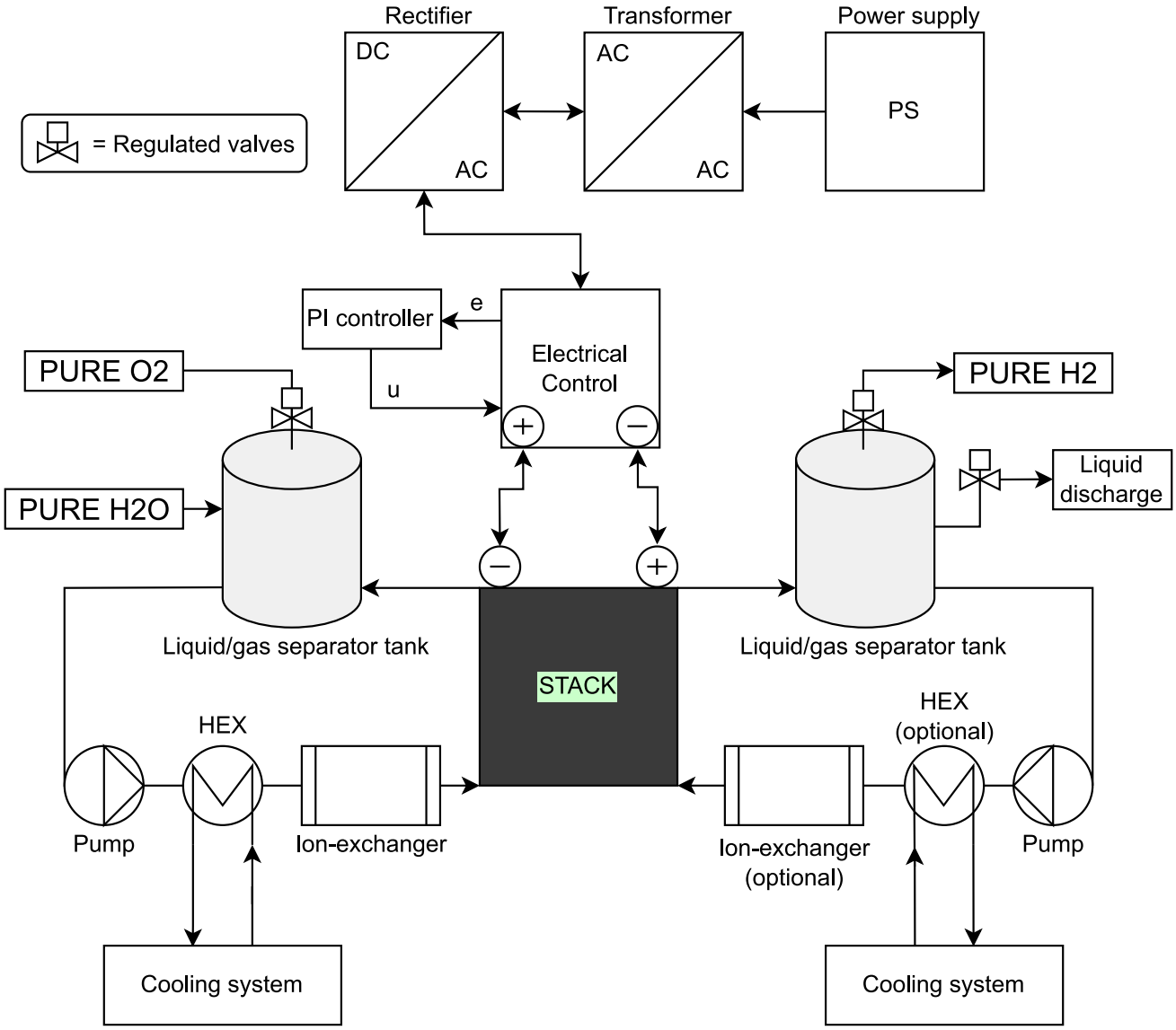

Figure 13: Schematic illustrating the combined BoPs of the digital twin within the scope of the thesis

The ion and heat exchanger on the cathode side is as illustrated in figure 13 denoted as optional. This can be neglected depending on the structural approach of the electrolysis system. The heat generated in the system can be extracted sufficiently from the anode side. However, it can also be included on both sides as a mirroring of the anode and cathode side. The same case is true for the ion-exchanger component. However, the HEX and ion-exchanger models are optional in the cathode flow unit as seen in figure 13.

All components in the anode flow unit and the cathode flow unit are connected with fluid ports previously explained in chapter 3.1. Information is interpreted from the inlets, processed from the governing equations, and continues through the outlets.

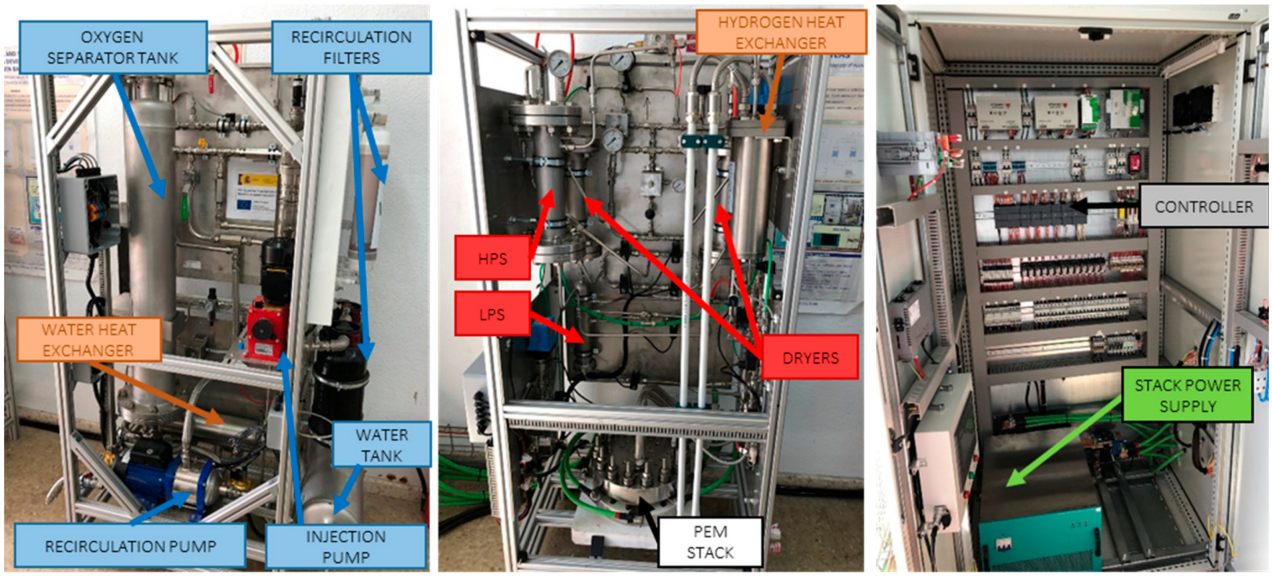

(a) (b) (c)

Figure 14: Detailed illustration of a laboratory PEM electrolysis system with included BoP equipment [46]

To showcase that the schematic presented in figure 13 reflects the reality of a PEM electrolyzer, a figure of a physical system is presented in figure 14. Figure 14a shows the liquid management system of the anode flow circuit. Figure 14b includes the PEM stack and the cathode side, where hydrogen gas is separated and stored. The separation differs from the one developed in the digital twin by having high pressure separators and low pressure separators. Additionally the dryers are excluded as the hydrogen purification unit is excluded from the digital twin. Figure 14c shows the power supply unit, as well as all controllers used in the PEM electrolysis system. This substantiates the digital twins structure with a reflection of reality.

4 Results

The results chapter presents simulations of all the developed components in the digital twin. Initially, the results are presented in separate sections to show that each model works individually before they eventually are merged into a combined system. When the models have been combined and connected to the electrolyzer stack provided by Hystar, simulations of the entire combined system can be run. Most of the simulations of the models use predetermined parameters, which are presented in tables. The relevant results are then presented graphically through figures and/or numerically in tables.

4.1 The liquid-gas separator unit

Simulations done involving the liquid-gas separator unit is presented in this section. As there are fluids present with fluid port connectors in all components, mass flow sources and ambient sinks from the Modelica library are used to simulate component behavior. To better grasp the function of certain components, there are multiple connected together, while others are simulated individually. This is explicitly stated.

4.1.1 Liquid-gas separator

For the liquid-gas separator, the vessel is being fed by pumps operating at 100 W through all three inlet ports. The pumps are coupled to atmospheric conditions at inlet side. Liquid water is pumped by two separate pumps into the electrolyzer inlet and the liquid feedwater inlet at 5 °C. Simple air is pumped through the last inlet port at 50 °C. At the outlet ports, both mediums are extracted at a rate of 0.1 kg/s. The liquid mass of the vessel starts at 500 kg, and the gas starts at 0.5 kg. The pressure is denoted in the unit of bar in simulations, and not in Pascal as previously. This is done as the unit bar is more suitable to be shown visually in the simulations done.

Table 23: Simulation parameters in the liquid-gas separator

Parameter	**Value**	**Unit**
V	1	m^3
k	1000	W/K
$\dot{m}_{gas,outlet}$	0.1	kg/s
$\dot{m}_{liquid,outlet}$	0.1	kg/s
T_{gas}	50	°C
T_{liquid}	5	°C

(a) Parameters for the simulation

Parameter	**Value**	**Unit**
m_{gas}	0.5	kg
m_{liquid}	500	kg
T_{gas}, T_{liquid}	20	°C

(b) Initial values for the simulation

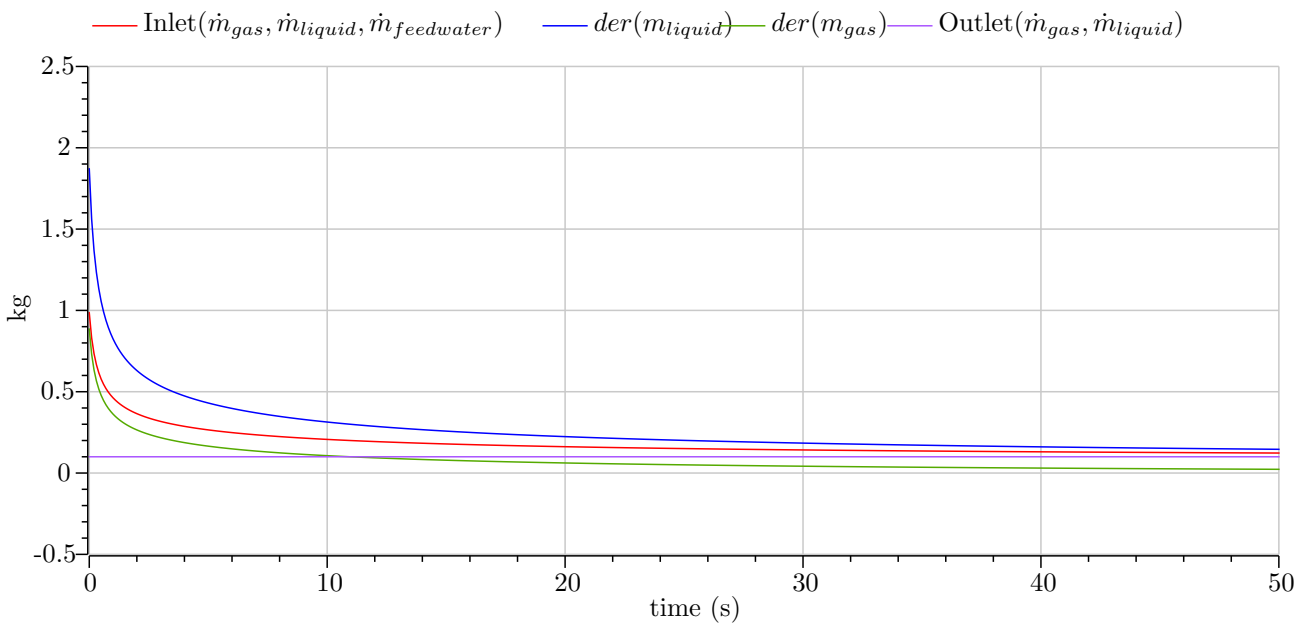

Figure 15: Simulation of the mass balance in liquid-gas separator

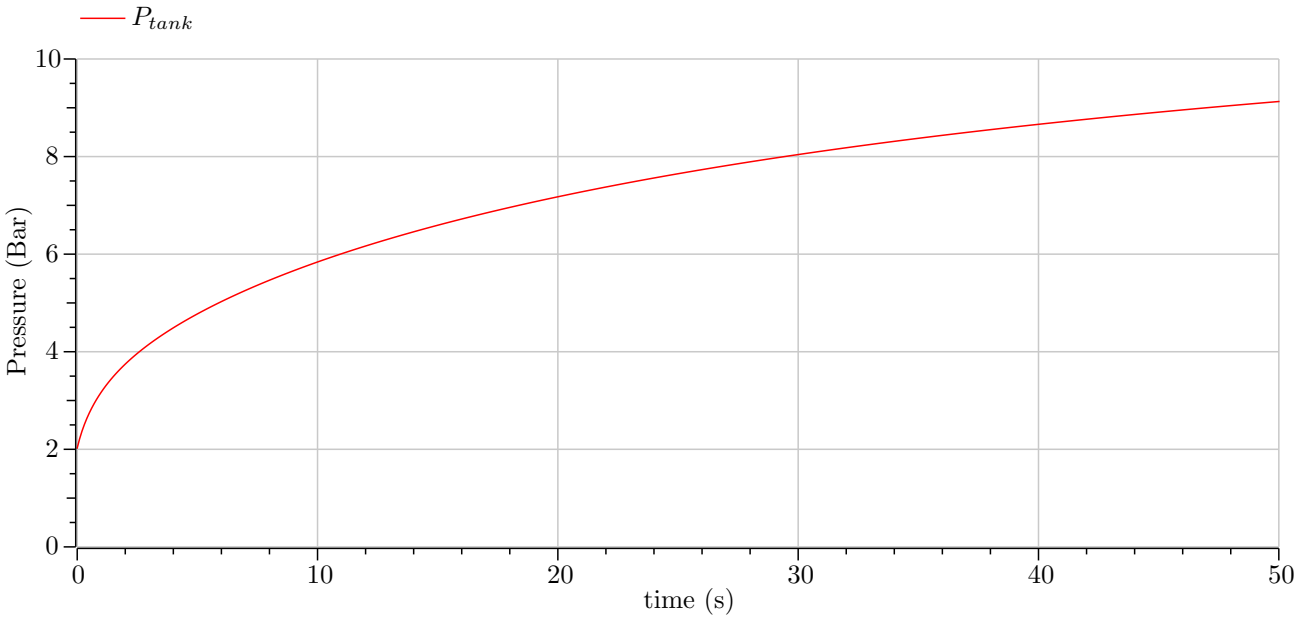

Figure 16: Simulation of the pressure inside the liquid-gas separator

Figure 15 shows the decrease in inlet mass flow rates for the liquid and the gas. This is due to the increase in pressure as shown in figure 16.

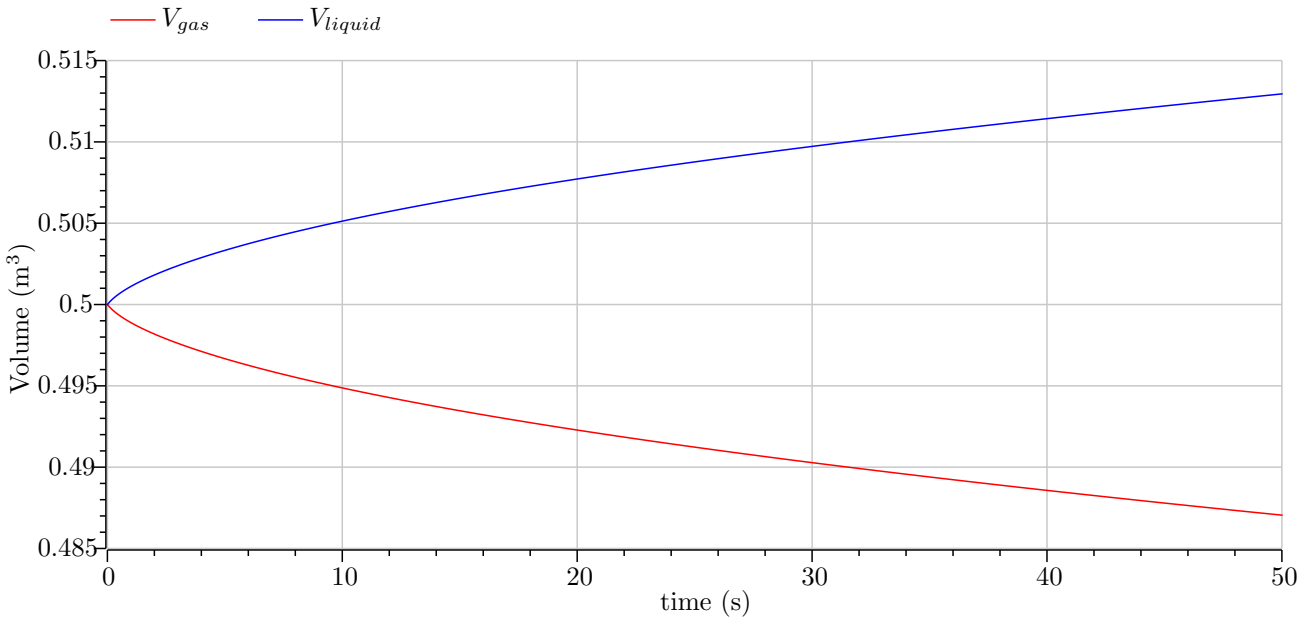

Figure 17: Simulation of volume of the gas and liquid inside the liquid-gas separator

Figure 17 shows the volume of both mediums inside the liquid-gas separator. This figure is interesting in relation to figure 16 as the liquid-gas separator model can be controlled, where pressure is controlled by the outlet of gas, and volume is controlled by the outlet of liquid.

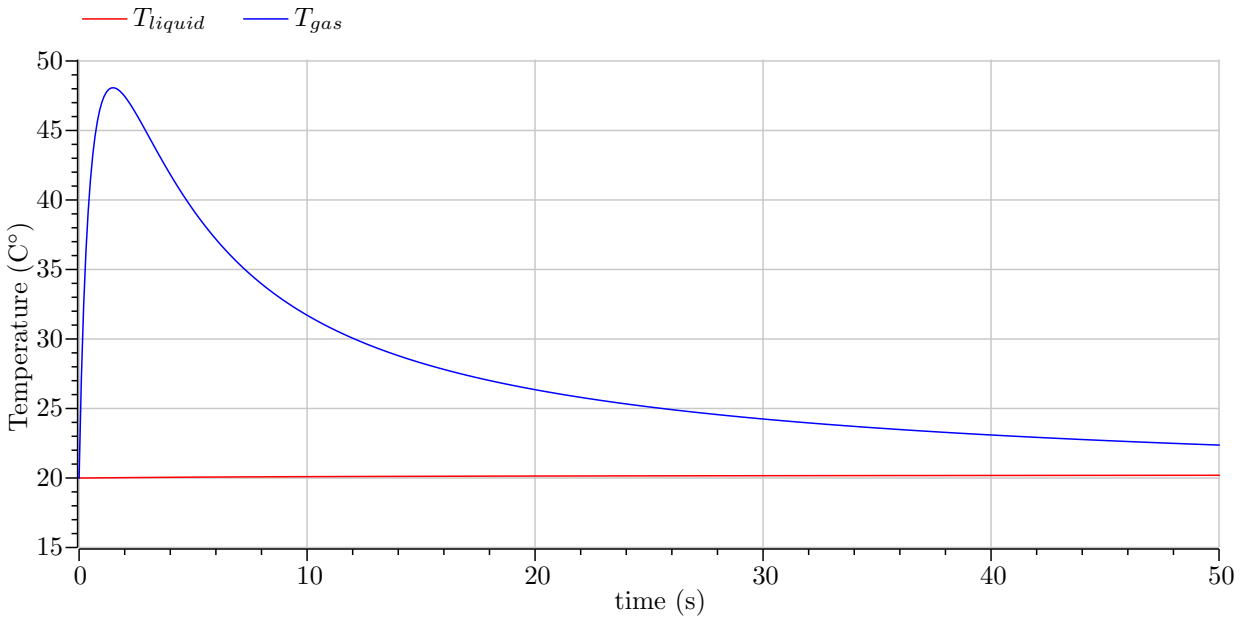

Figure 18: Simulation of the temperature in the liquid-gas separator

As seen in figure 18, there is a change of temperature in the vessel. The gas quickly increases its temperature as the inlet of gas is at 50 °C. The gas temperature then decreases due to the heat transfer from the gas to the liquid. Though it is hard to see, this heat transfer leads to an temperature increase in the liquid of 0.2 °C even though the liquid is constantly fed water at 5 °C. The small variation in the temperature of the liquid as opposed to the gas is due to there being way more liquid mass inside the vessel.

4.1.2 Valve at constant pressure

The valve works by regulating inlet pressure, and thereby also affecting the flow rate through the valve. For testing purposes a simulation of the valve exposed to two different, but constant, pressures are of interest. In this simulation the opening of the valve varies from 0 to 1.

Table 24: Simulation parameters in a valve

Parameter	Value	Unit
k_v	0.1	-
P_1	202650	Pa
P_2	101325	Pa

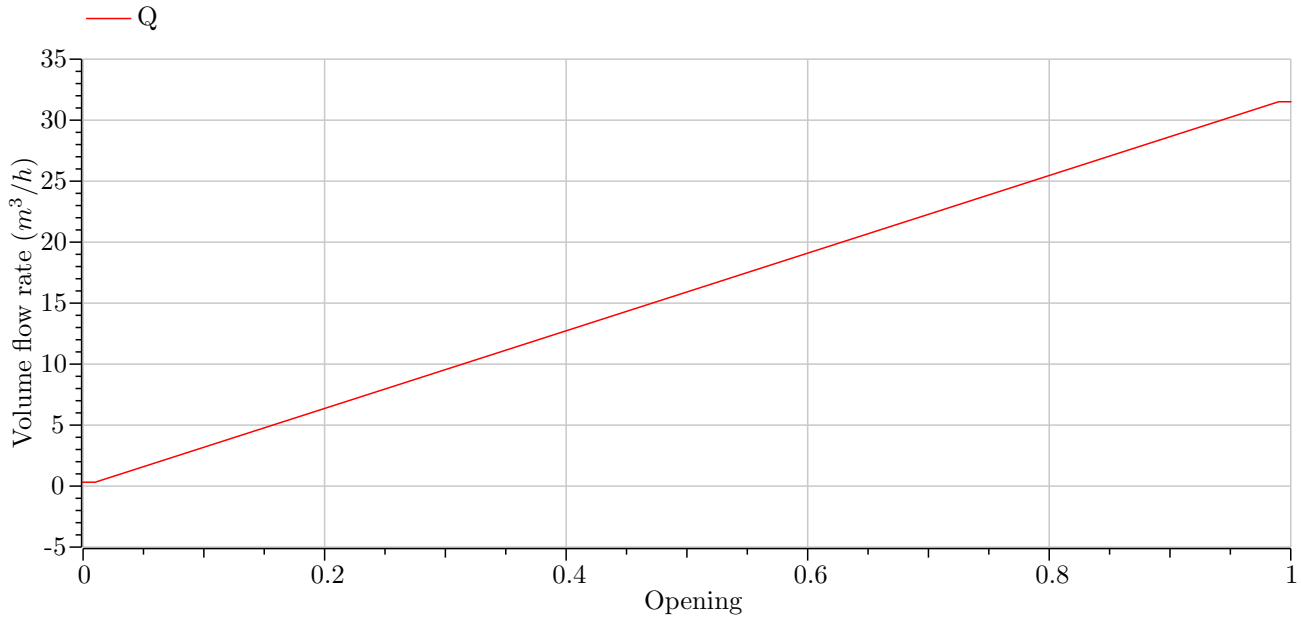

Figure 19: Simulation of the valve volume flow rate against opening at constant pressure

The valve curve is presented in figure 19 and shows that the valve design is of a linear type as established earlier.

4.1.3 Valve in series with a pump

In this simulation the valve is placed at the discharge outlet of a pump working at 100 W. In order to produce better simulation results, this pump does not have a pump curve. The opening of the valve is 0 at 1 second, before it rises linearly to a value of 1 at 4 seconds.

Table 25: Simulation parameters for a valve in series with a pump

Parameter	Value	Unit
P_{inlet}	101325	Pa
Power	100	W

(a) Pump parameters

Parameter	Value	Unit
k_v	4	-
P_{outlet}	101325	Pa

(b) Valve parameters

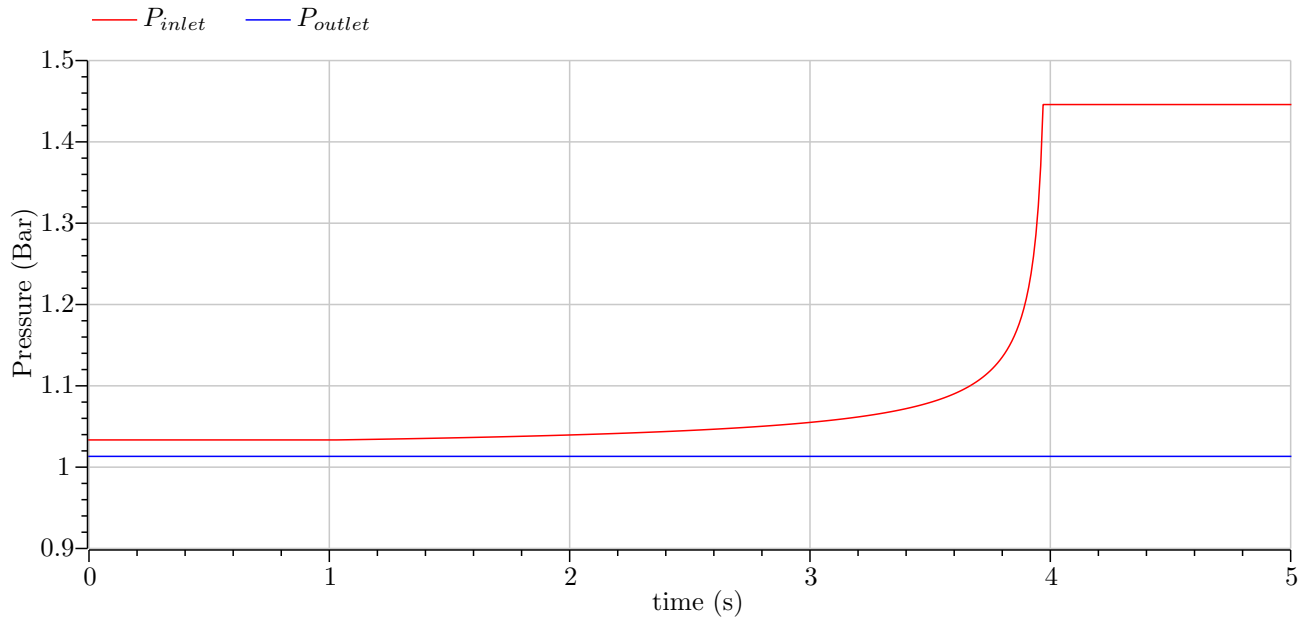

Figure 20: Simulation of the valve pressure in series with a pump

In figure 20 the inlet pressure slowly increase as the valve is opened. After 4 seconds the valve has been fully opened, making it stable at a constant pressure value. The outlet pressure is not changed at all since the valve does nothing to the outlet pressure.

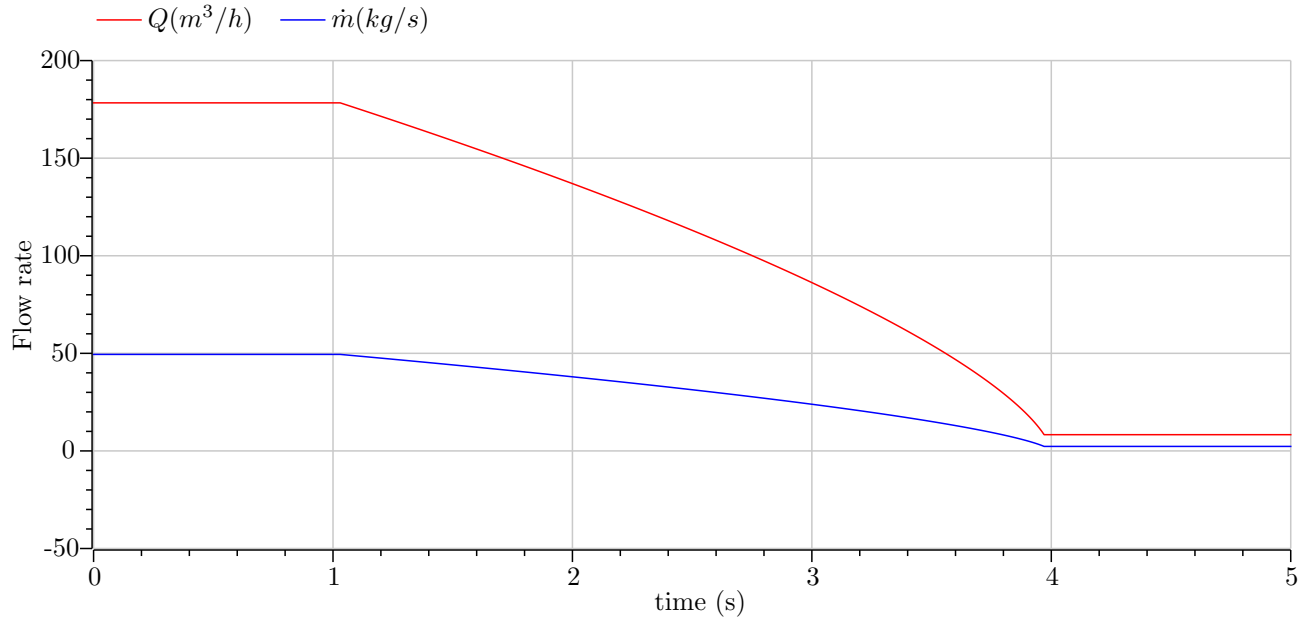

Figure 21: Simulation of the mass flow rate and volume flow rate through a valve in series with a pump

As seen from figure 21 when comparing to figure 20, the mass flow is decreasing as the pressure is increasing. This means that the valve is able to control inlet pressure by restricting the mass flow rate through the component.

4.1.4 Centrifugal pump

The simulation and test of the pump are connected with the power input of the pump. The pump is tested under varying pressure at discharge and its ability to produce mass flow rate at different head and power input. In this simulation the outlet pressure starts at ambient pressure and is increased until it reaches the point of no volume flow.

Parameter	**Value**	**Unit**
Power	100, 200, 300	W
P_1	101325	Pa
P_2	101325, and rising	Pa

Table 26: Simulation of pump parameters

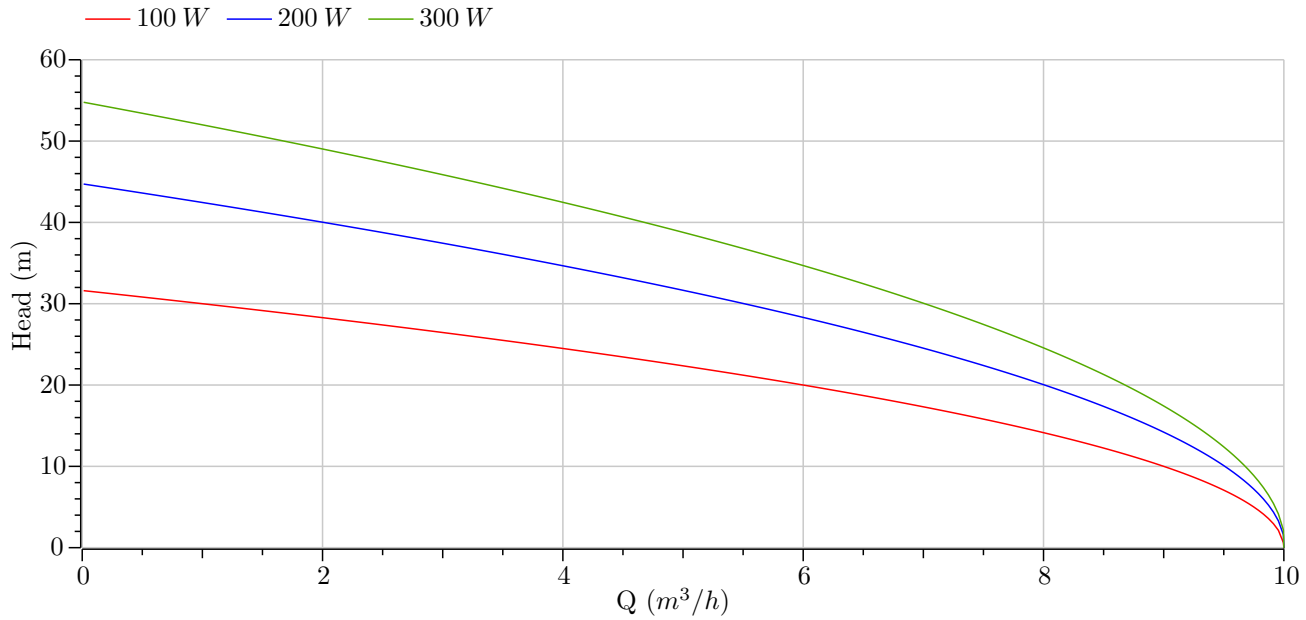

Figure 22: Simulation of the pump at varying power input

As seen from figure 22 an increase in power output increases the ability to to deliver flow at higher pressure. However there is a limit to the maximum volume flow rate. This is due to the pump curve equation mostly being a placeholder and meant for use only in low volume flow rate situations.

4.1.5 Ion exchanger

The simulation of the ion-exchanger is done by letting a predescribed mass flow rate flow through the ion-exchanger, towards an outlet pressure of 101325 Pa.

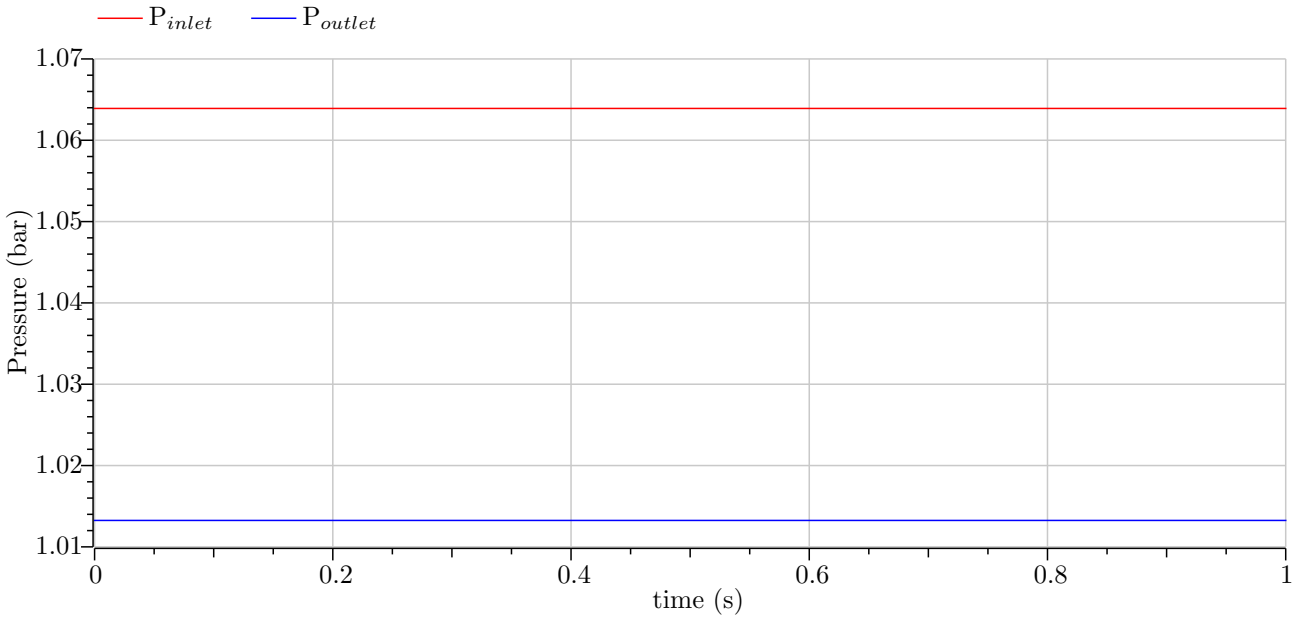

Figure 23: Simulation of the pressure drop through the ion exchanger

A simple simulation of the ion exchanger is shown in figure 23. It is modeled as a minor pressure drop, as previously explained in section 3.3.3, and as shown in this result.

4.2 The cooling system unit

Results from simulations done on the cooling system unit is presented in this section. The heat exchanger is first simulated independently before it is connected to the cooling system and simulated again.

4.2.1 Heat exchanger

Parameters used in the simulation are presented in table 27. Under these simulation conditions there are multiple interesting results presented in Table 28.

Table 27: Simulation parameters in the heat exchanger

Parameter	**Value**	**Unit**
$\dot{m}_{ab}$	0.1	kg/s
$\dot{m}_{cd}$	0.2	kg/s
T_a	353	K
T_c	293	K

Table 28: Simulation results of the heat exchanger

Variable	**Value**	**Unit**
A	0.31	m^2
q	27375	W
η	55%	-

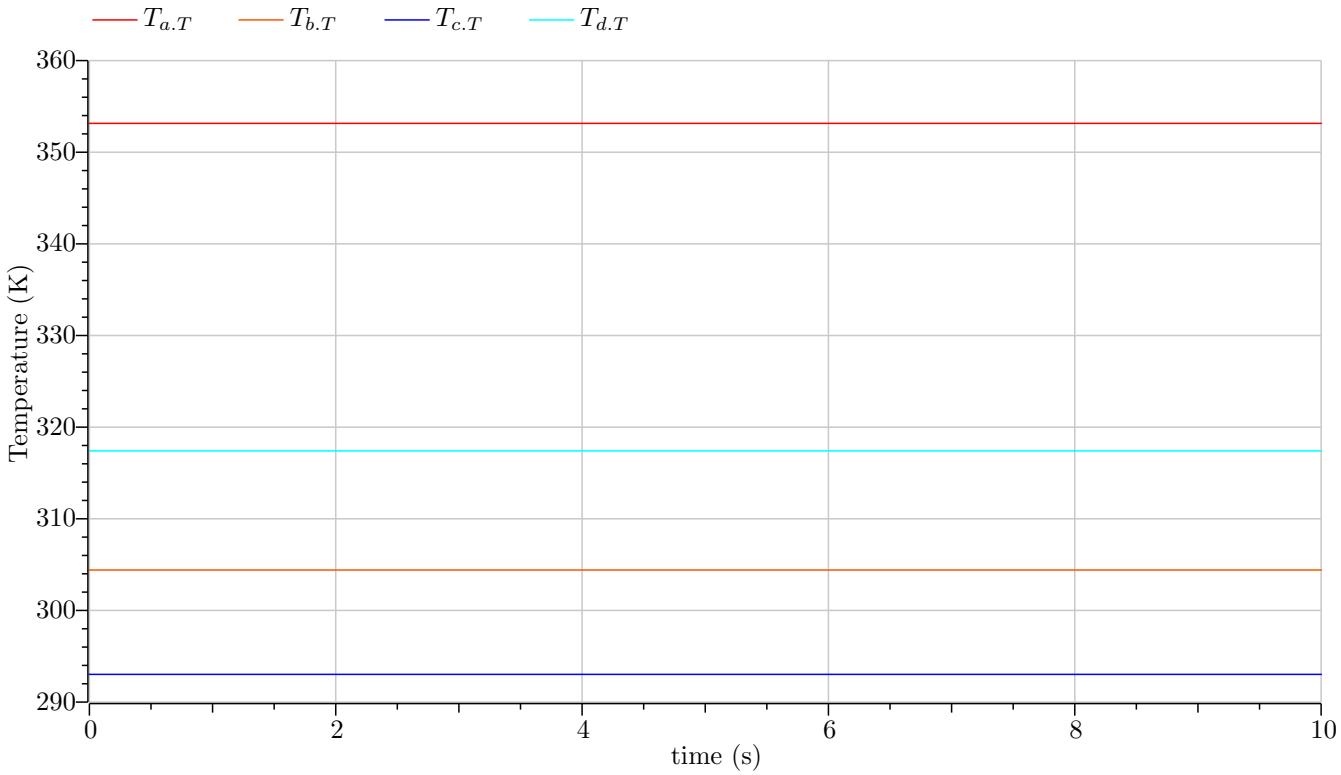

Figure 24: Simulation of the basic heat exchanger model

A simulation of the heat exchanger is shown in figure 24. Predescribed constant mass flow sources from Modelica are used during the simulation in order to show the basic behaviour of the model, with output temperatures measured with absolute temperature sensors.

4.2.2 Cooling system

The cooling side of the heat exchanger is connected to the cooling unit and the simulation of this is presented in figure 25 and figure 26. For the simulation of the cooling system unit, the system is simulated with a desired output temperature, and the cooling system unit alters the mass flow rate from the pump to the necessary value in order to provide sufficient cooling. The parameters of the simulation are presented in table 29.

Table 29: Simulation parameters in the cooling system

Parameter	**Value**	**Unit**
$T_{in,cooling}$	293.15	K
$T_{in,heated}$	$340 \mapsto 335$	K
$\dot{m}_{in,heated}$	0.1	kg/s
K_p	0.01	-

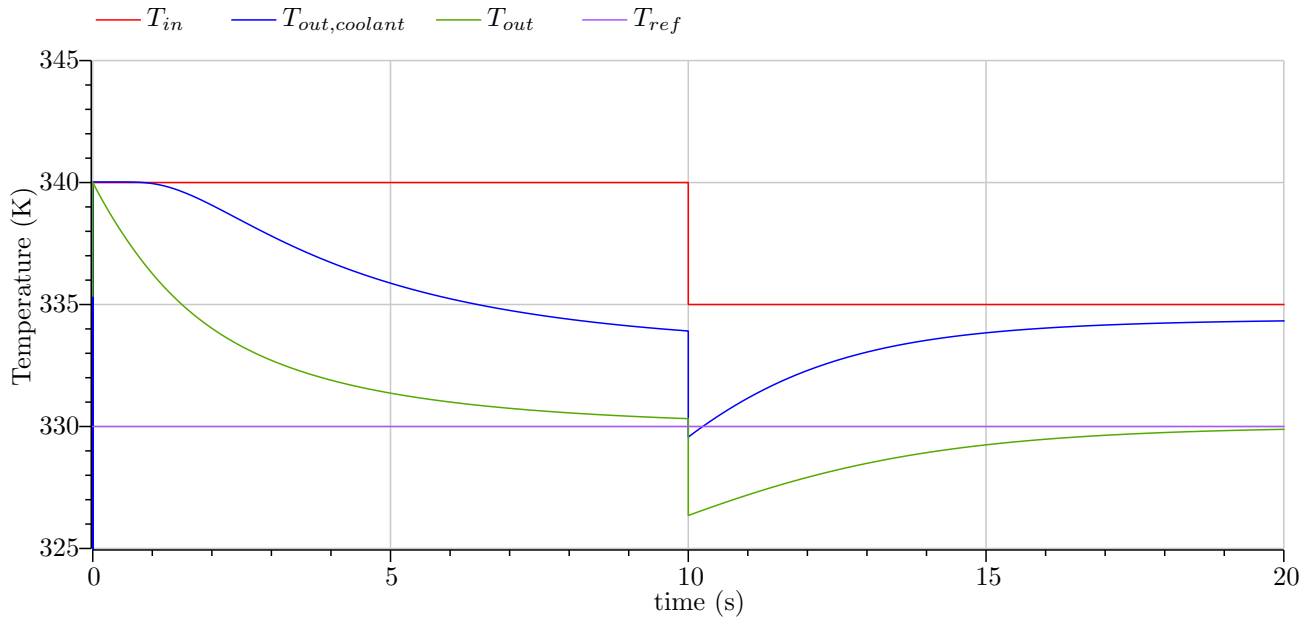

Figure 25: Simulation of the temperature change in the cooling system unit

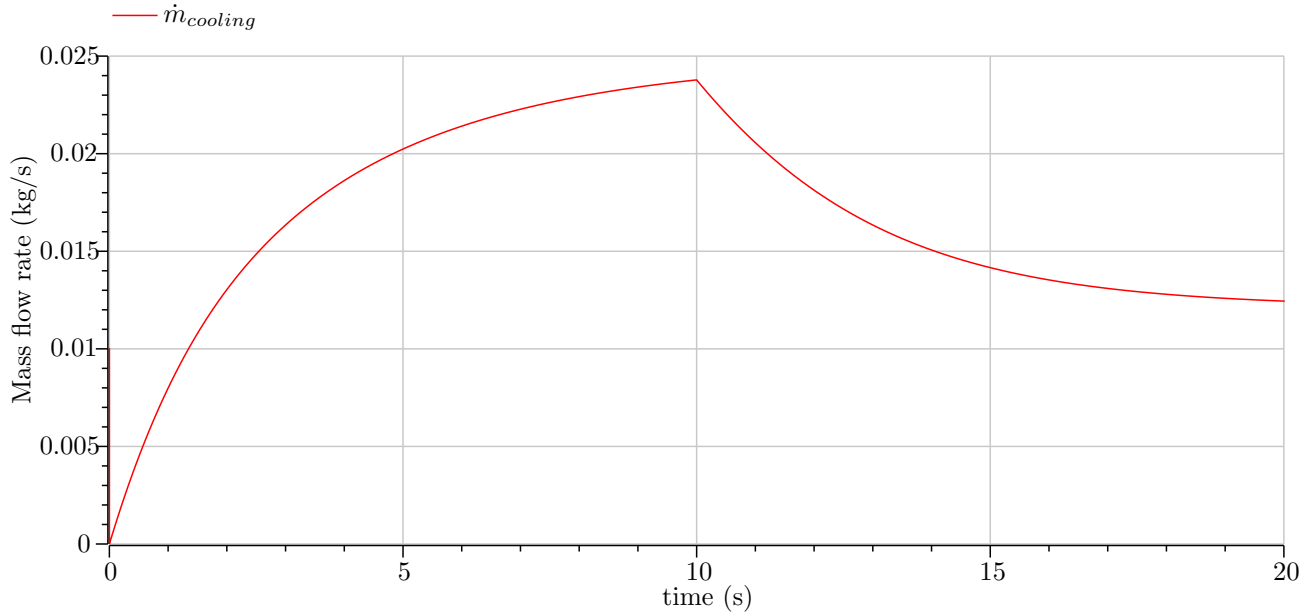

Figure 26: Simulation of the mass flow rate of coolant water

To show how the cooling system unit works, the system was subjected to an instream of hot water at 340 K from $0 \rightarrow 10$ seconds. After this the instream temperature was lowered to 335 K from $10 \rightarrow 20$ seconds. This change in temperature and mass flow rate is visible in both figure 25 and figure 26 at 10 seconds.

4.3 The Power Supply Unit

The models within the power supply unit are all dependent on each other, except for the power supply model, and are therefore all included as parts of the total results of the power supply unit.

4.3.1 Power supply

Since the power supply model acts as the source for the other models in the power supply unit, two different scenarios were simulated. This was done by using different input parameters in the power supply model in order to show that the models work as intended even with different starting parameters.

Table 30: Simulation parameters in the power supply

Parameter	Vp	Phase	f	point	startTime
Value	230	0	50	0	0
Unit	V	rad	Hz	-	s

(a) Parameters in simulation 1

Parameter	Vp	Phase	f	point	startTime
Value	400	$\frac{\pi}{3}$	60	0	0
Unit	V	rad	Hz	-	s

(b) Parameters in simulation 2

The parameters used in simulation 1, as seen in table 30a, were a Vp value of 230 V, which is the rms value of the standard line-to-neutral voltage in Norway, and a frequency of 50 Hz which is the standard frequency in Norway [47]. On the other hand, the parameters used in simulation 2 as seen in table 30b, were altered in order to show how the simulation of the three-phase AC voltage will change in both its amplitude, phase shift and frequency in comparison to simulation 1. The *point* parameter is kept at zero in both simulations since altering this value would cause the symmetrical waves to become unbalanced. This would in turn cause instability in the other models and the results would be inaccurate.

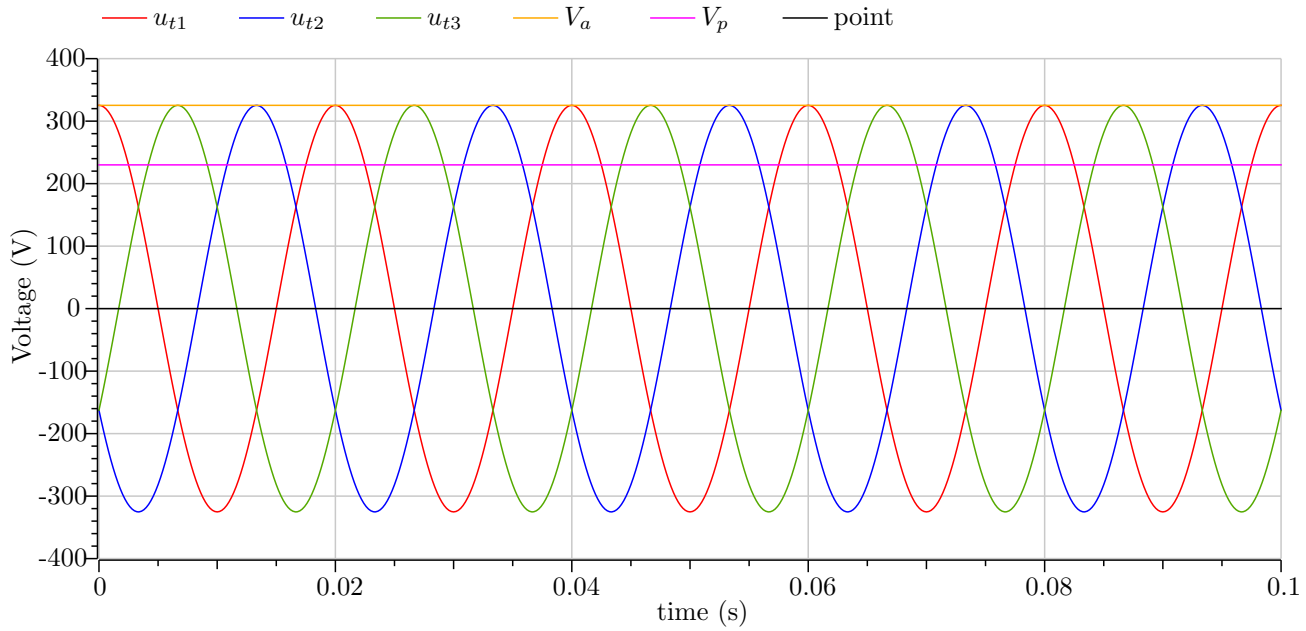

Figure 27: Simulation 1 of the power supply

In both figure 27 and figure 28, the simulation was run at a stop time of 0.1 seconds in order to show the three-phase AC voltage of the different simulations due to their frequencies. This will be the standard stop time for all the models within the power supply unit, except for the electrical control and PI-controller models.

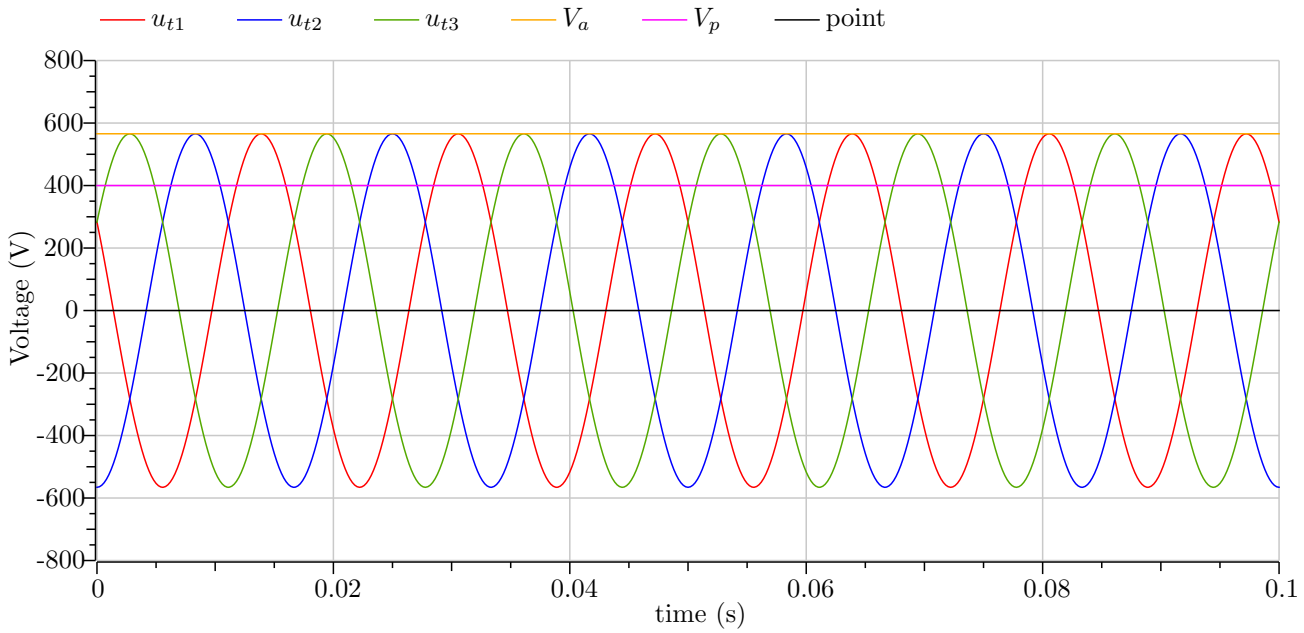

Figure 28: Simulation 2 of the power supply

Table 31: Simulation results of the power supply

Variable	Va	Phase2	Phase3
Value	325.3	$\frac{2\cdot\pi}{3}$	$\frac{-2\cdot\pi}{3}$
Unit	V	rad	rad

(a) Results from simulation 1

Variable	Va	Phase2	Phase3
Value	565.7	π	$-\frac{\pi}{3}$
Unit	V	rad	rad

(b) Results from simulation 2

The numerical results from both of the simulations of the power supply model are presented in tables 31a and 31b.

4.3.2 AC/AC transformer

Two different simulations, with different parameter inputs, were run for the transformer as well.

Table 32: Simulation parameters in the transformer

Parameter	Np	Ns	Pi	Pc	PF
Value	200	50	10	10	0.9
Unit	-	-	W	W	-

(a) Parameters in simulation 1

Parameter	Np	Ns	Pi	Pc	PF
Value	150	100	30	20	0.8
Unit	-	-	W	W	-

(b) Parameters in simulation 2

Tables 32a and 32b shows the different parameters used in the simulation of the transformer model. Since the transformer model is interconnected with the power supply model, and uses some of the power supply's variables, it is important to distinguish that table 32a is taking simulation 1 from section 4.3.1 into consideration, while 32b is taking simulation 2 from section 4.3.1 into consideration.

Simulation 1, visualized in figure 29, shows the lowered AC voltage, referred to as $Vs_{1/2/3}$, in comparison to the much higher AC voltage from the power supply model. Simulation 2 as seen in figure 30 technically shows the same as figure 29, except that with altered parameters specific to simulation 2 from tables 30b and 32b, the voltage values are much higher.

The results presented in tables 33a and 33b, show an increased power output and efficiency with the changed parameters. The varying values of variables P_{AC} and η_{trans} is caused by the changing current coming from the rectifier. This is further explained in section 4.3.4.

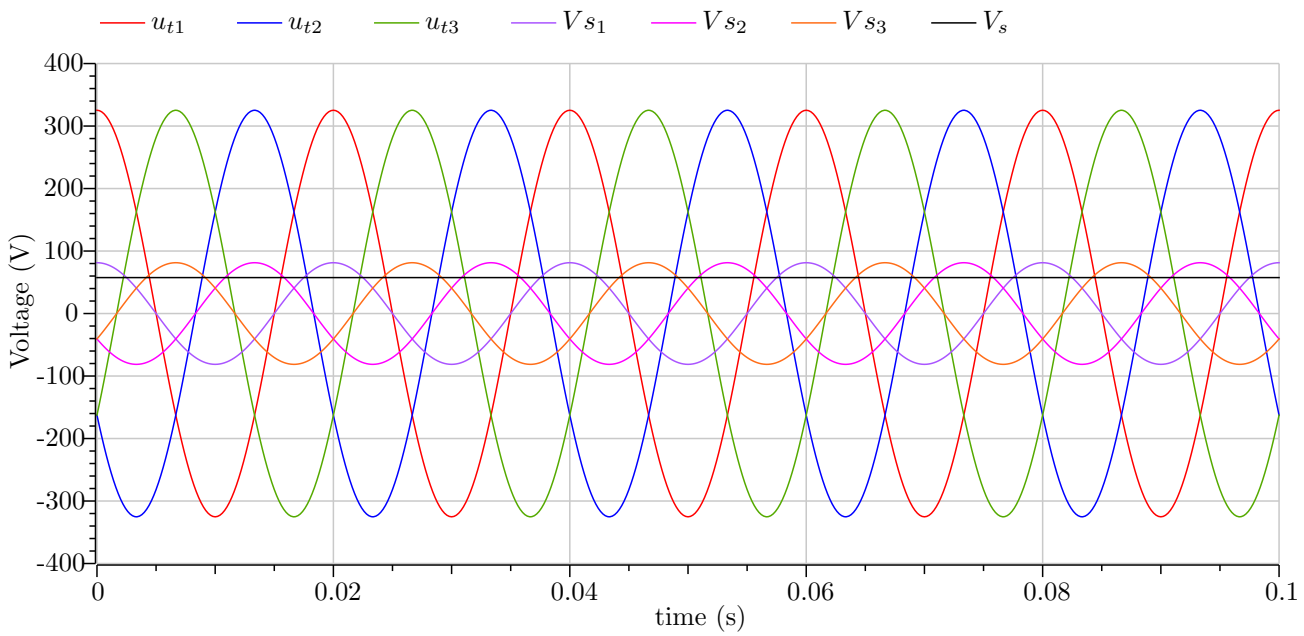

Figure 29: Simulation 1 of the transformer with $u_{t1/2/3}$ from figure 27 as reference

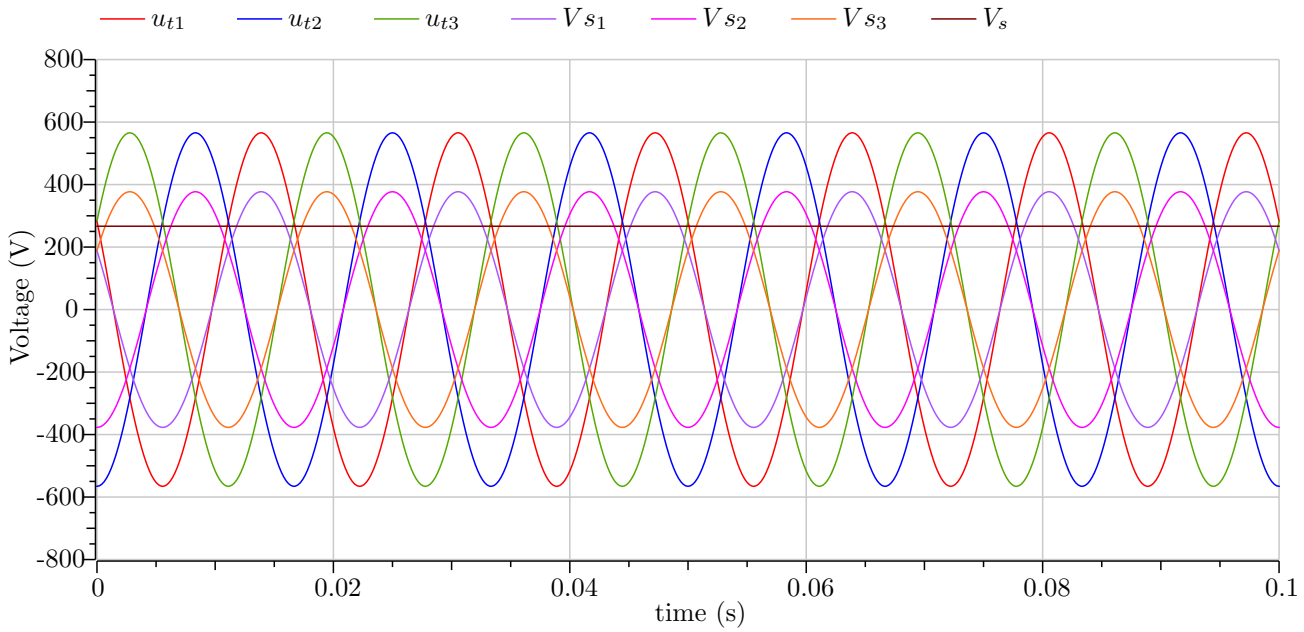

Figure 30: Simulation 2 of the transformer with $u_{t1/2/3}$ from figure 28 as reference

Table 33: Simulation results of the transformer

Variable	Vs	P_{AC}	η_{trans}
Value	57.5	317.2→143.6	96.1→91.8
Unit	V	W	%

(a) Results from simulation 1

Variable	Vs	P_{AC}	η_{trans}
Value	266.7	3045.3→442.9	98.8→92.5
Unit	V	W	%

(b) Results from simulation 2

4.3.3 AC/DC rectifier

In the rectifier model, much of the previous information from the transformer and power supply models are processed in order to simulate the rectified voltage.

In tables 34a and 36b, the efficiency of the rectifier for the different simulations is determined as an input parameter.

The rectified voltage can be seen in figure 31 and figure 32, alongside its boundaries between $V_{DC/top}$ and $V_{DC/bot}$.

Table 34: Simulation parameters in the rectifier

Variable	Value	Unit
η_{rect}	0.9	-

(a) Rectifier efficiency in simulation 1

Variable	Value	Unit
η_{rect}	0.8	-

(b) Rectifier efficiency in simulation 1

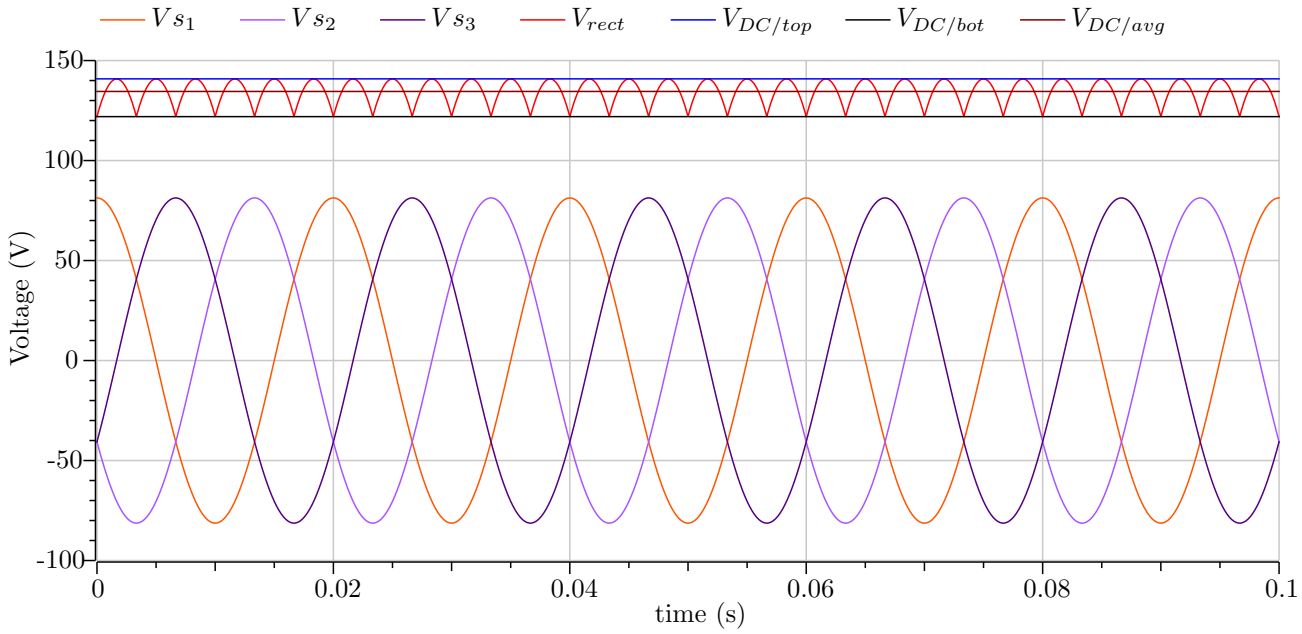

Figure 31: Simulation 1 of the rectifier

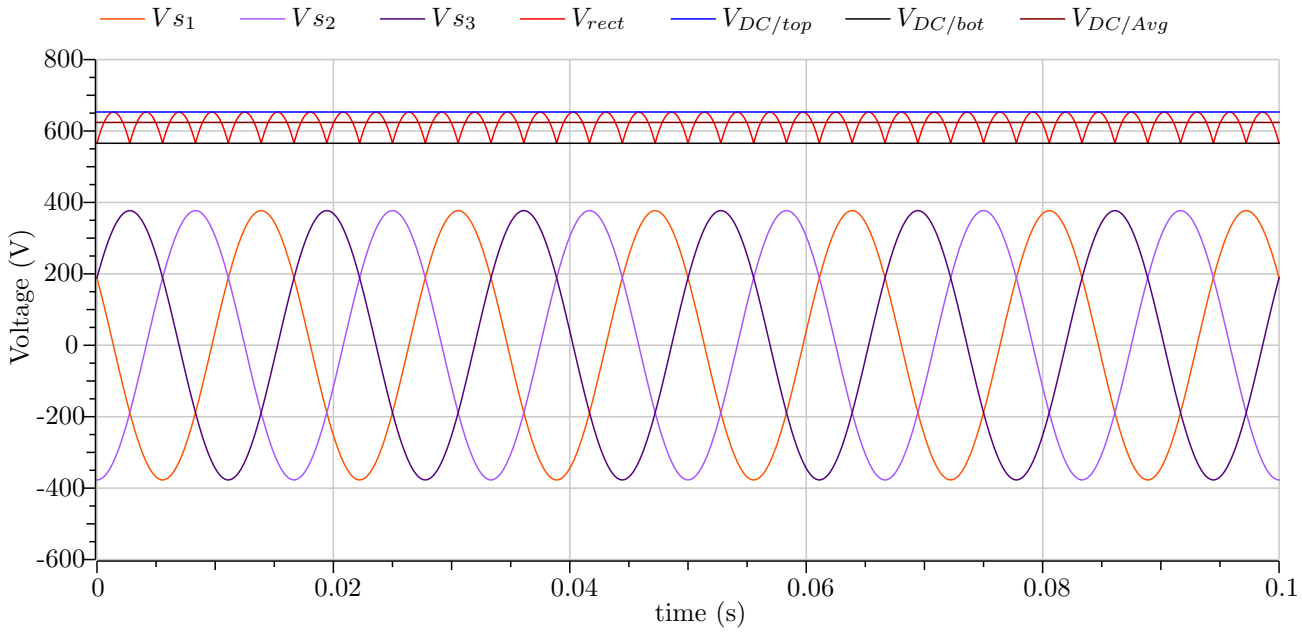

Figure 32: Simulation 2 of the rectifier

The lowered three-phase AC voltage from the transformer model can be seen in both figures as well.

The results from the rectifier simulations, presented in tables 35a and 35b, are affected by the results from the electrical control model. This is seen in the variable P_{DC} in both simulations as it varies based on the actual current from tables 36a and 36b.

Table 35: Simulation results of the rectifier

Variable	$V_{DC/avg}$	P_{DC}
Value	134.6	286→129.3
Unit	V	W

(a) Results from simulation 1

Variable	$V_{DC/avg}$	P_{DC}
Value	624	2436.2→354.3
Unit	V	W

(b) Results from simulation 2

4.3.4 Electrical control and PI-controller

The simulations of the electrical control and PI-controller models illustrate the behavior surrounding the implementation of the output voltage from the rectifier as the u signal.

Table 36: Simulation parameters in the electrical control and PI-controller

Parameter	R_{ref}	R_{load}	Kp	Ki	$I_{desired}$
Value	1	0.5	1	10	2→1
Unit	Ω	Ω	-	-	A

(a) Parameters in simulation 1

Parameter	R_{ref}	R_{load}	Kp	Ki	$I_{desired}$
Value	1	2	5	5	4→0.5
Unit	Ω	Ω	-	-	A

(b) Parameters in simulation 2

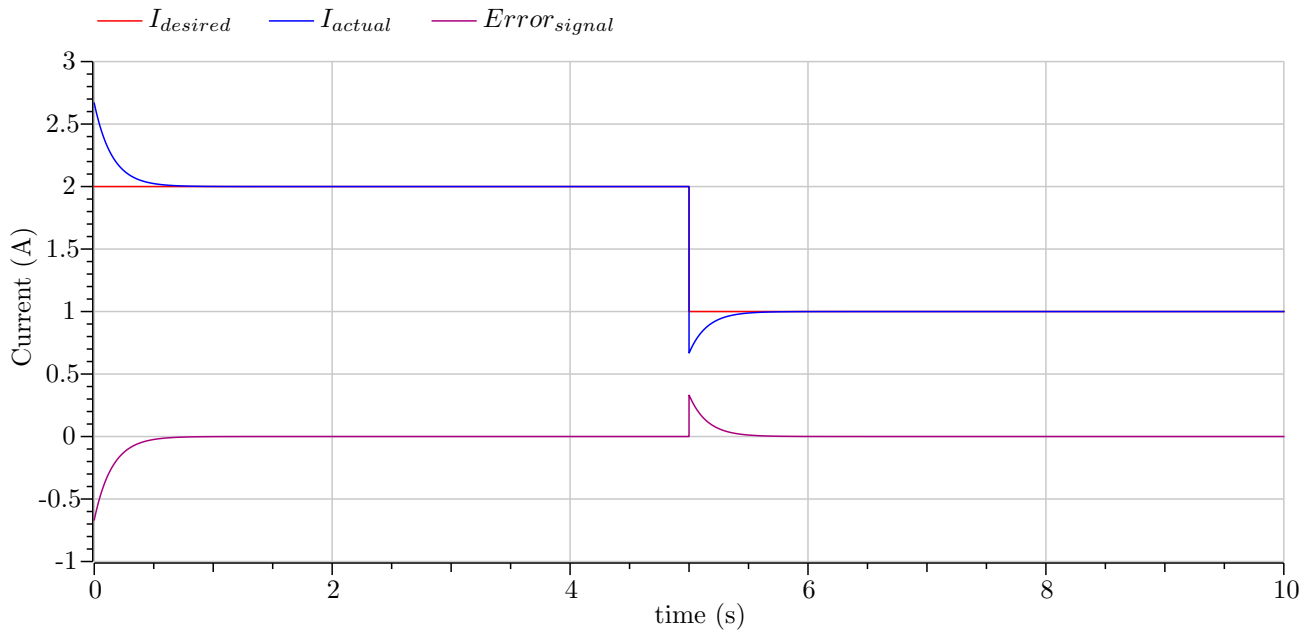

Figure 33: Simulation 1 of the electrical control and PI-controller

In tables 36a and 36b the parameters are presented. Note that in both of the simulations the desired current is changed midway through the simulations by using algorithm 5.

In figure 33 and figure 34, the error signal is gradually lowered as the error between the desired and actual current is corrected. The error signal eventually reaches a value of zero as the output current reaches the value of the desired current. There is no need for results presented in tables, since the simulation showcases that the error signal is corrected down towards zero and the desired current is reached by the actual current. Important to note is that the efficiencies and power outputs of the transformer and rectifier, presented in tables 33a, 33b, 35a and 35b, is derived from when time is equal to 5 seconds or 10 seconds into the simulation. This is when the current is closest to its desired value as seen in both figure 33 and figure 34.

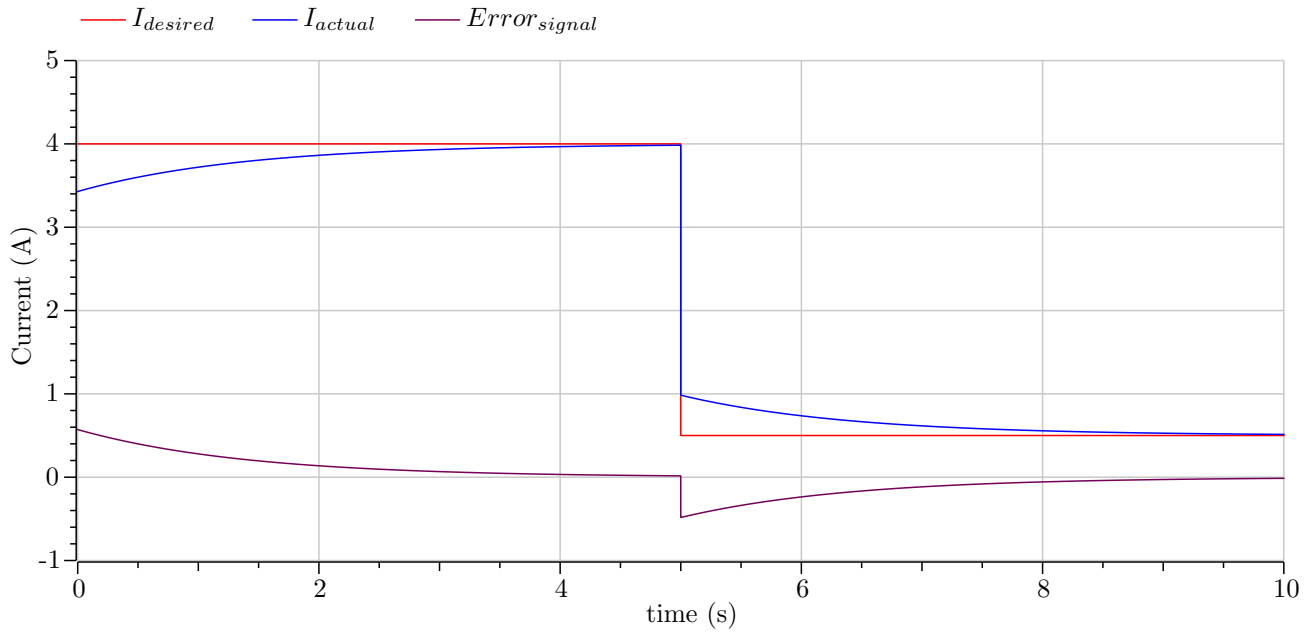

Figure 34: Simulation 2 of the electrical control and PI-controller

4.4 The combined system

The combined system is simulated under steady-state conditions where all the created models are connected to the electrolyzer stack. The models have been connected in similar fashion to the schematic previously presented in figure 13. The stack is as previously mentioned developed by Hystar, and the stack's structure and behavior will not be further elaborated in this thesis, other than its input parameters.

Table 37: Simulation parameters in the electrolyzer stack

Parameter	*No. of cells*	*Active area*	$Current_{stack}$	$Mass_{stack}$
Value	10	500	1500→1000	25
Unit	-	cm^2	A	kg

In table 37 the parameters used in the electrolyzer stack are presented. These specific parameters were provided by the thesis' supervisors, except for the mass of the stack.

Table 38: Initial values for the stack

Variable	**Value**	**Unit**
$m_{liquid,anode}$	9	kg
$m_{liquid,cathode}$	1	kg
$P_{gas,anode}$	4.99	bar
$P_{gas,cathode}$	29.9	bar
$T_{gas,anode}$	345	K
$T_{liquid,anode}$	345	K
$T_{gas,cathode}$	345	K
$T_{liquid,cathode}$	345	K

For a smooth initialization and simulation, the stack is dependent on appropriate initial values. The initial values used for the simulation are presented in table 38.

Table 39: Reference values for the full simulation

Sub model	**Variable**	**Value**	**Unit**
Cooling system, anode	T_{ref}	325	K
Liquid-gas separator, anode	P_{ref}	5	bar
Liquid-gas separator, cathode	P_{ref}	30	bar
Liquid-gas separator, anode	$V_{min,liquid}$	25%	-
Liquid-gas separator, cathode	$V_{max,liquid}$	90%	-

For the system to operate as desired, reference set points are set. These values are presented in table 39, and can easily be changed if different values should be desired. The volume values are representing the % of total volume.

Table 40: Mediums used in the combined system simulation

Medium	**Medium package**
LiquidMedium	$Modelica.Media.Water.StandardWaterOnePhase$
AnodeGasMedium	$Modelica.Media.IdealGases.SingleGases.O2$
CathodeGasMedium	$Modelica.Media.IdealGases.SingleGases.H2$
CoolantMedium	$Modelica.Media.Water.StandarsWaterOnePhase$

For the simulation of the full system several medium models were used. Table 40 lists all replaceable medium packages in the full system and their assigned medium package.

4.4.1 Anode flow unit

As previously established, the anode flow unit corresponds to the anode flow subsystem of the liquid-gas separator unit, seen in figure 10 in section 3.4.1

Table 41: Initial values for the anode flow unit

Sub model	**Variable**	**Value**	**Unit**
Liquid-gas separator	P	4.9	bar
Liquid-gas separator	T_{gas}	345	K
Liquid-gas separator	T_{liquid}	345	K
Liquid-gas separator	m_{liquid}	500	kg
Predescribed pump	$\dot{m}$	0.15	kg/s

All specified initial values given for the anode flow unit is presented in table 41. For this simulation initial values was given in order to emphasize desired behaviour. By having the pressure value from table 41 close to the reference pressure given in table 39, it becomes easier to show the regulation of the pressure.

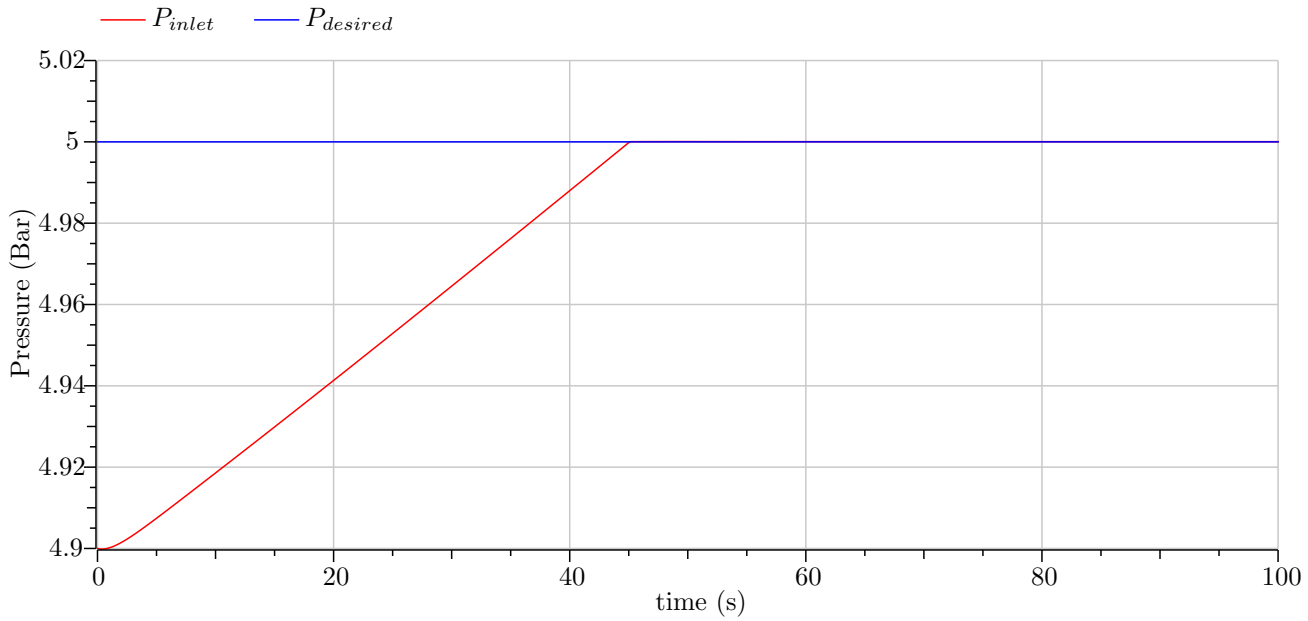

Figure 35: Simulation of the pressure in the liquid-gas separator on the anode side

Figure 35 shows the pressure of the anode system against the declared desired pressure of the liquid-gas separator. As seen in the figure the pressure increases until it reaches its reference value.

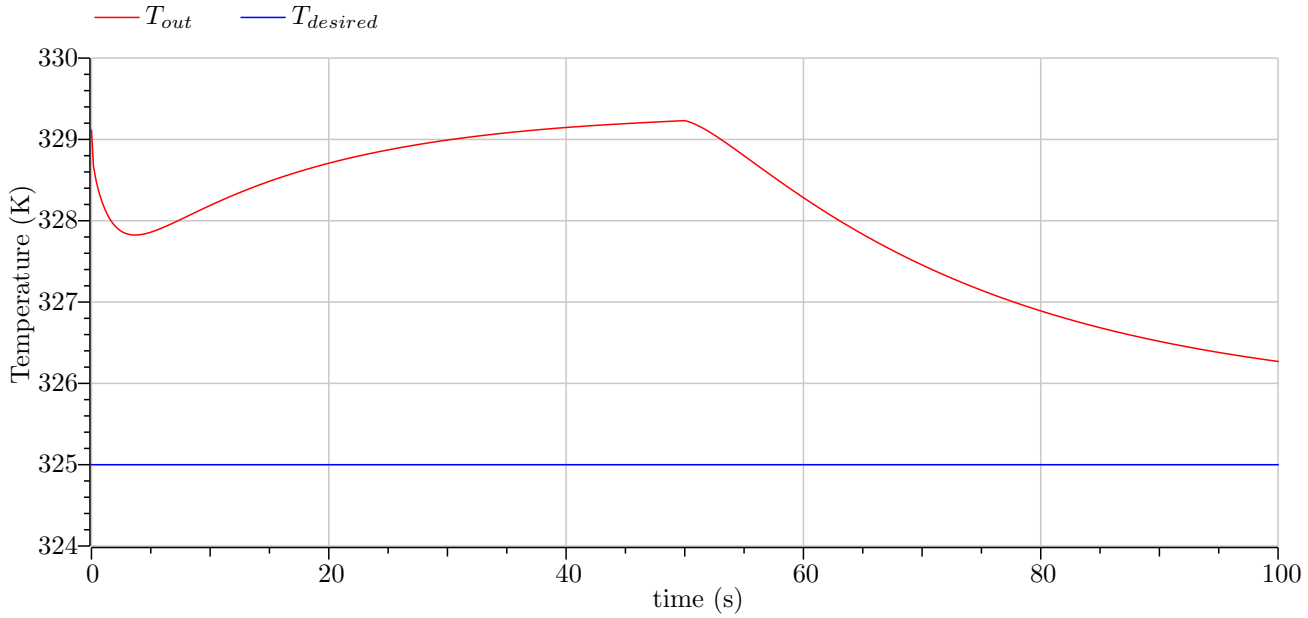

Figure 36: Simulation of the actual and desired temperature on the anode side

Figure 36 shows the difference between the desired temperature and the actual output temperature of the cooling system unit. The temperature T_{out} for this simulation is desired to constantly be approaching $T_{desired}$. However, the temperature into the cooling system unit is dependent on a number of other variables in the simulation which also affect the increase or decrease of the temperature output.

4.4.2 Cathode flow unit

Similarly to the anode flow unit, the cathode flow unit is also a subsystem of the liquid-gas separator unit, previously shown in figure 10 in section 3.4.1.

Table 42: Initial values for the cathode flow unit

Sub model	Variable	Value	Unit
Liquid-gas separator	P	29.8	bar
Liquid-gas separator	T_{gas}	345	K
Liquid-gas separator	T_{liquid}	345	K
Liquid-gas separator	m_{liquid}	500, but Modelica overrides this to 155	kg

The initial values for the cathode flow unit is presented in table 42. The ion-exchanger and HEX, which were optional on the cathode side, were discarded in the simulation. The initial values for the cathode flow unit were similarly to the anode flow unit given in order to emphasize desired behaviour.

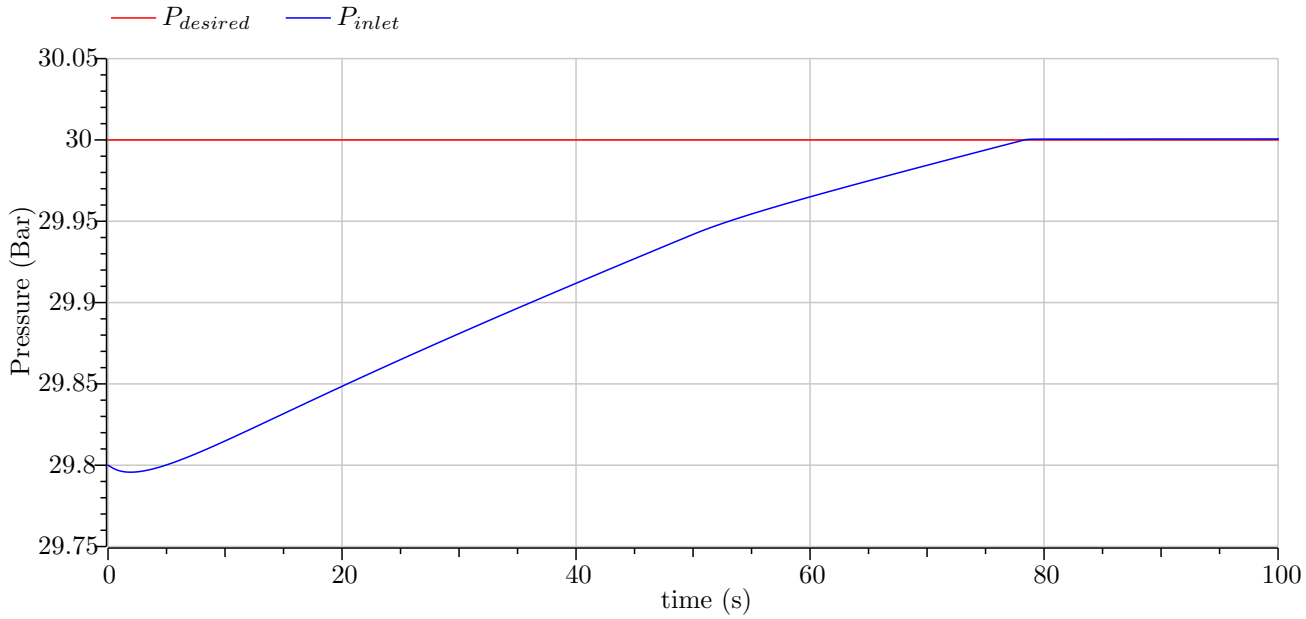

Figure 37: Simulation of the pressure in the liquid-gas separator on the cathode side

Just like the anode flow unit, the liquid-gas separator on the cathode flow unit is also regulated by a valve as can be seen in figure 37. The pressure in the cathode flow unit can be seen approaching the desired pressure value a lot slower than the pressure in the anode flow unit seen in figure 35. A small dent in the curve for P_{inlet} is also visible at the time of 50 seconds, which is when the current supplied to the electrolyzer stack is lowered.

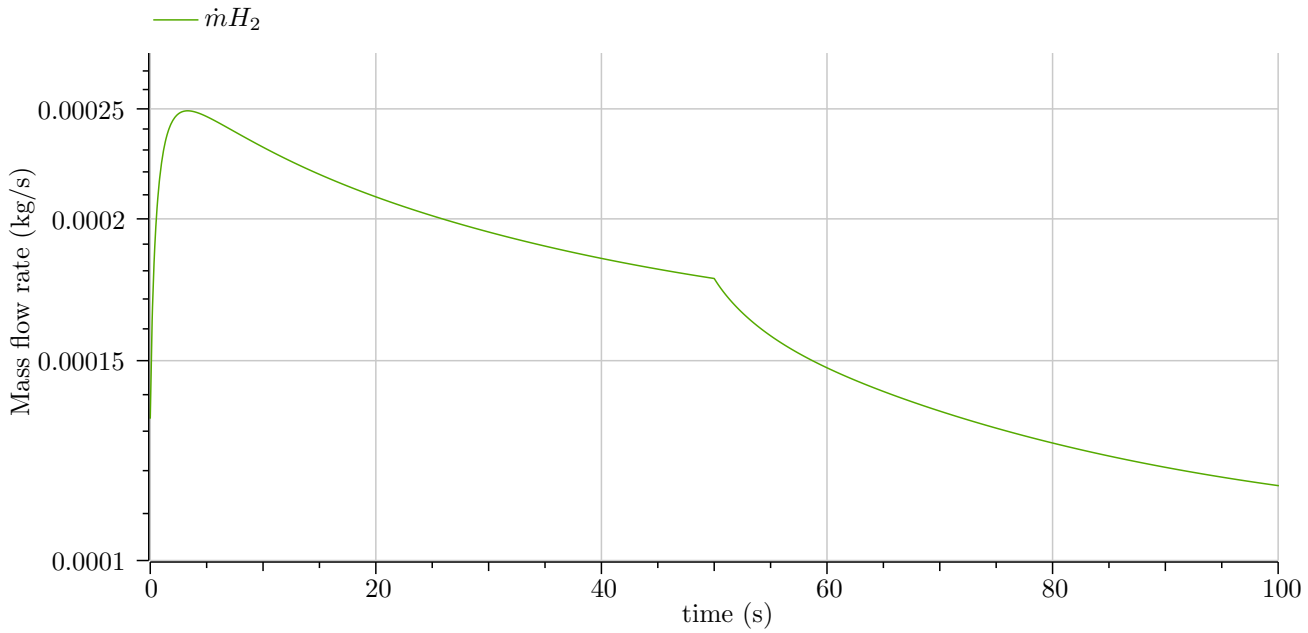

Figure 38: Simulation of the mass flow rate of H_2 on the cathode side

The actual mass flow rate of hydrogen gas, as an output from the electrolyzer stack, is presented in figure 38. This mass flow rate also be referred to as the hydrogen production rate of the electrolyzer stack.

4.4.3 Power supply unit

Table 43: Simulation parameters in the power supply unit

Parameter	Ki	Kp	R_{ref}	f
Value	5	5	2	1
Unit	-	-	Ω	Hz

In the combined system, where the power supply unit is also connected to the electrolyzer stack, input parameters are needed. The simulation parameters used in the power supply unit of the combined system is for simplicity's sake kept almost identical to the simulation parameters from simulation 1, which were previously presented in tables 30a, 32a and 34a in section 4.3. Still, some parameters have been altered from the previous simulation in order to make the simulations run more smoothly. These new parameter values are presented in table 43.

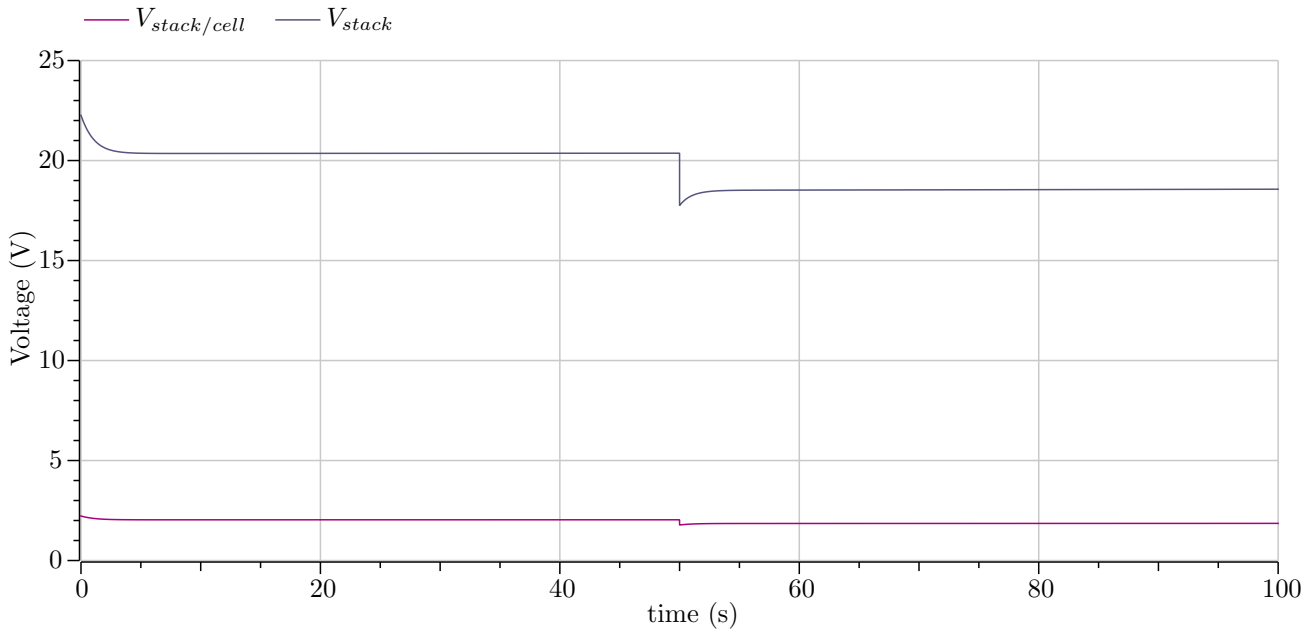

Figure 39: Simulation of the combined system showing the input voltage and cell voltage of the stack

In figure 39 the voltage from the power supply unit, as well as the cell voltage within the membrane of the electrolyzer stack, are presented.

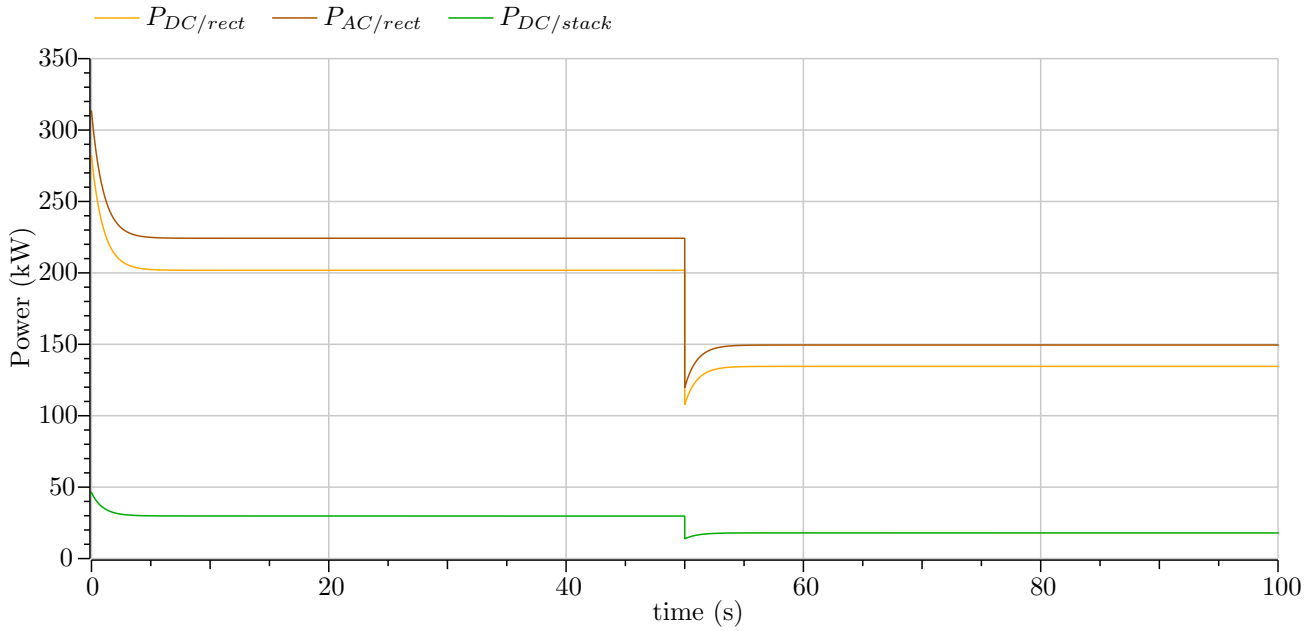

Figure 40: Simulation of the combined system showing the power outputs

Figure 40 shows the power outputs of the combined system. The power output of the transformer is shown as P_{AC} and the power output of the rectifier, which theoretically could be used in the electrolyzer stack, is shown as P_{DC}. The actual power output from the power supply unit to the electrolyzer stack is shown as $P_{DC/stack}$

4.4.4 Electrolyzer stack

The electrolyzer stack has already had its simulation parameters presented in table 37.

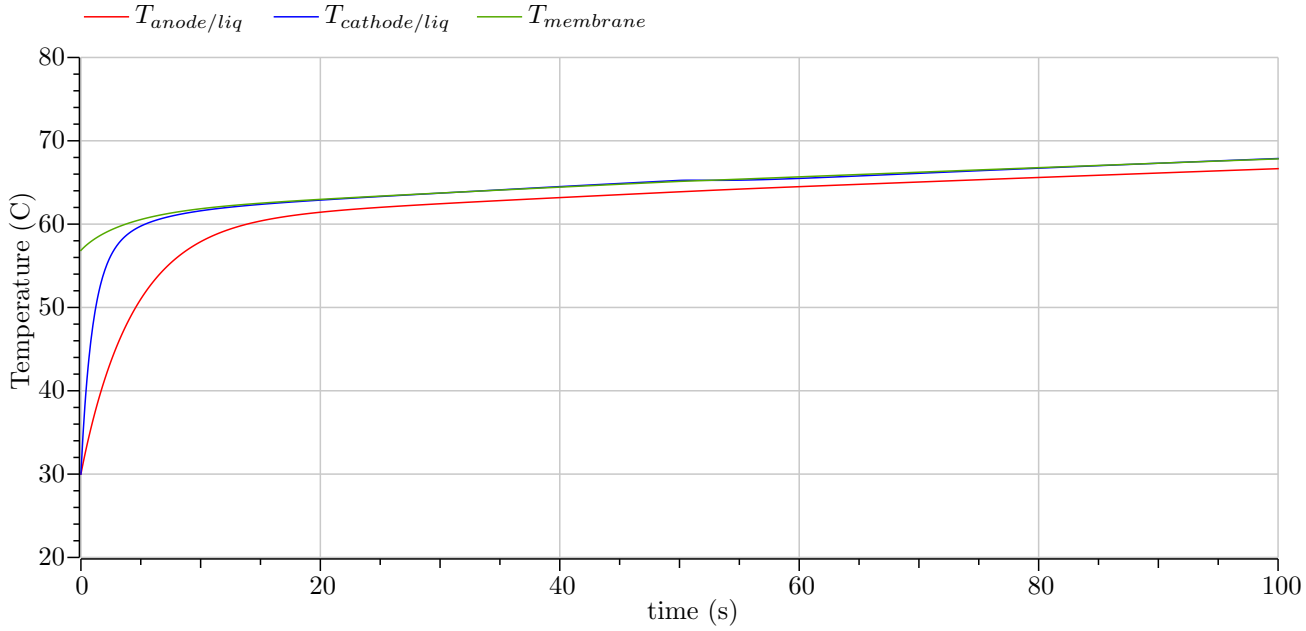

Figure 41: Simulation of the combined system showing the temperatures in the stack

In figure 41 the temperature of the stack membrane, anode liquid and cathode liquid are shown. It is important to note that the temperature is continuously increasing during the simulation run time. What this continuous temperature increase means, and how it affects the combined system will be discussed later in section 5.4.1.

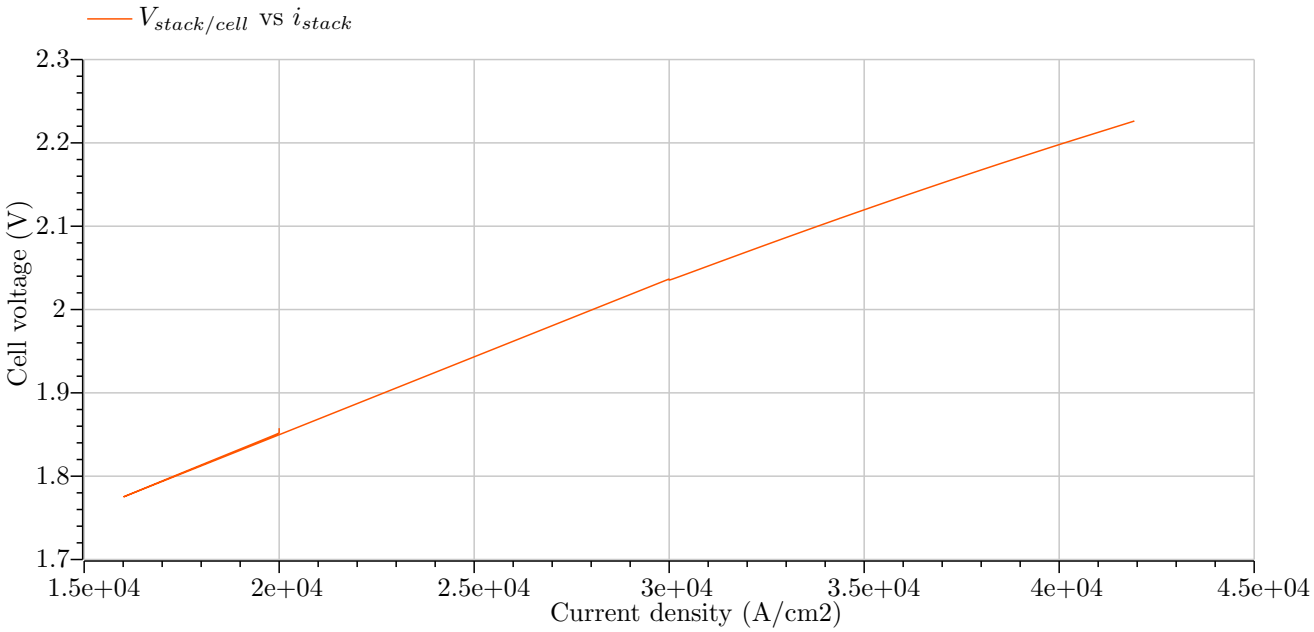

Figure 42: Simulation of the combined system showing the polarization curve in the stack membrane

The polarization curve of the electrolyzer stack can be seen in figure 42. The current density as the x-axis and the cell voltage as the y-axis are plotted against each other, showing a linear relation between both axes.

5 Discussion

It is important to reflect on and examine the gathered results in a thesis. The discussion chapter aims to examine the models in order to create an overview of the correctness and accuracy of the simulations. This section is structured as the previous chapters, with a general discussion of the subsystems and their results followed by discussion around the design choices, sources of error and validity of each individual model. The results and validity of the combined system of the entire digital twin, connected to the electrolyzer stack, is discussed as well. Future development and improvements of the digital twin are discussed in closing.

5.1 The liquid-gas separator unit

The liquid-gas separator unit consists of several components as previously explained in section 3.4.1. A discussion of relevant findings from the simulations done in section 4.1 is presented, as well as design choices and potential sources of errors in the subsystem.

5.1.1 Results

The pump has one of the more restrictive designs in the digital twin. Relating power, head, and volumetric flow rate into a pump curve can be a difficult task. Therefore, in the case of the pump model, a pump with plausible values around the working point was chosen. As the pump is to be operating at somewhere around 4 m^3/h for this model, the pump curve equation 4 works as a gross estimation of curve behavior. However, as seen from the result in figure 22 these results can only be thought of as an estimation around a certain flow rate. Due to the nature of the estimated pump curve, a flow rate of 10 m^3/h will always happen due to the pump curve equation, equation 4. If the pump was to operate at higher flow rates, this issue would need to be addressed by linking the power to the second degree part of equation 4.

As shown in figure 20 and figure 21, the valve is working as intended by controlling the flow rate which in turn increases the inlet pressure. From figure 19 it is also apparent that the valve curve is of type linear as desired, as the figure shows the linear relationship between the opening and the flow rate through the valve. The ion exchanger does what it is intended to as seen in figure 23. However, this is as previously explained, due to it only being a minor pressure drop.

The liquid-gas separator vessel includes the internal energy balances for both of the included fluids as well as their mass balances. Some physical phenomenas within the volume was simplified, but the results still show desired behavior. As seen in figure 13, 15 and 16, all values of variables and parameters are related to each other. Increasing liquid inside the volume leads to a compression of the gas, which again leads to an increase in the pressure of the vessel. The vessel also includes the change in internal energy for both mediums and their change in mass. The change in internal energy also includes heat transfer between mediums, where medium temperatures can be seen in figure 18. The results from the simulations done in section 4.1.1 are plausible, though validating these results to real-world data is difficult. This will be further discussed in section 5.5.5.

5.1.2 Design choices and limitations

The design choices for the pump were mainly driven by a desire to create a pump able to handle a pump curve in addition to keeping the structure and governing equations fairly simple. This included adding the possibility of a pump curve, where a generic one was used as a placeholder. The estimation of the pump curve is therefore a major design limitation as developing an actual general pump curve equation relating power, head and flow rate proved difficult. The major limitation here is the pumps inability to deliver more than 10 m^3/h. The included predescribed mass flow pump does not have this problem as the pump curve given by equation 4 is discarded.

For the valve, some assumptions and simplifications were done. For a modeled valve, nominal pressure drop at full opening and nominal leakage at the full opening would normally be included. This is however harder to model, since it can create some problems with dividing by zero and similar issues. Instead, an *if loop* was created in order to limit the opening to be between 0.01 and 0.99. This solves the aforementioned problem, and also helps with the ease of use of the model. This is a major simplification and should therefore be addressed in future work. Having the valve highly sensitive to the k_v factor and the opening was an intended behavior for the model. For easier controlling of inlet pressure an equal percentage valve could also have been implemented.

For the ion exchanger, multiple simplifications were done. The ion exchanger is modeled simply as a minor pressure drop given by some constant k as previously explained. This was agreed with the supervisors of the thesis to be sufficient behavior. The main reason for this is that the complexity it would take to model an actual ion exchanger is beyond the scope of this thesis. The water is instead assumed to be of desired conductivity. This assumption makes it so that the ion exchanger, in addition to achieving the desired conductivity, contributes to a minor pressure loss in the flowing stream.

The liquid-gas separator is modeled as a volume with unspecified geometry, as this greatly decreased the complexity of the model. This meant neglecting the actual geometry of the volume. For the internal energy balance, a function base properties was used, where the base properties of a medium is constantly calculated from the state of each fluid. This was done as it was proven to be an efficient way to model the vessel whilst taking pressure-volume changes into consideration. For further simplification of the vessel, and the model as a whole, it was decided to split the instream of the multi component stream into two separate streams. This means that the vessel is not actually separating the fluids. For the sake of simplicity, the mixing of fluids was assumed to be immediate and the the overall heat transfer coefficient was assumed to be a constant.

5.1.3 Sources of error

The pump is subject to multiple sources of error, the major one being the difficulties around the approaching of a pump curve. As the pump curve was modeled as a generic curve meant to fit the working range of the pump in the full system, it is not assumed to be valid outside of its operating range. Other major sources of error are the simplifications made in the sizing of the pump. For the predescribed mass flow pump the major source of error is the absence of a pump curve.

The major source of error for the modeled valve is, as stated earlier, inherently a combination of the valve equation 8 and Modelica's inability to handle dividing by zero. This is the reason the valve never completely opens and is never completely closed, whereas in reality the valve should include a predescribed pressure drop at full opening and some leakage at full closed. The approach works well for running a simulation smoothly but does include some inaccuracies in the actual values.

The vessel is modeled using several simplifications, which undoubtedly is a source of error. The assumption of enthalpy outflow at the exact enthalpy of the vessel disregards the physics behind the mixing of vessel medium and inflowing medium. Another source of error is the heat transfer between mediums in the vessel. This is for now is given by a coefficient and temperature difference.

5.2 Cooling system unit

The cooling system unit is made up of three main components, the heat exchanger, the cooler unit, and a centrifugal pump. All of these components have been described in detail previously. Simulations from the cooling unit that creates the foundation for discussion have been presented previously in section 4.2. Interesting aspects from the simulations are discussed, as well as design choices and assumptions made. Potential causes for errors are also looked into.

5.2.1 Results

As figure 28 seems to indicate, the results are close to what one would expect from a counter-current HEX as the temperature gradients have crossed. It is also apparent that the mass flow rates and medium type greatly affect the total heat exchange as well as the outlet temperatures in the HEX. When the mass flow rate of either the hot or the cold fluid deviates greatly, the heat capacity ratio is strongly affected, and in return the effectiveness as well.

The cooler with its control system is working as intended, as illustrated from the simulation in figure 25. The temperature outlet from the heat exchanger is controlled by the set temperature in the regulator. This enables the electrolyzer stacks inlet water to be at its optimally desired temperature of 330 Kelvin. The centrifugal pump shows a change in the mass flow rate of the coolant medium as expected, with belonging power input increase being calculated. For the last half of the simulation in figure 26 the set temperature is lowered and the coolant flow rate required is shown decreasing as well.

5.2.2 Design choices and limitations

The heat exchanger model developed in the project is created with certain simplifications and assumptions, which again affects the models behavior. As there is insufficient information to calculate the Log-Mean Temperature Difference, the NTU method is applied as previously explained in section 3.3.5. During simulations of the heat exchanger, the efficiency was calculated to be in the lower end, and with great dependency on the mass flow rates of the system. The efficiency of a liquid/liquid heat exchanger is expected to be higher, but this is dependant of the HEX design and operational values. However, the models behavior still is as expected, with a transfer of heat from the hot to the cold fluid at plausible values.

Initially the heat exchanger model had an increased complexity, with the overall heat transfer coefficient being a variable calculated. As explained in section 3.3.5, this proved to difficult as the heat transfer coefficients greatly depends on the nusselts number. This also depends on the geometric design of the heat exchanger, as well as the laminar and turbulent flow boundary, dependant of the Rayleigh's number. Therefore a constant overall heat transfer coefficient were chosen, with a value of *1250* $W/(m^2 \cdot K)$, based on representative values found online for a liquid/liquid plate heat exchanger [48]. This being the average of a selected range of values. A geometrical design of the heat exchanger had to be defined. These were estimated values based on what a reasonable sizing for the heat exchange required. A diameter of *0.05 m* were chosen, and a length of *2 m*. This gives an area, A, of *0.31* m^2. These values are unknown, and are only estimates based on what the authors found to be appropriate sizing for the heat exchanger's purpose.

The temperature control of the cooling system unit is controlled by a regulated signal. The proportional gain signal, K_p, can be varied to regulate how quick the response time of the change is. An important advantage of the PEM electrolysis technology is its quick response time. This indicates that important auxiliary equipment also requires to be subject of quick changes in the system.

5.2.3 Sources of error

It is of great importance to acknowledge potential sources of error in order to document and evaluate the models created. The model includes fundamental equations from both heat and mass transfer and fluid dynamics. These equations are interpreted by the Modelica compiler, and although the resulting values are plausible, there are room for potential human errors.

When constructing a digital model it is important to have profound knowledge of the respective physical system. When this is not the case, estimates and assumptions has to be made. A potential cause of error could emerge from this. As the geometrical design of the HEX is a required parameter for the NTU method, estimations had to be made, potentially deviating from a realistic sizing.

The modeling program used, Modelica, was unknown at the start of the project period, meaning that the program in some aspects was learnt as parts of the model were created. This could be a source of error, as early code implementation could differ from the desired behavior.

5.3 The power supply unit

This section of the thesis provides discussion around the specific results, design choices, limitations and sources of error relevant to the power supply unit.

5.3.1 Results

The results from the power supply unit, which were presented in section 4.3, generally show the expected behavior of the electrical models which were designed and explained in section 3.3.7 to section 3.3.11.

The power supply model managed to generate three symmetric sine waves to imitate three-phase AC voltage. This was achieved in both of the simulations that were run as can be seen in figure 27 and figure 28. The change of parameter values in simulation 2, where both the input rms voltage and frequency were increased, returned expected results as well. The higher frequency caused a shorter distance between the sine waves and the higher input voltage generated higher amplitudes of the sine waves. The results of the power supply model provided in tables 31a and 31b also return numerical values that are consistent with equations 27, 28 and 29 from section 3.3.7 in both simulations.

For the AC/AC transformer model, the lowering of the three-phase AC voltage from the power supply model was achieved in both simulations as can be seen in figure 29 and figure 30. It became apparent the large impact the number of windings on either side of the transformer had. In simulation 1 the number of windings was a lot higher on the primary side than on the secondary side in comparison to simulation 2, which can be seen in tables 32a and 32b. This caused the lowered sine waves in figure 30 to be much closer to the sine waves from the power supply. This was expected since the calculations of the lowered sine waves were based on equation 31, where the ratio of windings between the primary and secondary side of the transformer is directly taken into consideration. The other results of the transformer, presented in tables 33a and 33b, all show expected behavior as well in relation to each of their respective equations. The transformer efficiencies in both simulations will be looked more into when discussing the validity of the transformer model in section 5.5.7.

The rectifier model managed to turn the three sine waves into a single wave, reflective of the rectified voltage derived from an AC voltage source. As can be seen in figure 31 and figure 32, the rectified voltage is higher than the lowered AC voltage in both cases. This is expected since the rectifier model was based on a three-phase full wave six diode bridge rectifier which, as explained previously in section 3.3.9. In figure 31 and figure 32 the ripple of the rectified voltage is visible as small fluctuations on the variable V_{rect} in the simulation. What ripple does and why it occurs was briefly explained in section 3.3.9 as well. The numerical results of the rectifier presented in tables 35a and 35b are interesting to have a closer look at. Since the current in the rectifier is derived from a connected load, the values for the DC power output, P_{DC}, have different values in both simulations. This is due to the change in the rectifier current since the desired current in the electrical control model was changed after 5 seconds as previously mentioned. Additionally, the parameter input of the rectifier efficiency was hard to determine correctly. Whether the used rectifier efficiencies, presented in tables 34a and 32, are accurate or not will be further discussed when validating the rectifier model in section 5.5.8.

When looking at the results from simulations 1 and 2 of the electrical control and PI-controller, it seems that the models were able to correctly determine the error signal and in turn, control the output current of the power supply unit. This can be seen in both figure 33 and figure 34. The rate at which the slope of the current I_{actual} is either rising or falling over time is also affected by the input parameters presented in tables 36a and 36b.

The error signal in both simulations was determined by taking the difference between the actual output current and the desired output current as previously done in equation 38. In conclusion, the electrical control and PI-controller models managed to create a feedback loop which in turn gradually lowered the error signal until there was no difference left between the desired and actual output currents.

5.3.2 Design choices and limitations

When designing the power supply unit of the digital twin, the main task was to create an interactive, three-phase AC voltage source and some intermediate models which could be used to supply the electrolyzer stack with electricity. Through discussions with the thesis' supervisors, it was agreed upon that the models did not have to include the electrical circuits. The inclusion of power components like inductors, capacitors, diodes, and so on was therefore not necessary in the electrical models of the digital twin. The idea was then instead to find relevant equations, either online or through literature, to imitate the behavior of the specific power electronics that were to be modeled.

As stated previously, the information from the power supply model was used in all the other electrical models. To be able to transport this information, some sort of connectors between the models had to be used. Normally for electrical models in Modelica, electrical pin connectors are used. Electrical pin connectors allow for the voltage and current to flow from one model to another. However, this type of connector was not used on most of the electrical models as it allowed little customization for defining which variables should be transferred. Therefore, custom connectors were created in the power supply unit and implemented on the electrical models. These custom connectors allowed the transport of multiple variables, for example, the three different sine wave variables from the power supply model, to be transported to the transformer model and used. Doing this made it relatively easy to transfer desired values from one model to another. However, the downside to using this method is that the electrical balances of the models are not upheld. The electrical values are instead treated like information with no flow. Fortunately, due to the simplicity of the electrical models in the digital twin, treating the electrical values as information works just fine since they are compatible with the implemented equations and provide expected results as discussed earlier in section 5.3.1.

5.3.3 Sources of error

Human error in the form of misinterpreting literature or failing to understand the desired behavior of a model is undoubtedly some of the largest sources of error within the power supply unit. Finding the correct equations for a model for example proved difficult, as many of these equations can be found online. These equations are then often based on specifics like if there is a single phase or three-phase AC voltage being supplied. How many diodes a rectifier has and whether it is a full wave, half wave, three-phase full wave, or three-phase half wave are examples of specifics that are important to keep in mind when simply looking for the correct equations. Often, especially when found online, the equations are not labeled regarding these critical specifics. This may cause the models to behave inaccurately. The authors had little to no experience with power electronics prior to this thesis, hence why finding the correct information in the electrical models could be difficult. Therefore, critical thinking, cross-reference checking of sources, and some guidance from the supervisors were measurements taken to minimize these sources of error.

Another possible source of error is the simplified nature of the electrical models. Since electrical circuits were not modeled, a great layer of depth was lost. This makes it more difficult to assume and calculate the power losses, power output and efficiencies in the electrical models, especially the models imitating the power electronics. This is due to the fact that some expected losses can only be input as parameters in the models and several different types of losses are not taken into consideration at all. The impact of these simplifications does not necessarily act as a source of error regarding the design choices and the following results presented in section 4.3, but acts instead as a source of error in regards to the model's real-world validity. This will be discussed more thoroughly in section 5.5.

A general weakness of the power supply unit is how much a high frequency on the three-phase AC voltage slows down the simulation time in Modelica. This became especially apparent when the combined system was simulated in section 4.4. Due to this, the frequency parameter in the power supply model was set to 1 Hz as specified in table 43 in order to simulate. Although this did not cause any problems during this simulation, it might cause some in the future. As the complexity of the models within the digital twin are increased, more components which utilise frequency will most likely be added. An example could be in the case that a switch is added. A switch operates often in the kHz range in order to control the current or voltage going into the electrolyzer stack [44]. Having such a high frequency on a switch would undoubtedly cause very long simulation times and lowering the switching frequency might cause it to no longer work . This does not necessarily act as a source of error, since letting the simulation run for a longer period of time with the needed frequency should still work. However, if the simulation crashes midway through or the parameter inputs were wrong, it will be a timely process.

Lastly, input of the wrong or unrealistic parameters is also a great source of error in the power supply unit that will affect the results of the models greatly. It is for example possible to create situations where the efficiency of some models might exceed 100%. This should not occur if built in values in the Modelica Standard Library, like efficiency, are used when defining the different variables. Modelica will still simulate if it can, but the user will be informed through the message toolbar if any unrealistic values occur. Therefore, determining which parameters work together in the power supply unit and in general, is instrumental in order to have the models behave as they were designed to.

5.4 The combined system

Discussion around the results and possible sources of error of the combined system is presented in this section. Design choices and limitations are not discussed for the combined systems due to the fact that all the connected subsystems, like the power supply unit, have already been discussed. The electrolyzer stack, which was provided by Hystar, was not created by the authors of this thesis. Therefore, discussing design choices and limitations of the stack itself would be difficult and most likely inaccurate.

5.4.1 Results

The desired pressure of the system is maintained for both the anode and cathode side, as shown in figure 35 and figure 37 respectively. These values are as expected, and show that the system is responding well to the predetermined reference pressures. The change in actual pressure is somewhat abrupt, but this is mainly due to the pressure being controlled by a simplified control loop instead of an actual regulator with appropriate settings.

The temperature outlet of the anode flow is presented in figure 36, and is highly dependent on the other models of the combined system. Initially the temperature rises when the current is high. When the current is reduced from 1500 ampere to 1000 ampere at 50 seconds, the temperature starts decreasing down towards its reference value. The desired current is presented in table 37. The fact that the temperature still increases when the current is high, and that it seemingly does not reach its desired temperature even when the current is lowered, might indicate that the cooling is insufficient. Still, the fact that the temperature is affected by the current at all shows that the combined system is at least simulating correctly.

The hydrogen production rate is presented in figure 38. The decreased production rate at 50 seconds is expected, most likely due to the sudden change of the current. However, the continuous decrease under most of the simulation is an abnormality. Exactly why this happens is unknown, since explaining and understanding all the code within the electrolyzer stack is outside the scope of the project.

The voltage into the electrolyzer stack from the power supply behaved as expected in the simulation of the combined system. The voltage, which can be seen in figure 39, was initially at around 20 volts before it dropped down to about 18 volts when the current, which was presented as an input parameter in table 43, was reduced 50 seconds into the simulation. The AC power input and the DC power output of the rectifier, as well as the actual DC power input into the electrolyzer stack is shown in figure 40. The actual DC power input into the stack is greatly different from the DC power output of the rectifier. This is due to the fact that the output voltage of the electrical control model was calculated from the u signal as mentioned earlier. This output voltage is then multiplied with the I_{actual} current in order to find the actual DC power output.

The calculated temperature of the electrolyzer stack's membrane, anode liquid and cathode liquid, presented in figure 41, shows an initially steep increase the first 10 seconds before it eventually is cooled and increases at a much slower rate. Still, the fact that the temperature continues to increase means that the cooling system is not correctly tuned to the electrolyzer stack, or that an additional cooling system unit should be directly connected to the stack as well. The polarization curve for a single cell in the stack is presented in figure 42. The polarization curve is an important parameter for any electrochemical reaction, as it is often used to assess the performance of the PEM electrolyzer. In the polarization curve, it is possible to often see losses such as activation losses, ohmic losses and concentration losses [49]. The polarization curve appears to be mostly linear, meaning that the ohmic losses are most likely present in the model. As for the activation losses and concentration losses, they do not seem to occur. Whether or not this is due to the stack model from Hystar, or the incorrect use of input parameters in the other models is unknown.

5.4.2 Sources of error

During the simulations of the combined system, the compatibility of the input parameters and initialization values between all models played a major role in whether or not the simulation was able to initialize and run. If the cooling system was not tuned to the electrolyzer stack's heat generation, or the wrong initialization values were used then the simulation would often crash. Lack of sufficient real-world data to use in the created models made the process of getting the simulation to run one of trial and error. The supervisors provided some parameters which could be used in the stack, but for the other models the values had to be guessed. Still, the simulation of the combined system was eventually able to run, returning mostly expected results.

Other sources of error include the DC power output of the rectifier not being supplied to the stack. This source of error is similar to the error in the power supply unit where the output voltage is not derived from the rectifier either. Still, these values can later be implemented which will be discussed in section 5.6.3. The complexity of the combined system, with long simulation times, several crashes and many new parameters introduced in the stack, made the consistent use of the same simulation parameters often difficult. Sometimes Modelica would behave strangely and seemingly delete several packages from the combined file. Measures were taken in order to keep the input parameters and initialization values as similar as possible between the simulations done and presented in section 4.4.

5.5 Validation

To determine the validity of the created models, each component is compared individually to its real-world behavior where it is possible to do so. Preferably the validation process of each model also consists of results from a great amount of sources. This is done in order to prevent the models in the digital twin from being an exact replica of a real-world component from a single source, but rather having them as generic and robust models that are flexible while still returning expected results compared to their real-world behaviour from several sources.

5.5.1 Centrifugal pump

As the centrifugal pump operates as a generic pump, validation of this pump is hard. One can assume that there are great differences in expected and actual results due to an inaccurate pump curve. However, the working principles of the pump is theoretically valid as shown in section 5.1.1. The flow is dependent on the inlet and outlet pressure, as well as the power output.

5.5.2 Valve

Since the valve is modeled as a way to control pressure drop and resistance to mass flow, results presented in figure 20 and figure 19 indicate this working principle. Further validation against real world data requires an actual valve and knowledge regarding its curve. This valve can simply be validated as a working linear valve from figure 19.

5.5.3 Heat exchanger

As explained in section 5.2, the heat exchangers efficiency is on the lower end, with a value of *55%*. Compared to a physical heat exchanger based on counter-current flow and the use of the NTU method, higher efficiency is expected. It proved difficult to find a way to accurately validate the heat exchanger, therefore a comparison to known behavior is done. The digital heat exchanger model's efficiency is greatly dependent on the mass flow rates of both the cooled and heated medium. In addition to this the area of the heat exchanger is an important factor, an area that was assumed to be *0.31* m^2.

5.5.4 Cooler

The cooler is primarily built up around the centrifugal pump, which controls the desired amount of coolant medium circulated. Therefore, a validation of the cooling system is greatly contiguous with the validity of the centrifugal pump. As previously explained, validating this component proved to be difficult as there are no experimental data available to accurately compare the simulated data to. However, conclusions can be drawn by evaluating the cooler's ability to dissipate heat with already known physical behavior in a system.

5.5.5 Liquid-gas separator

The liquid-gas separator model is hard to validate as its behaviour depends on multiple parameters, variables, assumptions and initial values. To perform some form of validation for the model would require an elaborate experiment or data from an actual volume operating in the same matter as the liquid-gas separator. Validating that the volume operates exactly as a physical volume would is hard, but validating the working principles can be done and has been simulated and shown in section 4.1.1.

5.5.6 Power supply

Verifying the exact real-world behavior of the model for the power supply proved difficult due to the complexity of a three-phase AC source. The behavioral data used to create the model for the power supply were theoretical approximations. These approximations were assumed to resemble the model's real-world behavior close enough for the model to be valid, at least within the scope of this thesis. Validating the power supply model any further would therefore be a difficult task without a laboratory with electrical equipment or data provided from real-world experiments. The use of a laboratory was outside the scope of the thesis and was not deemed necessary as the development of the models themselves was instead prioritized. Still, there are undoubtedly going to be losses of some sort that will diminish the validity of the power supply model. These losses might for example occur either through voltage drop due to internal resistances of wiring or heat dissipation. These types of losses are neglected in the model. The power supply model is, as shown previously in section 3.3.7, solely based on equations used to determine its expected behavior, like the sinusoidal nature of the AC voltage.

5.5.7 AC/AC transformer

The transformer model faces a lot of the same problems as the power supply model does when it comes to performing a validation process. For example, the relation between the number of windings on the primary and secondary side and the consequential lowering of the AC voltage seems like behavior that did not exactly need to be modeled more complicated than how it already has been done.

However, the transformer model does, unlike the model for the power supply, include some losses as input parameters. These losses have been explained in detail previously in chapter 3.3.8, and add more realism to the transformer model as it directly affects the efficiency. The power factor, as previously explained in section 3.3.8, is also a parameter that can be given an input value to increase its validity. These steps are measures taken in order to make the model more realistic. As seen in tables 32a and 32b, the efficiency of the transformer model lies between $92.5 - 98.8\%$ in the two simulations that were run.

When comparing these simulated transformer efficiencies to the results from an efficiency analysis on transformers done in a heavy current laboratory [50], it becomes apparent that the simulated efficiencies might be too high. Even if the transformer model is assumed to be constantly operating at 100% of the rated load, which it is in the transformer model, the range of $92.5 - 98.8\%$ seems unlikely when compared to the results from the heavy current laboratory where the efficiency range was from 88% to 90.5%. However, this discrepancy is most likely due to the use of different parameters in the Modelica simulations and the efficiency analysis in heavy current lab simulations. The lack of complexity in the transformer model compared to the real transformer used in the heavy current lab is also important to keep in mind. Even if this analysis seem to indicate that the transformer model is wrong, another source claim that transformer efficiencies, especially in low voltage distribution transformers, can be anywhere between 97% to 99.3% depending on how many phases there are, type of transformer, and the voltage [51]. Still, more data would preferably be available in order to compare the transformer model to several other transformers, as this would greatly help in further improving the model's source code as well as validating it. However, no more usable data to validate the transformer model was found or received.

5.5.8 AC/DC Rectifier

The rectifier model is perhaps one of the most simplified models within the power supply unit compared to its intended real-world counterpart. As established, the rectifier is based on a three-phase six diode bridge full wave rectifier, so finding real-world data derived from such a rectifier would be useful to draw some comparisons. However, this proved to be quite difficult.

An attempt to determine whether or not the high input efficiency of the rectifier model, presented in tables 34a and 34b in section 4.3.3, were plausible was done. In an article found online, called "Performances/efficiency analysis for high efficiency three-phase buck-type PFC rectifiers", the rectifier efficiencies were found to be between 97.6% and 98.7% depending on the output power and the specific type of rectifier presented in the article [52]. In another article found online called "Rectifier efficiency analysis for DC distributed data centers", efficiencies for a multi-pulse rectifier at different loads were found to be between 96.5% to 98.1%. In the same paper, efficiencies of a three-phase buck-type current source rectifier at different loads were found to be between 97.6% and 99.2% [53]. Although these efficiencies are specific to the type of rectifiers used in the articles, the results from these articles imply at least that efficiencies above 90% are possible for three-phase rectifiers. It is important to note that the results from these articles were based on digital models and simulations as well, meaning that these are not real-world data. Still, the complexity of the rectifiers in these articles is much higher than that of the rectifier model in this thesis. Therefore, they help to validate that at least the relatively high input rectifier efficiencies in the rectifier model is not blatantly wrong.

5.5.9 Electrical control and PI-controller

The electrical control and PI-controller models might be the most difficult models to validate, at least within the power supply unit. This is because of how much they are simplified in order to produce the output voltage. As already established, the output voltage is calculated based on the u signal and the feed forward. Since this is not the correct use of the u signal, the best way to validate the electrical control and PI-controller would be to improve the power supply unit as a whole so that the u signal could be implemented realistically. This will be further discussed in section 5.6.3.

5.6 Further development

The digital twin developed in this project is created over the duration of one semester. Consequently, the complexity of certain components is diminished to keep the project within its scope. Therefore, the inclusion of recommended further developments is of great potential use. Comments and recommendations are structured into the model's subsystems, and lastly the combined system. Further development of model validation is also included, as increased validity is greatly of use to the digital twin's accuracy and reliability.

5.6.1 The liquid-gas separator unit

The liquid-gas separator includes, as stated earlier, several simplifications and assumptions. The assumption of instantaneous mixing between in flowing medium and the medium occupying the volume is a simplification which could be elaborated with further work by adding a constant or actual equations for the mixing of a volume. The heat transfer between the mediums inside the volume is also a simplification which can be more accurately defined. Further work would include adding heat transfer coefficients for both mediums and from there calculate an overall heat transfer coefficient to calculate the heat transfer rate. To do this the area of heat exchange would also have to be known, so including the geometry of the volume should also be added.

The simplification made to transfer the gas and liquid out of the stack in its constituent phases were described previously, as the complexity of multi-phase compounds proved to be high. To further increase the realism of the liquid-gas separator unit further development of the medium composition would be beneficial to mirror the real-world behavior of the mediums to a greater extent.

As previously mentioned, the purification unit of both the water and the hydrogen gas were excluded in order to limit the scope of the project. However, having this subsystem implemented as part of the future development would likely increase the validity of the digital twin.

Including an actual pump curve relating both power, head and flow should be implemented as a part of the further development. It should also be possible to add the pump efficiency as part of this relation, where the efficiency varies according to the operating point of the pump. The generic placeholder for the pump curve only allows a maximum volume flow rate of $10 m^3/h$. This should be addressed and fixed. Adding an actual pump curve to the pump of type predescribed mass flow rate could also be done.

Another limitation of the pump is the pump's inability to handle a reverse flowing stream. Should this occur, the simulation will fail. This can be avoided by providing plausible parameters and operating conditions, but an extra override algorithm setting the mass flow to zero at reverse flow conditions could also have been added. Further development should also include a way to secure no reverse flow initial values, as the pump often has reverse flow for no apparent reason. This however is only of interest for the pump with a pump curve, as the pump with predescribed mass flow does no experience these problems.

The valve is working as it should but further development is advised. The main concept that should be introduced is the inclusion of a nominal pressure drop at full opening, and a nominal leakage at full closure. These additions should replace the if loop that strictly makes the opening never fully open and never fully closed. The addition of an equal percentage valve option could also be of interest if this was to be the desired type of valve for a user of the digital twin.

5.6.2 The cooling system unit

The cooling system unit can be further developed in several ways to enhance the accuracy and increase the system's complexity to resemble its physical counterpart to a greater extent. For the heat exchangers part, taking basis in an actual heat exchanger used for PEM electrolysis could be beneficial. As the model created in the project is solely based on equations, some parameters potentially deviate from the actual heat exchanger desired in the physical system. This is especially applicable for the geometric design of the exchanger, as this would make the area an accurate parameter.

If physical properties are known to a greater extent, the HEX digital model could calculate the heat transfer more accurately by factoring in the boundary layer and the mediums type of flow. This would make the overall heat transfer coefficient, U, a variable and thus the model more accurate and suitable to change. In addition, the digital model of the heat exchanger could be further developed to be capable of certain scenarios. The developed HEX model had some initialization problems, as it would consider the mass flow equal to zero at zero seconds. This could be further developed and fixed by improving the model's flexibility by defining stricter initial values.

The cooler model also has the potential for improvement. This could include the implementation of a heat sink model in the circuit to increase the heat dissipated.

5.6.3 The power supply unit

The power supply unit could drastically increase its accuracy and validity if the models were made more akin to their real-world counterparts, which was concluded when discussing each of the power supply models' validity in section 5.5.6. By implementing and modeling the electrical circuits specific to each of the power electronics, a new layer of depth will be added which allows for more accurate behavior of the power supply unit. If power components like capacitors, inductors, diodes, and so on are included, it will be much easier to calculate for example the losses in each model as well as to be able to simulate the models' real-world behavior more accurately.

By modeling the electrical circuits of each power electronic in the power supply unit, a smoothing capacitor could have been added to the circuit of the rectifier to reduce the ripple of the rectified voltage [54]. Although the rectified voltage is not used directly in the electrical control model to supply the electrolyzer stack as of now, reducing the ripple will still remove some of the expected losses of the actual DC power output in an updated model. Implementation of equations and models addressing other losses, such as internal resistance through wiring between the models or within, would also greatly increase the models' validity and in turn the digital twin's validity.

Updating the electrical control model would also be useful as a part of the digital twins' further development. With added electrical circuits to the power electronic models, new parameters and variables are introduced that can more easily utilize the u signal in a more realistic manner than how it currently is being used. This will in turn make it easier to implement for example a switch and thereby regulate the output voltage and current more efficiently. If this is implemented, the output voltage and current of the power supply unit will then be able to be derived from the rectifier model directly, instead of input in the electrical control model as predetermined parameters. This would in turn allow for nuances like the ripple to have an impact on the performance of the electrolyzer stack, as well as the power supply unit. As of now, the output voltage is solely determined by the input desired current in the electrical control model, which unfortunately does not take into consideration the rectified voltage variable at all as previously established.

Sensors in the power supply unit are something that also could be added as a part of future development. The sensors could then for example be used to keep track of the behavior of the power components within the electrical circuits as well as on the connectors between the power electronic models. If further development of the power supply unit incorporates the electrical circuits within the models, the customized connectors which are currently used can be replaced with the electrical pin ports. By doing this, the electrical balance of the entire power supply should be much easier to check and maintain, removing potential sources of error and unrealistic behavior.

Implementation of electrical circuits and an overly complex control system was initially not necessary when discussing modeling of the power supply unit with the thesis' supervisors. Still, for future development of the power supply unit these aspects, as well as implementation of sensors, could be worth looking into since the options to optimize something in Modelica are endless. Doing measures like these would also greatly benefit the models' further validation process. The only limit when using Modelica is the user's creativity, experience, and knowledge of desired model behavior.

5.6.4 The combined system

The further development of the combined system is related to the improvements provided for each unit previously. However, a few new aspects can be of interest. One of these being the interactions between the components combined in the combined system. As the Balance of Plant and the electrolysis stack is created by different developers, potential differences in the way the models behave arises. To minimize the potential effects of this, it would be beneficial to further examine and look into both models in greater depth.

The digital models were previously validated individually, this required experimental data that were unavailable for some of the components developed. If the combined system could undergo an additional validation by comparing real-world data to the digital twin ran at equal parameters it could reinforce the models validity further. However, this might prove difficult and counter-intuitive since the main purpose of creating a digital twin is to save money by not having to buy physical components. If real-world data were gathered by buying physical components and test them, the point of having the digital twin in the first place would be lost.

Including regulators with appropriate settings would create a smoother regulation of the system. This would also potentially contribute to a quicker response time of the combined system.

6 Conclusion

The objective of this study was to develop a digital twin of a next generation PEM electrolyzer. The thesis aimed to describe and document the end product developed by using the object-oriented programming language Modelica. To conclude the work done it is important to evaluate the results produced.

It is apparent that the main objective of the thesis is fulfilled. A digital twin of the PEM electrolyzer's Balance of Plant has been developed, and has been proven to be compatible with the electrolysis stack developed by Hystar. Supplementary, documentation of the work done have been presented in this thesis. Still, there are certain aspects of the digital models behavior that needs to be addressed, especially when the system is combined.

During simulations of each component individually, realistic behavior was achieved to a great extent. The developed pump worked as desired and facilitated for an accurate representation when given a fitting pump curve. The valve model achieved the desired behavior, as well as containing the necessary fail safe additions preventing the model from crashing a simulation at specific adverse values. The liquid-gas separator, though containing some simplifications, simulated and ran well despite being a highly complex and extensive model. It was also easy to implement it into a bigger system. The heat exchanger showed some discrepancies regarding the effectiveness, and a validation compared to normal behavior proved to be difficult without experimental data. However, the HEX generally showed expected behavior in regards to heat transfer when combined with the cooling system unit. The electrical models of the power supply unit managed to create a voltage source for the electrolyzer stack. This voltage source was then able to be both lowered and rectified. The power supply unit also managed to lay the foundation for further and more complex development of the power supply unit, where for example the rectified voltage can be directly controlled and supplied to the electrolyzer stack. Validation of the created models proved to be difficult due to limitations in resources and relevant literature.

Combining the system increased the overall complexity of the system. Still, simulations were able to run and desired results were gathered. Although many of the results received from the simulation of the combined system were as expected, there were still some major issues regarding inadequate cooling of the electrolyzer stack and some problems with initialization. Future implementation of a cooling system directly connected to the stack is highly recommended in order to counter the inadequate cooling of the electrolyzer stack.

In conclusion, many of the thesis' goals were achieved. The models behaved for the most part according to their design, and could be combined into larger and more complex models with relative ease. Still, further development is necessary in order to increase the overall accuracy, validity and compatibility of the digital twin created in this thesis.

Reference List

[1] Hannah Ritchie, Max Roser and Pablo Rosado. 'CO and Greenhouse Gas Emissions'. In: *Our World in Data* (May 2020). URL: https://ourworldindata.org/emissions-by-sector (visited on 09/05/2022).

[2] *Hydrogen - energy system disruptor?* URL: https://www.dnv.com/to2030/technology/hydrogen-energy-system-disruptor.html (visited on 15/05/2022).

[3] *Hydrogen Council - "Hydrogen, Scaling Up"*. URL: https://hydrogencouncil.com/en/study-hydrogen-scaling-up/ (visited on 08/04/2022).

[4] nationalgrid. *The hydrogen colour spectrum*. URL: https://www.nationalgrid.com/stories/energy-explained/hydrogen-colour-spectrum. (Accessed: 01.04.2022).

[5] *Hydrogen production by PEM water electrolysis A review — Elsevier Enhanced Reader*. URL: https://reader.elsevier.com/reader/sd/pii/S2589299119300035?token=705165F792B6100654E841387638596C6E58CAB8CB4F78A36470FDDE5FDAE0D7B96C711302AD03136EAC459E1E46BD2B&originRegion=eu-west-1&originCreation=20220408124309 (visited on 08/04/2022).

[6] Sumit Sood et al. 'Generic Dynamical Model of PEM Electrolyser under Intermittent Sources'. In: *Energies* 13.24 (Jan. 2020). Number: 24 Publisher: Multidisciplinary Digital Publishing Institute, p. 6556. ISSN: 1996-1073. URL: https://www.mdpi.com/1996-1073/13/24/6556 (visited on 29/03/2022).

[7] Bo Han et al. 'Electrochemical performance modeling of a proton exchange membrane electrolyzer cell for hydrogen energy'. In: *International Journal of Hydrogen Energy* 40.22 (June 2015), pp. 7006–7016. ISSN: 0360-3199. URL: https://www.sciencedirect.com/science/article/pii/S036031991500837X (visited on 02/05/2022).

[8] *The Future of Hydrogen – Analysis*. URL: https://www.iea.org/reports/the-future-of-hydrogen (visited on 11/04/2022).

[9] *What is Digital Twin Technology and How Does it Work?* en-GB. URL: https://www.twi-global.com/technical-knowledge/faqs/what-is-digital-twin.aspx (visited on 10/05/2022).

[10] *Diagram Software and Flowchart Maker*. URL: https://www.diagrams.net/ (visited on 19/05/2022).

[11] *The Modelica Association — Modelica Association*. URL: https://modelica.org/ (visited on 28/03/2022).

[12] Modelica association. *Download Modelica for windows*. URL: https://openmodelica.org/download/download-windows. (Accessed: 28.03.2022).

[13] Modelica. *Modelica by Example*. URL: https://mbe.modelica.university/ (visited on 28/03/2022).

[14] Syed Adeel Asghar and Sonia Tariq. *Design and Implementation of a User Friendly OpenModelica Graphical Connection Editor*. 2010. URL: http://urn.kb.se/resolve?urn=urn:nbn:se:liu:diva-65864 (visited on 11/04/2022).

[15] *A review on PEM electrolyzer modelling: Guidelines for beginners — Elsevier Enhanced Reader*. URL: https://reader.elsevier.com/reader/sd/pii/S0959652620312312?token=96BBAEEA83A27045C9F1E0DC4C51094BF7B328A4D488701E800D74BCF3BF6DC16594256E49DE07659352B2F6489783E1&originRegion=eu-west-1&originCreation=20220329105830 (visited on 29/03/2022).

[16] *VIRTUAL-FCS*. en. URL: https://www.sintef.no/projectweb/virtual-fcs/ (visited on 14/05/2022).

[17] Michael Smith Engineers ltd. *Useful information on centrifugal pumps*. URL: https://www.michael-smith-engineers.co.uk/resources/useful-info/centrifugal-pumps. (Accessed: 05.04.2022).

[18] John M. Cimbala Yunus A. Cengel. *Fluid Mechanics. Chapter 5.4 - The Bernoulli Equation*. Third Edition. McGraw-Hill, 2014, pp. 199–207.

[19] Pumps&Systems Jim Swetye. *Useful information on centrifugal pumps*. URL: https://www.pumpsandsystems.com/pumps/reading-centrifugal-pump-curve. (Accessed: 11.04.2022).

[20] John M. Cimbala Yunus A. Cengel. *Fluid Mechanics. Chapter 8 - Internal Flow.* Third Edition. McGraw-Hill, 2014, pp. 347–419.

[21] Editorial Staff. *Valve Characteristics - Quick Opening, Linear & Equal Percentage.* en-US. Feb. 2019. URL: https://instrumentationtools.com/valve-characteristics/ (visited on 12/05/2022).

[22] *Control Valve performance parameters.* en-US. Dec. 2020. URL: https://theinstrumentguru.com/control-valve-performance-parameters/ (visited on 12/05/2022).

[23] John M. Cimbala Yunus A. Cengel. *Fluid Mechanics. Properties of Fluids.* Third Edition. McGraw-Hill, 2014, pp. 37–63.

[24] *PEM Water Electrolysis, Volume 1 - 1st Edition.* URL: https://www.elsevier.com/books/pem-water-electrolysis/bessarabov/978-0-12-811145-1 (visited on 05/04/2022).

[25] John M. Cimbala Yunus A. Cengel. *Fluid Mechanics. Fundementals and Applications.* Third Edition. McGraw-Hill, 2014, pp. 186–191.

[26] John M. Cimbala Yunus A. Cengel. *Fluid Mechanics. Fundementals and Applications.* Third Edition. McGraw-Hill, 2014, pp. 214–230.

[27] Theodore L. Bergman & Adrienne S. Lavine Frank P. Incropera Drew P. DeWitt. *Fundamentals of heat and mass transfer. Chapter 11 - Heat Exchangers.* John Wiley & Sons US, 2006, pp. 492–534. ISBN: 978-0-12-811407-0.

[28] Nick Connor. *What is Logarithmic Mean Temperature Difference – LMTD – Definition.* URL: https://www.thermal-engineering.org/what-is-logarithmic-mean-temperature-difference-lmtd-definition/. (Accessed: 11.04.2022).

[29] Robert L. Boylestad. *Introductory Circuit Analysis. Chapter 13 - Sinusoidal Alternating Waveforms.* 13th edition. Pearson, 2016, pp. 570–621.

[30] A.G. Tsikalakis and Z.N. Vrontisi. '3.10 - Energy Networks'. In: *Climate Vulnerability.* Ed. by Roger A. Pielke. Oxford: Academic Press, 2013, pp. 135–147. ISBN: 978-0-12-384704-1. URL: https://www.sciencedirect.com/science/article/pii/B9780123847034003191.

[31] Thomas Shoemaker James E. Mack. *The Lineman's and Cableman's Handbook. Chapter 15 – Distribution Transformers.* 11th edition. New York: McGraw-Hill, 2006.

[32] Linquip. *What is the Efficiency of Transformer?* URL: https://www.linquip.com/blog/efficiency-of-transformer/. (visited on 22/04/2022).

[33] Blackhawk Supply. *SINGLE AND THREE-PHASE AC POWER CALCULATOR. Kilowatts from Amps (line-to-neutral voltage).* URL: https://blackhawksupply.com/pages/single-and-three-phase-ac-power-calculator-amps-to-kilowatts?fbclid=IwAR1Ohj-SwjuC4too-uUk7Jm7IOBCdxF2st0kZzXDlxZ5LbQA7HroSoowRD8. (visited on 22/04/2022).

[34] Britannica. *Hysteresis losses.* URL: https://www.britannica.com/science/hysteresis-loss. (visited on 21/04/2022).

[35] Farnell. *Eddy current losses.* URL: https://il.farnell.com/eddy-current-loss-definition. (visited on 21/04/2022).

[36] J.F. Manwell. *Hybrid Energy Systems.* Ed. by Cutler J. Cleveland. New York: Elsevier, 2004, pp. 215–229. ISBN: 978-0-12-176480-7. DOI: https://doi.org/10.1016/B0-12-176480-X/00360-0. URL: https://www.sciencedirect.com/science/article/pii/B012176480X003600.

[37] ElectronicsTutorials. *Three Phase Rectification.* URL: https://www.electronics-tutorials.ws/power/three-phase-rectification.html. (visited on 02/05/2022).

[38] Electronicscoach. *3 Phase Rectifier. 3 Phase Bridge Rectifier.* URL: https://electronicscoach.com/3-phase-rectifier.html. (visited on 5/05/2022).

[39] Yim-Shu Lee and Martin H.L. Chow. *7 - Diode Rectifiers*. Ed. by Muhammad H. Rashid. Fourth Edition. Butterworth-Heinemann, 2018, pp. 177–208. ISBN: 978-0-12-811407-0. DOI: https://doi.org/10.1016/B978-0-12-811407-0.00007-6. URL: https://www.sciencedirect.com/science/article/pii/B9780128114070000076.

[40] electricalbaba. *What is Ripple and Ripple Factor? – Formula of Ripple Factor*. URL: https://electricalbaba.com/ripple-factor-definition-formula-derivation/. (visited on 11/05/2022).

[41] Muhammad H. Rashid. '9 - Three-Phase Controlled Rectifiers'. In: *Power Electronics Handbook (Fourth Edition)*. Ed. by Muhammad H. Rashid. Fourth Edition. Butterworth-Heinemann, 2018, pp. 233–273. ISBN: 978-0-12-811407-0. DOI: https://doi.org/10.1016/B978-0-12-811407-0.00009-X. URL: https://www.sciencedirect.com/science/article/pii/B978012811407000009X.

[42] Robert L. Boylestad. *Introductory Circuit Analysis. Chapter 4 - Ohm's Law, Power and Energy Objectives*. 13th edition. Pearson, 2016, pp. 120–157.

[43] Saeid Mokhatab and William A. Poe. *Chapter 14 - Process Control Fundamentals*. Ed. by Saeid Mokhatab and William A. Poe. Second Edition. Boston: Gulf Professional Publishing, 2012, pp. 473–509. ISBN: 978-0-12-386914-2. DOI: https://doi.org/10.1016/B978-0-12-386914-2.00014-5. URL: https://www.sciencedirect.com/science/article/pii/B9780123869142000145.

[44] Steven Frank Barrett and Daniel J. Pack. *Microcontrollers Fundamentals for Engineers and Scientists. "Timing subsystem"*. Morgan and Claypool Publishers, 2006, pp. 51–64. ISBN: 1-598-29058-4.

[45] Synopsys. *What are power electronics?* URL: https://www.synopsys.com/glossary/what-are-power-electronics.html. (visited on 04/05/2022).

[46] Julio José Caparrós Mancera et al. 'An Optimized Balance of Plant for a Medium-Size PEM Electrolyzer: Design, Control and Physical Implementation'. en. In: *Electronics* 9.5 (May 2020). Number: 5 Publisher: Multidisciplinary Digital Publishing Institute, p. 871. ISSN: 2079-9292. DOI: 10.3390/electronics9050871. URL: https://www.mdpi.com/2079-9292/9/5/871 (visited on 19/05/2022).

[47] Worldstandards. *Norway – Power plug, socket & mains voltage in Norway*. URL: https://www.worldstandards.eu/electricity/plug-voltage-by-country/norway/. (visited on 22/04/2022).

[48] *Overall Heat Transfer Coefficients in Heat Exchangers*. URL: https://www.engineersedge.com/heat_transfer/overall_heat_transfer_coefficients_13827.htm (visited on 15/05/2022).

[49] P. Millet. *18 - Membrane electrolysers for hydrogen (H2) production*. Ed. by Angelo Basile and Suzana Pereira Nunes. Woodhead Publishing Series in Energy. Woodhead Publishing, 2011, pp. 568–609. ISBN: 978-1-84569-969-7. DOI: https://doi.org/10.1533/9780857093790.4.568. URL: https://www.sciencedirect.com/science/article/pii/B9781845699697500187.

[50] R. Gouws and O. Dobzhanskyi. 'Efficiency analysis of a three-phase power transformer for industry applications operated under different load conditions'. In: *2013 Proceedings of the 10th Industrial and Commercial Use of Energy Conference*. 2013, pp. 1–5.

[51] OLSUNElectornics. *Efficiency of distribution transformers*. URL: https://www.olsun.com/distribution-transformer-efficiency/. (Accessed: 10.05.2022).

[52] Nicola-Valeriu Olarescu et al. 'Performances/efficiency analysis for high efficiency three-phase buck-type PFC rectifiers'. In: *2015 17th European Conference on Power Electronics and Applications (EPE'15 ECCE-Europe)*. 2015, pp. 1–9. DOI: 10.1109/EPE.2015.7311752.

[53] Seyed Ahmad Hamidi, Adel Nasiri and Zhao Tiefu. 'Rectifier efficiency analysis for DC distributed data centers'. In: *2014 International Conference on Renewable Energy Research and Application (ICRERA)*. 2014, pp. 776–779. DOI: 10.1109/ICRERA.2014.7016490.

[54] electronicsnotes. *Capacitor Smoothing Circuits & Calculations*. URL: https://www.electronics-notes.com/articles/analogue_circuits/power-supply-electronics/capacitor-smoothing-circuits.php. (visited on 10/05/2022).

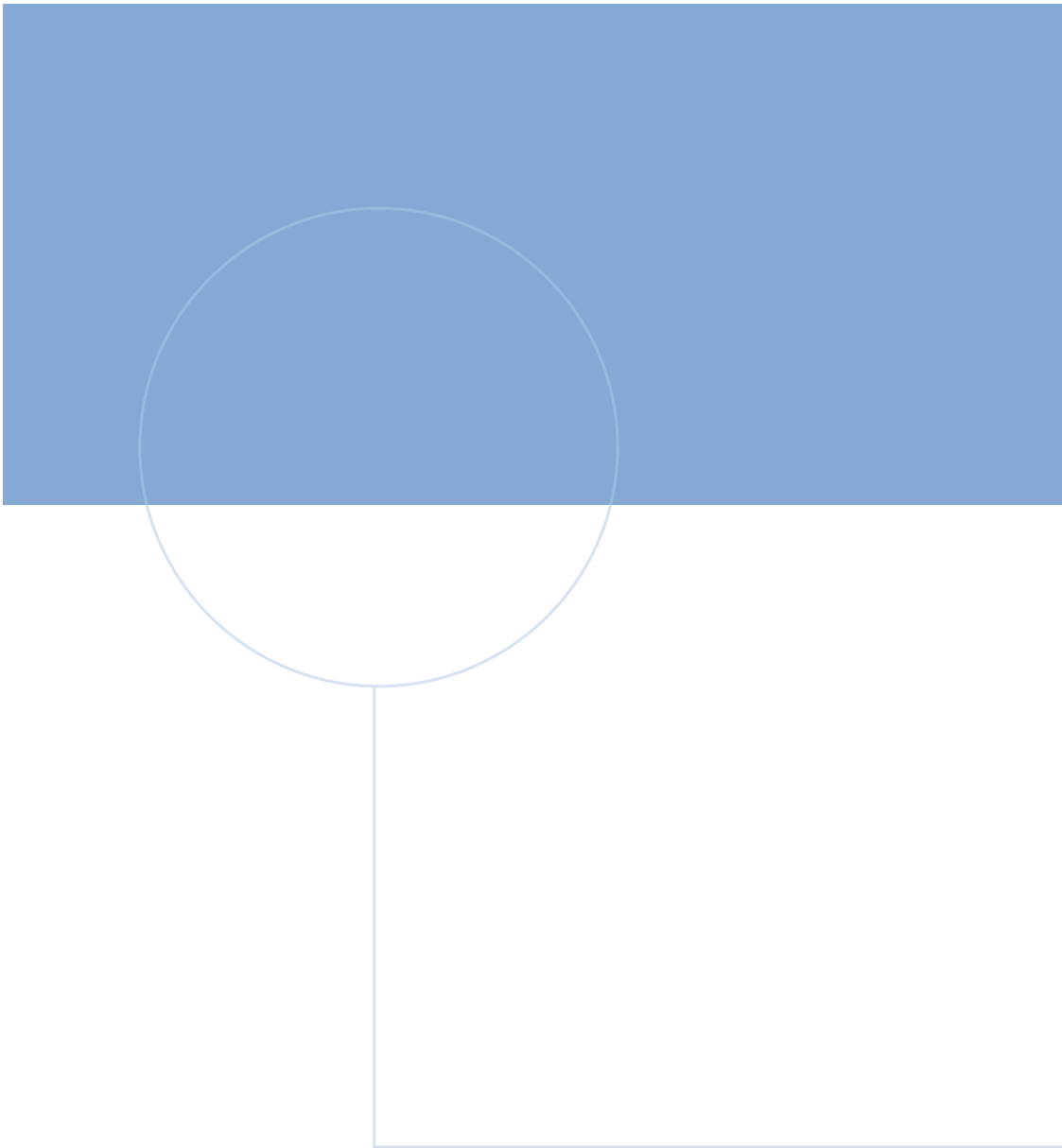

NTNU

Norwegian University of
Science and Technology